Received: 1 October 2020 | Revised: 21 April 2021 | Accepted: 27 April 2021

DOI: 10.1002/dep2.147

ORIGINAL RESEARCH ARTICLE

The Depositional Record Open Access
A journal of the International Association of Sedimentologists
IAS WILEY

The influence of microbial mats on travertine precipitation in active hydrothermal systems (Central Italy)

Giovanna Della Porta[1] | **Michael Hoppert**[2] | **Christine Hallmann**[2] | **Dominik Schneider**[2] | **Joachim Reitner**[3]

[1]Earth Sciences Department, University of Milan, Milan, Italy

[2]Institute of Microbiology and Genetics, Georg-August-University Göttingen, Göttingen, Germany

[3]Geobiology, Göttingen Centre of Geosciences, Georg-August-University Göttingen, Göttingen, Germany

Correspondence
Giovanna Della Porta, Earth Sciences Department, University of Milan, via Mangiagalli 34, 20133 Milan, Italy.
Email: giovanna.dellaporta@unimi.it

Funding information
Deutscher Akademischer Austauschdienst; German Research Council DFG, Grant/Award Number: DFG-For 571

Abstract

The study of hydrothermal travertines contributes to the understanding of the interaction between physico-chemical processes and microbial mats in carbonate precipitation. Three active travertine sites were investigated in Central Italy to characterise the types of carbonate precipitates and the associated microbial mats at varying physico-chemical parameters. Carbonate precipitated fabrics at the decimetre to millimetre-scale and microbial mat composition vary with decreasing water temperature: (a) at relatively higher temperature (55–44°C) calcite and aragonite crystals precipitate on microbial mats of Chloroflexi and sulphur-oxidizing microbes forming filamentous streamer fabrics with sparse cyanobacteria, (b) at intermediate temperature (44–40°C), rafts, coated gas bubbles and dendrites are associated with *Spirulina* cyanobacteria and other filamentous and rod-shaped cyanobacteria, (c) low temperature (34–33°C) laminated crusts and oncoids forming in a terraced slope system are associated with diverse Oscillatoriales and Nostocales filamentous cyanobacteria, *Spirulina* and diatoms. At the microscale, carbonate precipitates are similar in the three sites consisting of prismatic calcite crystals organised in radial rosettes or fibrous aragonite spherulites (40–300 μm in diameter), overlying or embedded in Extracellular Polymeric Substances. Clotted peloidal micrite dominates at temperatures <40°C, also encrusting filamentous microbes. Carbonates are associated with gypsum crystals; extracellular polymeric substances are enriched in silicon, aluminium, magnesium, calcium, phosphorous and sulphur; authigenic aluminium-silicates form aggregates on Extracellular Polymeric Substances. This study confirms that microbial communities in hydrothermal settings vary as a function of water temperature. Carbonate precipitates at the microscale are similar in the three settings, despite different microbial communities, suggesting that travertine precipitation, driven by carbon dioxide degassing, is influenced by biofilm extracellular polymeric substances acting as a substrate for crystal nucleation (Extracellular Polymeric Substances-mediated mineralization) and affecting the resultant fabric types, independently from specific microbial community composition and metabolism.

KEYWORDS
Central Italy, EPS-mediated mineralization, extracellular polymeric substances (EPS), microbial mat, terrestrial thermal spring, travertine

1 | INTRODUCTION

Travertines are terrestrial carbonates precipitated in hydrothermal settings (Capezzuoli et al., 2014; Pedley, 1990), which thrive with microbial mats comprising a wide spectrum of thermophilic Archaea and Bacteria, including sulphide-oxidizing bacteria, sulphate-reducing bacteria, anoxygenic phototrophs, oxygenic photosynthetic cyanobacteria and eukaryotic algae (Farmer, 2000; Fouke et al., 2003; Konhauser, 2007; Pentecost, 2003, 2005). Sedimentological and microbiological investigations on present-day active hydrothermal systems are fundamental because these extreme aquatic terrestrial environments store important palaeobiological information due to the high rates of mineralization (Campbell et al., 2015; Farmer, 2000). The study of microbial mats in warm to hot hydrothermal vent environments and their interaction with siliceous and carbonate mineral precipitation is linked to the understanding of early life forms on Earth and could also be important for the search of biosignatures on putative habitable planets and moons (cf. Cady & Farmer, 1996; Cady & Noffke, 2009; Cady et al., 2018; Farmer, 1998; Franchi & Frisia, 2020; Reinhardt et al., 2019; Reysenbach & Cady, 2001; Reysenbach et al., 1999; Reysenbach & Shock, 2002; Rothshield & Mancinelli, 2001; Ruff & Farmer, 2016; Sanchez-Garcia et al., 2019; Westall et al., 2000). Geomicrobiological research on the origin of life has recently shifted from high temperature submarine Black Smokers to terrestrial thermal springs, because the relatively lower temperatures of terrestrial geothermal sites facilitate the preservation of organic molecules (Des Marais & Walter, 2019). Despite the abundance of Cenozoic terrestrial thermal spring settings with precipitation of siliceous sinter and/or carbonate travertine (Capezzuoli et al., 2014; Jones & Renaut, 2010, 2011; Pentecost, 2005), these deposits are scarce in the pre-Cenozoic fossil record (Des Marais & Walter, 2019). The oldest reported terrestrial travertine deposits, attributed to deep-sourced carbon dioxide fluids at high temperature, are hosted in the Palaeoproterozoic (*ca* 2.2 Ga) Kuetsjärvi Sedimentary Formation (Pechenga Greenstone Belt; Fennoscandian Shield; Brasier, 2011; Melezhik & Fallick, 2001; Salminen et al., 2014). These dolomitic travertines and stromatolites might have formed through similar processes to present-day hydrothermal springs, but they do not contain traces of organic carbon (Salminen et al., 2014). The oldest siliceous deposits attributed to terrestrial thermal springs are known from the *ca* 3.5 Ga Dresser Formation (Pilbara, Western Australia) and were interpreted as putative geyser environments (Djokic et al., 2017).

Widespread active terrestrial thermal springs and fossil travertines in Central Italy represent key localities to investigate carbonate precipitation under warm thermal water conditions. In subaerial hydrothermal systems, supersaturation for carbonate minerals is primarily achieved by carbon dioxide evasion from thermal water issuing out of a vent and flowing along the topographic profile (Pentecost, 2005 and references therein). The precipitation of carbonate minerals might be primarily driven by physico-chemical processes (Pentecost & Coletta, 2007) or the diverse travertine facies might result from a combination of inorganic, biologically induced and influenced processes in association with microbial mats (Chafetz & Folk, 1984; Chafetz & Guidry, 1999; Della Porta, 2015; Erthal et al., 2017; Folk, 1994; Fouke, 2011; Fouke et al., 2000; Gandin & Capezzuoli, 2014; Guo et al., 1996; Guo & Riding, 1994; Jones & Peng, 2014a; Pentecost, 1995a; Rainey & Jones, 2009; Riding, 2008). There is, however, not a full understanding of the geomicrobiological processes acting in these carbonate-dominated hydrothermal systems including the role played by diverse microorganisms, their metabolic pathways, biofilm organic substrates and the physico-chemical and biochemical factors enhancing or inhibiting the precipitation of carbonate and other minerals.

In travertine hydrothermal systems, where water is supersaturated with respect to calcium carbonate due to physico-chemical processes, more research is required to unravel the controls exerted by microbial biofilms on carbonate mineral precipitation. This study aims to improve the understanding of the interaction among water physico-chemical parameters, microbial mats and the specific travertine precipitated fabrics focussing on the investigation of the character and spatial distribution of carbonate mineral precipitates with respect to the microbial mat substrates in three active travertine sites in Central Italy, with different thermal water chemistry and temperature (from 33 to 55°C).

1.1 | Review of mechanisms of carbonate mineral precipitation associated with microbial mats

Numerous studies on present-day marine and terrestrial settings, from the geological record and through laboratory experiments, have demonstrated that carbonate mineral precipitation

associated with microbial mats can take place in aquatic environments through different mechanisms. These mechanisms depend on environmental conditions, types of microbial communities and the nature of organic substrates. Carbonate precipitation associated with organic substrates in aqueous fluids, under favourable physico-chemical conditions, can be both the result of: (a) metabolic activity of live microbes (Castanier et al., 1999; Chafetz & Buczynski, 1992; Knorre & Krumbein, 2000; biologically induced mineralization sensu Dupraz et al., 2009; Lowenstam & Weiner, 1989 and/or (b) the result of mineralization of non-living organic substrates with acidic macromolecules able to bind calcium and magnesium ions (organomineralization sensu Défarge & Trichet, 1995; Défarge et al., 1996, 2009; Neuweiler et al., 1999; Reitner et al., 1995a, 1995b, 2000, 2001; Trichet & Défarge, 1995; organomineralization sensu *strictu* and biologically influenced mineralization sensu Dupraz et al., 2009; organic-compound catalyzed mineralization sensu Franchi & Frisia, 2020). Organomineralization has been identified associated with various organic substrates such as EPS (Extracellular Polymeric Substances) from microbial biofilms, post-mortem encrustation of bacterial cells, sponge tissues or even abiotic organic compounds (Défarge et al., 2009; Reitner, 1993, 2004).

Among the microbial metabolic pathways that appear to play a key role in carbonate precipitation by modifying the microenvironment, driving increased alkalinity and carbonate supersaturation, the most significant appear to be: (a) photosynthesis by autotrophic oxygenic cyanobacteria (Bissett et al., 2008; Castanier et al., 1999; Eymard et al., 2020; Golubic et al., 2000; Merz, 1992; Merz-Preiß, 2000; Merz-Preiß & Riding, 1999; Obst et al., 2009; Pentecost & Riding, 1986; Plée et al., 2010; Robbins & Blackwelder, 1992), with eventually carbonate encrustation of microbial cells in settings with low dissolved inorganic carbon (DIC) and high calcium (Arp et al., 2001, 2003, 2010; Défarge et al., 1996; Kamennaya et al., 2012; Merz, 1992; and (b) ammonification of aminoacids and sulphate reduction by heterotrophic bacteria (Andres et al., 2006; Baumgartner et al., 2006; Castanier et al., 1999; Dupraz & Visscher, 2005; Dupraz et al., 2004, 2009; Knorre & Krumbein, 2000; Pace et al., 2016; Visscher et al., 2000).

Microbial biofilm EPS play a key role on the precipitation of carbonate and other minerals (Decho, 2010; Decho & Gutierrez, 2017; Défarge & Trichet, 1995; Reitner et al., 1995; Westall et al., 2000; Wingender et al., 1999). Microbial cells and eukaryotic algae in marine and terrestrial environments can secrete diverse arrays of EPS. Dominant macromolecules are often acidic polysaccharides and (glycol-) proteins, including lectins, which are rich in negatively charged carboxylic and sulphate groups that may bond divalent cations. The EPS also facilitate attachment to surfaces that lead to the formation of microbial mats, stabilising cells and protecting them from physical stresses (e.g., changes in salinity, temperature, UV irradiation, desiccation). One function of EPS is the inhibition of fast precipitation of various minerals, mainly calcium carbonate, to avoid the blockade of ionic exchange between cells and ambient water (Arp et al., 1999, 2001, 2003; Défarge & Trichet, 1995; Reitner et al., 1995). The EPS acidic macromolecules have a matrix and template function of mineralization and inhibit precipitation by providing bonding of divalent cations, such as calcium, strontium and magnesium (Arp et al., 1999, 2012; Ionescu et al., 2014). Therefore, EPS can either promote calcium carbonate precipitation by acting as a template for crystal nucleation (EPS-mediated mineralization; Reitner, 1993; Reitner et al., 1995) or inhibit precipitation by binding free calcium ions (Arp et al., 1999, 2001, 2003; Ionescu et al., 2014). Crystal nucleation is promoted by highly ordered acidic groups at defined distances that correspond to the crystal lattice, whereas disordered organic matrices as EPS inhibit precipitation (Arp et al., 2001). Nucleation of calcium carbonate only occurs at acidic groups, which are suitably arranged mainly by accident, after a sufficient diffusive calcium supply surpasses the complexation capacity of EPS. The binding capabilities of EPS acidic macromolecules and the inhibiting effect increase with pH and are stronger in alkaline settings and in the phototrophic zone (Arp et al., 1999, 2003; Ionescu et al., 2014). The EPS inhibiting capability is surpassed by degradation that releases calcium, increasing calcium carbonate supersaturation and enhancing mineral precipitation (Arp et al., 1999; Braissant et al., 2007, 2009; Ionescu et al., 2014; Reitner et al., 1996, 1997). Various studies suggest that biofilm EPS degradation through bacterial sulphate reduction is pivotal to carbonate precipitation in present-day microbialites (Baumgartner et al., 2006; Dupraz & Visscher, 2005; Dupraz et al., 2004, 2009; Glunk et al., 2011).

Hence, carbonate precipitation can be induced by living microorganisms and their metabolic pathways, but it can also occur without the contribution of microbial metabolism, mediated by organic compounds independently from the microorganisms from which these compounds may derive (Défarge et al., 2009). These two mechanisms must have been both active in the geological record together with physico-chemically driven abiotic mineralization (Défarge et al., 1996; Riding, 2000, 2008). The first probable EPS-mediated mineralization deposits are suggested to be the Strelley Pool stromatolites (*ca* 3.35 Ga) from Pilbara Craton, Western Australia (Allwood et al., 2006; Viehmann et al., 2020).

2 | GEOLOGICAL BACKGROUND OF STUDIED TRAVERTINE DEPOSITS

Since the Neogene, Central Italy has been the site of widespread deposition of hydrothermal travertines, in particular during the Pleistocene and Holocene times (Brogi &

Capezzuoli, 2009; Brogi et al., 2016; Capezzuoli et al., 2014; Chafetz & Folk, 1984; Croci et al., 2016; Della Porta, 2015; Della Porta et al., 2017a, 2017b; Erthal et al., 2017; Faccenna et al., 2008; Guo & Riding, 1992, 1994, 1998, 1999; Mancini et al., 2019; Minissale, 2004; Minissale et al., 2002a, 2002b; Pentecost, 1995a, 1995b). Travertine deposits in Central Italy are associated with Neogene and Quaternary magmatic activity and extensional tectonics superimposed on the Apennine Mesozoic and Cenozoic thrust sheets (Figure 1). The western side of the Apennine fold-and-thrust belt was affected by extensional and strike-slip tectonics from late Miocene time due to back-arc related extension of the Tyrrhenian Sea in the west, while in the east, the Adriatic plate was in subduction westwards and the Apennine thrusts propagated eastwards (Carminati & Doglioni, 2012; Doglioni, 1991; Malinverno & Ryan, 1986). Due to Neogene tectonics, several sedimentary basins developed with preferential orientation NW-SE and were filled by Miocene to Quaternary marine and terrestrial deposits (Carminati & Doglioni, 2012; Faccenna et al., 2008). In these extensional and strike-slip basins, hydrothermal activity with Ca-SO_4-HCO_3 water composition (Minissale, 2004) and related travertine deposition are common features due to: (a) Pliocene–Holocene intrusive and effusive rocks with up to present-day volcanic activity; (b) faults acting as fluid conduits; (c) humid climate and mountain relief driving atmospheric precipitation; and (d) substrate rocks consisting of hundreds of metres thick Mesozoic carbonate successions providing calcium and carbonate ions and hydrogen sulphide derived from Triassic evaporites (Minissale, 2004). In present-day active hydrothermal systems in Central Italy (Figure 1), water (temperatures 20–65°C) emerges at the surface and degasses carbon dioxide precipitating travertine while outflowing away from the vent. The origin of carbon dioxide is debated and has been attributed to: (a) hydrolysis of regionally extensive Mesozoic limestones; (b) metamorphism of limestones within the Palaeozoic basement; and (c) mantle derived carbon dioxide (Minissale, 2004). Based on stable isotope data of thermal water and travertine deposits, the

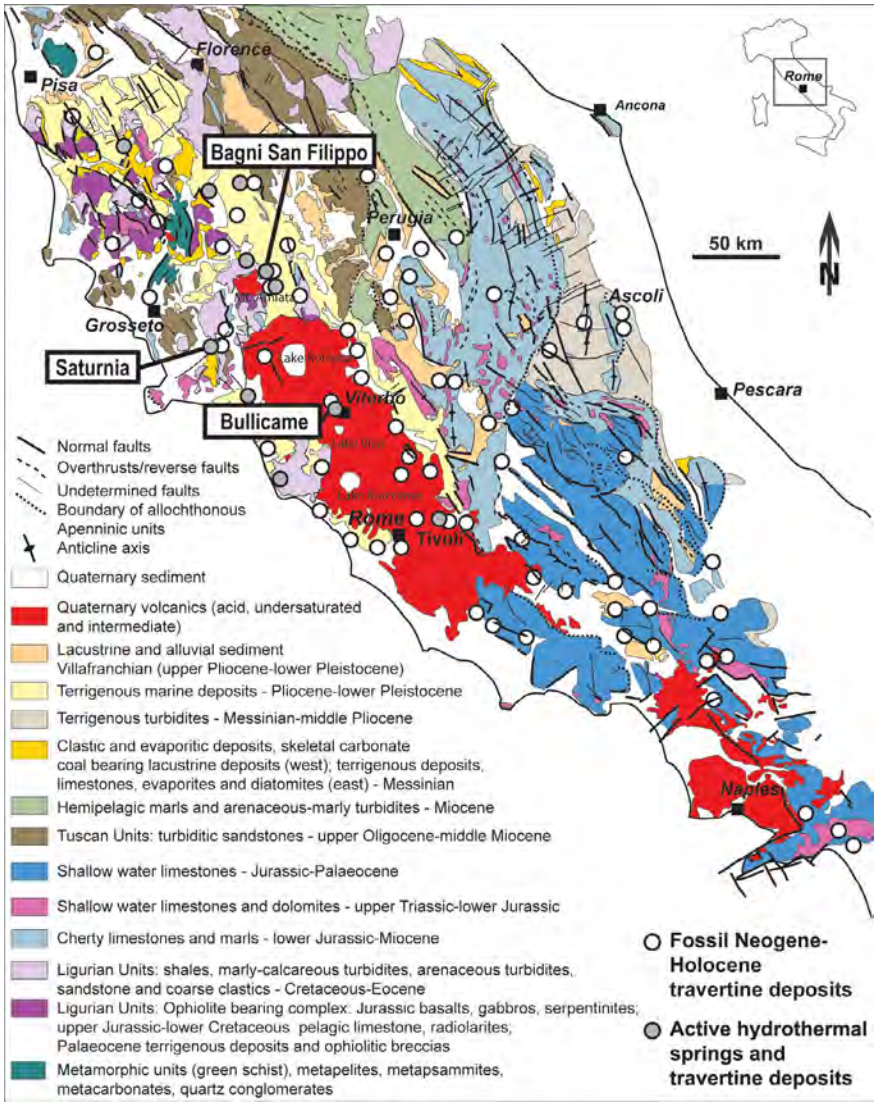

FIGURE 1 Generalised geological map of Central Italy (modified after Bigi et al., 1990; Della Porta, 2015) with sites of active and fossil hydrothermal springs as reported by Minissale (2004). The three active hydrothermal travertine sites sampled in this study are indicated: Bullicame (near the town of Viterbo, north of Rome), Bagni San Filippo (north-east of the volcanic complex of Monte Amiata) and Saturnia

main source of carbon dioxide is related to decarbonation of limestones triggered by the presence of shallow mantle intrusions in the crust (Minissale, 2004).

The selected sites of active hydrothermal travertine deposition investigated in this study in Central Italy (Figure 1) are located in the Latium region, near the town of Viterbo (Bullicame) and in Southern Tuscany, close to the villages of Bagni San Filippo and Saturnia. The Bullicame vent issues water with temperatures of 55–58°C and a pH of 6.3 (Pentecost, 1995a; Piscopo et al., 2006). Thermal water from different vents around the village of Bagni San Filippo has temperatures ranging from 47 to 52°C and a pH range of 6.7–6.4 (Brogi & Fabbrini, 2009; Minissale, 2004; Pentecost, 1995a). At Saturnia, the travertine system consists of a waterfall and travertine apron (Gorello Waterfall) developed more than 1 km away from the vent, where thermal water temperature is 37°C and pH 6.3 (Minissale, 2004; Ronchi & Cruciani, 2015).

3 | METHODS

Travertine and thermal water were sampled from active hydrothermal systems in three localities in Central Italy (Figure 1), during the summer month of July with high air temperature and limited atmospheric precipitation. The investigated travertine sites are: (a) Bullicame, near Viterbo (N 42°25′ 13.53″, E 12° 04′ 22.58″, elevation 293 m a.s.l.); (b) Bollore, close to the village of Bagni San Filippo, northeast of the Mount Amiata volcanic complex (N 42°55′38″, E 11°41′41.5″, 597 m a.s.l.); (c) Gorello Waterfall, near the village of Saturnia (N 42° 38′53.30″, E 11°30′45.45″, 138 m a.s.l.). Water temperature, pH and total alkalinity (Tables 1 through 3) were measured in the field with a hand-held pH-meter and titrator, Mortimer solution and sulphuric acid cartridges. Sixteen samples of travertine and the adherent microbial mat were collected in 50 ml falcon tubes and fixed either in formaldehyde 4% (v/v) in phosphate buffer solution (PBS) or in glutaraldehyde at a concentration of 4% (v/v) in PBS. Samples were stored in a refrigerator at 4°C during transportation.

Travertine samples were processed within 4 days from collection at the Geobiology Department of the Georg-August-University Göttingen (Germany). The fixative was removed, samples were dehydrated in graded ethanol series (15–30–50–70–90%–99%) and embedded in a resin (LR White, London Resin Company, UK). Once hardened, 70 thin sections were prepared for petrographic analysis with a Zeiss AX10 microscope equipped with a digital camera. Prior to resin embedding, subsamples were stained with the fluorochrome calcein, tetracycline, DAPI (6-Diamidino-2-Phenylindole, Dihydrochloride) and toluidine blue. Calcein and tetracycline allow detection of calcium-binding areas. Calcein penetrates the cell membrane into vital cells where the acetoxymethyl-group is enzymatically cleaved by esterases; calcein spreads throughout the cell, including the mitochondria and the cell nucleus. Intracellularly, calcein is able to bind calcium and thus leads to a bright green fluorescence (Fox et al., 2018; Reitner, 1993; Reitner & Gautret, 1996). The DAPI fluorochrome detects DNA. Toluidine blue is a basic thiazine metachromatic dye with a high affinity for acidic tissue components. Thirteen thin sections stained with calcein and DAPI were analysed with a confocal laser scanning microscope (Nikon A1) at the Unitech laboratory of the University of Milan. Eight subsamples of prevalent organic soft microbial mat were prepared for embedding in paraffin wax after decalcification. Paraffin embedded samples were stained with alcian blue, cell centre red staining (nuclear fast red, Kernechtrot) and Masson-Goldener solution (Romeis, 1989). Alcian blue is a polysaccharide stain characterising EPS. It stains carboxyl and sulphate groups in acidic solution, but not nucleic acids. The dissociation of the carboxyl groups can be suppressed by lowering the pH or by adding high salt concentrations so that only sulphate groups bind the dye (Hoffmann et al., 2003; Reitner et al., 2004; Scott & Dorling, 1965).

Thirteen subsamples, previously fixed with glutaraldehyde 4% (v/v) in PBS, were prepared for scanning electron microscope (SEM) analysis. Samples were dehydrated in graded ethanol series (15–30–50–70–80–90–95–98%–99%) and air-dried after ethanol removal. Samples were mounted on stubs, coated with platinum 13 nm thick and analysed with a field emission SEM LEO 1530 with a Gemini column operating at 3.8–15 kV, equipped with INCA Energy EDX system from Oxford Instruments at the Geobiology Department of the Georg-August-University, Göttingen. Additional SEM analyses were performed on six gold-coated samples, with a Cambridge Stereoscan 360, operating at 20 kV with a working distance of 15 mm at the Earth Sciences Department, University of Milan. The mineralogy of carbonate precipitates was determined through X-ray powder diffraction analysis of six travertine samples with an X-ray powder diffractometer Philips X'Pert MPD with high temperature chamber at the University of Milan.

Stable oxygen and carbon isotope analyses of 48 carbonate powder samples (9 Bullicame, 15 Bollore, 24 Gorello; Table S1) were performed using an automated carbonate preparation device (GasBench II) connected to a Delta V Advantage (Thermo Fisher Scientific Inc.) isotopic ratio mass spectrometer at the Earth Sciences Department, University of Milan. Carbonate powders were extracted with a dental microdrill and were reacted with >99% orthophosphoric acid at 70°C. The oxygen and carbon isotope compositions are expressed in the conventional delta notation calibrated to the Vienna Pee-Dee Belemnite (V-PDB) scale by the international standards IAEA-603 and NBS-18. Analytical

TABLE 1 Physico-chemical properties of thermal water, travertine characteristics and microbial mat features from proximal to distal at the Bullicame (Viterbo) travertine mound. The vent is fenced and the first possible sampling site is along a channel nearly 12.5 m from the centre of the vent pool. Water chemistry information is extracted from Pentecost (1995a) and Piscopo et al. (2006). The saturation index (SI) for carbonate minerals calculated with WEB-PHREEQ (Parkhurst & Appelo, 1999) are similar to published values, resulting in values of 2.67 and 1.91 for calcite and 2.55 and 1.78 for aragonite, using ion concentrations by Pentecost (1995a) and Piscopo et al. (2006), respectively

	Thermal Water					
Bullicame mound	**Temperature (*T*, °C)**	**pH**	**Alkalinity (meq/L)**	**Water chemistry at vent from Pentecost (1995a) and Piscopo et al. (2006) in mg/L**	**Travertine**	**Microbial mats**
Proximal channel (20 cm wide, 1–2 cm deep)						
Channel 12.5 m from centre of the vent	55	6.7	15.6	At vent: *T* 55.5, 58.4°C; pH 6.30, 6.25; Ca 573, 500; Mg 137, 139; Na 76, 39; K 33, 38 HCO_3^- 964, 1,000; SO_4^{2-} 1,106, 1,050; Cl 9, 17. SI calcite 3.94 SI aragonite 2.74 SI gypsum 0.87 (Pentecost, 1995a) SI calcite 0.54 SI gypsum −0.32 (Piscopo et al., 2006)	Millimetre-thick carbonate crust at channel margin	Channel floor: dark orange/purple microbial mat; uncalcified filamentous microbes (Chloroflexi, sulphur-oxidizing, sulphate-reducing bacteria, cyanobacteria). Channel margin: orange/yellow to green mat with uncoated mm-size gas bubbles (cyanobacteria, *Phormidium*, *Spirulina, Synechococcus*)
15.5 m	54.6	6.7				
17.5 m	54.3	6.7				
21.5 m	53.9	6.8	15.76			
26.5 m	53.4	6.8			Channel centre: cm-size bundles of white carbonate-encrusted filaments oriented with flow direction (bacterial streamers)	Channel floor: dark green mat below white fans of calcified filamentous microbes (Chloroflexi, sulphur-oxidizing bacteria, cyanobacteria). Channel margin: orange/yellow to green mat with uncoated mm-size gas bubbles (cyanobacteria, *Phormidium*, *Spirulina, Synechococcus*)
30.5 m	53.1	6.9				
35.5 m	52.5	6.9				
41.5 m	52	7.1				
48.5 m	50	7.3				
55.5 m	50.5	7.2				
Distal channel (30–40 cm wide, 2–4 cm deep)						
60.5 m	50	7.3	14.52		Channel centre: carbonate coated gas bubbles and mm-thick crusts. Channel margin: calcified gas bubbles, mm to cm-thick carbonate crusts and paper-thin rafts	Channel floor: light green to yellow mat. Channel margin: light orange to green mat (cyanobacteria, *Spirulina, Phormidium*)
73.5 m; in water at centre of channel	49	7.4				
73.5 m; in green microbial mat at channel margin	48.4	7.3				
83.5 m	48.2	7.4				

TABLE 2 Physico-chemical properties of thermal water, travertine characteristics and microbial mat features from proximal to distal at the Bollore (Bagni San Filippo) travertine mound. The main vent is located at the mound top and consists of a circular pool with three orifices labelled as A, B, C; the second vent is at the base of the mound flank. Water chemistry information is extracted from Minissale (2004) and Pentecost (1995a). The saturation index (SI) for carbonate minerals calculated with WEB-PHREEQ (Parkhurst & Appelo, 1999) are different from those calculated by Pentecost (1995a), resulting in values of 1.63 for calcite and 1.5 for aragonite

	Thermal water					
Bollore mound	**Temperature (°C)**	**pH**	**Alkalinity (meq/L)**	**Water chemistry from Pentecost (1995a) and Minissale (2004) in mg/L**	**Travertine**	**Microbial mats**
Main vent (3 orifices, 20–50 cm in diameter)						
Vent pool A	46.5	6.5	31.65	At vent: *T* 47, 52°C; pH 6.3, 6.5; Ca 721, 798; Mg 197, 182; Na 115, 28; K 2, 11; HCO_3^- 1,696, 1,836; SO_4^{2-} 1,514, 1,200; Cl 67, 14.5 SI calcite 14.8 SI aragonite 10 SI gypsum 1.23 (Pentecost, 1995a)	Carbonate-encrusted filamentous bundles (bacterial streamers, 1–3 cm wide, 5–8 cm long) oriented with water flow; dm-size stagnant pools covered by white, mm-thick paper-thin rafts	Vent pool: white to light orange-pink mat; dm-size stagnant pools with green microbial mat adherent to raft lower surface (Chloroflexi, sulphur-oxidizing, sulphate-reducing bacteria, cyanobacteria); in winter vent pools support abundant green to brown/pink microbial mat
Vent pool B	46.1	6.6				
Vent pool C	49.5	6.5				
Proximal channel (15–30 cm wide, 1 cm deep)						
Channel at 0.4 m from vent C	49	6.6			Carbonate-encrusted filamentous bundles (bacterial streamers 1-3 cm wide, 5-8 cm long)	Channel floor: white to light pink/ orange mat (Chloroflexi, sulphur-oxidizing, sulphate-reducing bacteria, cyanobacteria *Synechococcus, Spirulina*)
3.10 m	47.3	6.8				
8.10 m	44	7.1				
Distal channel (30 cm wide, 1–2 cm deep, 10 m from vent)						
14 m	41.4	7.3	21.55		Millimetre-size carbonate coated gas bubbles and rafts	Channel floor: light green microbial mat (cyanobacteria, *Spirulina, Phormidium*, *Synechococcus,* Chloroflexi, sulphur-oxidizing bacteria)
20.3 m (increase in topographic gradient)	38.2	7.4			Centimetre-size terraces and pools with coated gas bubbles, coated grains and dendrites	Channel floor: light pink to green mat
24.5 m	36.4	7.5				
27 m	33.6	7.9				
28 m	33.5	7.9				

(Continues)

TABLE 2 (Continued)

Bollore mound	Thermal water: Temperature (°C)	Thermal water: pH	Thermal water: Alkalinity (meq/L)	Water chemistry from Pentecost (1995a) and Minissale (2004) in mg/L	Travertine	Microbial mats
Second vent and channel						
Vent	49.3	6.5				
Channel (30 cm wide, 1 cm deep) at 2 m from vent	48.4	6.5			Dark grey carbonate-encrusted filamentous bundles (bacterial streamer 2–4 cm wide, 6–8 cm long); yellow sulphur precipitates; carbonate and detrital sediments black stained by sulphide coatings	Channel floor and margins: bright yellow sulphur, dark grey and yellow and mat (Chloroflexi, sulphur-oxidizing, sulphate-reducing bacteria, cyanobacteria *Synechococcus*, *Spirulina*)
5 m	40.6	7				

reproducibility for these analyses was better than ±0.1‰ for both $\delta^{18}O$ and $\delta^{13}C$ values.

The identification of microbial communities at Bullicame, Bollore and Gorello Waterfall sampled sites is tentative and based on morphological criteria (cf. Pentecost, 2003; Reysenbach & Cady, 2001), on published metagenomic analyses on the same study sites and comparable hydrothermal vents in Central Italy and worldwide. Form-taxa classifications based upon morphological characters provide an overview aiding future sampling strategies and a taxonomic platform upon which to assess the ensuing molecular approaches, but molecular methods are fundamental for the determination of microbial taxa (Pentecost, 2003). Samples collected from Bullicame, Bollore and Gorello Waterfall for molecular analyses did not provide reliable results due to sample contamination and degradation during transportation and storage. Therefore, an additional sampling site for geomicrobiological analyses was selected close to the currently inactive Bollore vent near the village of Bagni San Filippo. Samples were collected approximately 650 m east of the Bollore vent, between the locality labelled as the Fosso Bianco (white creek; N 42°55′40, E 11°42′10, 521 m a.s.l.) and the Balena Bianca (white whale; N 42°55′45, E 11°42′12, 497 m a.s.l.), in a wide range of water temperatures varying between 46 and 29°C. Nine representative samples of travertine deposits and microbial mats were collected for molecular analyses from a cascade with thermal water flowing into a stream along a transect 520 m long; temperature and pH were measured at the sampling sites (Table 4). These nine samples were inspected, within a few hours after sampling through light microscopy, to confirm the presence of microbial morphotypes along with precipitates of calcite or other minerals, using a Motic BA310E microscope (Motic GmbH) equipped with phase contrast optics, simple crossed polarizers and an epiflourescence unit (exciter: 470 nm, dichroic mirror: 495 nm/long-pass, barrier: 515 nm/long-pass; suitable for chlorophyll autofluorescence excitation). Images were recorded with a Colour view III camera (Motic GmbH). Samples were collected as described in Kamran et al. (2021); they were refrigerated and kept frozen until further processing. Samples were processed for extraction of environmental DNA, amplification of 16S and 18S marker genes for Bacteria and Eukaryotes, *Illumina* next generation sequencing and sequencing data processing as described by von Hoyningen-Huene et al. (2019), Schulz et al. (2019) and Kamran et al. (2021). Raw reads were processed as described in Hoyningen-Huene et al. (2019) and, as a result, amplicon sequence variants (ASVs), which could be assigned to a taxon, were generated (Callahan et al., 2017). All sequences are available via the Biosample database of the NCBI (National Centre for Biotechnology Information, Bethesda, MD, USA) under Bioproject accession no. PRJNA723265 (https://www.ncbi.nlm.nih.gov/bioproject/PRJNA723265).

TABLE 3 Physico-chemical properties of thermal water, travertine characteristics and microbial mat features at the Gorello Waterfall (Saturnia) travertine terraced slope system located nearly 1,170 m from the vent with thermal water running through a channel terminating in a waterfall. Water chemistry parameters at hydrothermal vent (used as thermal spa) are extracted from Minissale (2004). Saturation indexes (SI) for carbonate minerals calculated with WEB-PHREEQ (Parkhurst & Appelo, 1999) result in values of 1.74 for calcite and 1.61 for aragonite

	Thermal water					
Gorello Waterfall (*ca* at 1,170 m from vent)	**Temperature (*T*, °C)**	**pH**	**Alkalinity (meq/L)**	**Water parameters at vent from Minissale (2004) in mg/L**	**Travertine**	**Microbial mats**
Proximal terraced slope (20 m long)						
At waterfall (5 m high)	33.8	7.8		At vent: *T* 37°C, pH 6.3; Ca 556; Mg 120; Na 72; K 11 HCO_3^- 665; SO_4^{2-} 1,420; Cl 67	Metre-scale sub-horizontal pools separated by rounded rims and sub-vertical walls 0.1–1.5 m high. Pool rims and walls: laminated travertine boundstone	Pool rims: olive green mm-thick mat; pool walls: white to dark to light green filamentous mat encrusted by carbonate (diverse filamentous cyanobacteria; Oscillatoriales, Nostocales, *Phormidium, Spirulina, Synechococcus*)
1 m from waterfall in pools of terraced slope	33.4	7.8				
2 m	33.6	7.8				
3 m	33.6	7.9				
4 m	33.7	7.8				
Distal terraced slope						
5 m	33	7.9	9.07; 9.04		Areas of pools temporarily not flooded by thermal water are sites of vegetation growth, mostly reeds, encrusted by carbonate at renewed flows. Pool floor: mm to cm-size carbonate coated grains (oncoids); terrigenous mud to sand-size detrital sediment (fragments of fluvial tufa with coated plants and calcified cyanobacteria, peloidal packstone, sandstone, quartz grains, planktonic and benthic foraminifers from the Pliocene marine claystone), carbonate coated plant fragments	Pool rims: olive green mm-thick mat; pool walls: white to dark to light green filamentous mat encrusted by carbonate (diverse filamentous cyanobacteria, Oscillatoriales, Nostocales, *Phormidium, Spirulina, Synechococcus*). Oncoid surface with green microbial mat
6 m	33.5	7.9				
7 m	33.6	7.9				
8 m	33.5	7.9				

TABLE 4 Location and microbial mat features and composition of the samples collected at Bagni San Filippo (Fosso Bianco and Balena Bianca) for geomicrobiological analyses (Figures S9 and S10). Measured water temperature and pH at the sampling sites are reported

Sample	Location (Latitude N; Longitude E)	Water temperature (°C)	pH	Microbial mat field features	Microbial communities
I4.1	42°55′39.9″; 11°42′10.4″	44.8	6.37	Fosso Bianco; whitish pale yellow to greenish on cascade	Cyanobacteria (*Phormidium*) Bacteroidota Chloroflexaceae Anaerolineaceae
I4.2	42°55′39.7″; 11°42′10.2″	45.8	6.4	Fosso Bianco; greenish at the creek margin side	Proteobacteria (*Thiofaba*) Cyanobacteria (*Spirulina*) Chloroflexaceae Anaerolineaceae
I4.3	42°55′39.7″; 11°42′10.2″	45.8	6.4	Fosso Bianco; whitish pale yellow filamentous streamers in creek floor centre	Anaerolineaceae, Chloroflexaceae (*Oscillochloris*) other Chloroflexi Cyanobacteria (Desertifilaceae and *Spirulina*)
I4.4	42°55′39.7″; 11°42′10.2″	45.8	6.4	Fosso Bianco; purple to green on creek margin side	Anaerolineaceae other Chloroflexi Cyanobacteria (*Spirulina*) Proteobacteria (*Thiofaba*)
I4.5	42°55′40.6″; 11°42′12.3″	41.1	6.29	Fosso Bianco; green to brownish on terrace wall/ cascade along stream with mixing thermal and freshwater	Patescibacteria Nitrospirota Actinobacteriota (*Streptomyces*) Proteobacteria (Sulfuritalea, Gallionellaceae)
I4.6	42°55′42.7″; 11°42′12.9″	31.6	7.72	Fosso Bianco; green to light brown in pool behind terrace wall along stream with mixing thermal and freshwater	Cyanobacteria Chloroflexaceae
I4.7-8	42°55′45.3″; 11°42′11.8″	29	7.7	Balena Bianca; white to pale pink in pool at the toe of the cascade	Proteobacteria (*Thiotricales, Hydrogenophaga*) Cyanobacteria (*Spirulina*)
I4.9	42°55′45.3″; 11°42′11.8″	29	7.7	Balena Bianca: white to pale greenish and yellow on vertical micro-terraced wall at the toe of the cascade	Cyanobacteria (*Spirulina*) Spirochaetota, Leptonema Proteobacteria (*Thiofaba*) Anaerolineaceae other Chloroflexi

4 | RESULTS

4.1 | Travertine precipitates and microbial mat features

4.1.1 | Bullicame

The Bullicame travertine mound consists of a central vent issuing thermal water conveyed along a channel (Figure 2A,B; Figure S1). Information about the travertine deposits, measured thermal water parameters and characteristics of the microbial mats along the channel is summarised in Table 1 and Supporting Information. In the proximal channel centre (Figure 2C,D), carbonate precipitates overlie or are embedded within microbial mats of filamentous microbes forming bacterial streamers (sensu Farmer, 2000). Precipitated carbonate crystals follow the spatial distribution of organic substrates (Figure 3A through E). The bundles of carbonate-coated EPS and filamentous microbes are 100 μm to several millimetres thick and a few centimetres long. In the proximal channel samples, precipitated calcite crystals consist of microsparite to fine sparite with euhedral prismatic crystals with a spindle shape (10–80 μm long, 5–40 μm wide), radially arranged to form rosettes (Figures 3E,F and 4A through C). Calcite crystals are embedded in EPS with filamentous microbes (Figure 4D through F; Figure S2), associated with rare rod-shaped microbes. Calcite rosettes (40–120 μm in diameter), also embedded in EPS and filamentous microbes (Figure 4A through C), may show a micrite clot and/or organic matter nucleus, 10–40 μm in diameter (Figures 3F and 4A). Calcite crystal size increases downstream reaching 40–120 μm in length and 20–40 μm in width; the diameter of crystal rosettes increases from

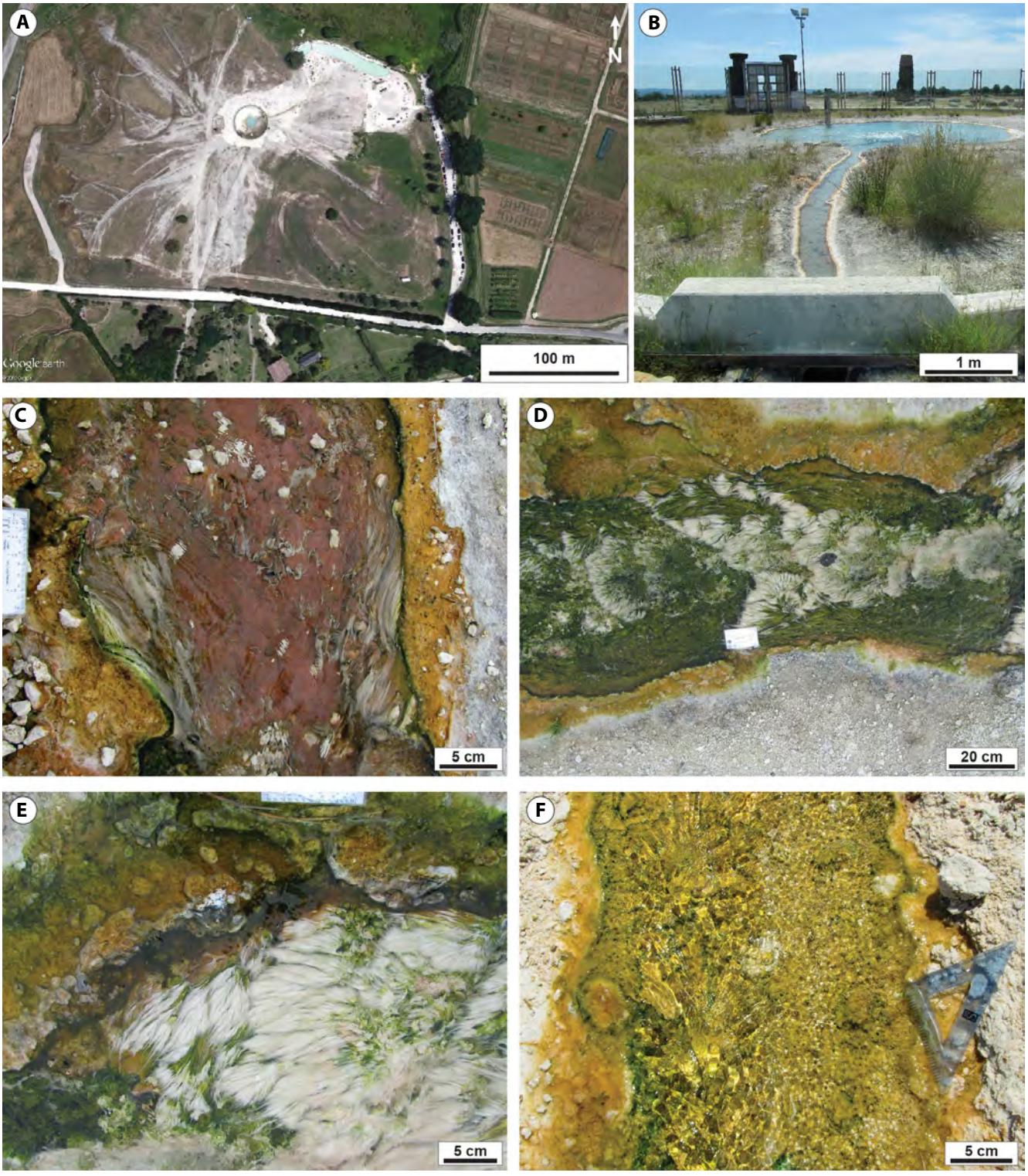

FIGURE 2 Bullicame (Viterbo) active hydrothermal travertine system. (A) Google Earth Pro satellite image showing the Bullicame travertine mound with the fenced active vent in the centre. (B) Image of the vent circular pool across the inaccessible glass fence. (C) Proximal channel, 14 m from the vent centre, draped by dark orange/purple microbial mats in the centre, with sparse bundles of white filamentous organic structures oriented according to the current flow direction and with orange to green microbial mat on the channel margins. (D) Proximal channel further downstream at 22 m from vent centre: the bundles of carbonate-coated filaments are abundant and the channel floor is draped by green microbial mat, while the channel margins are orange to green in colour with gas bubbles. (E) Close-up view of proximal channel at 30 m from the vent centre with bundles of carbonate-coated filaments (bacterial streamers sensu Farmer, 2000). (F) Distal channel at 60 m from the vent with centre and margins draped by light green to yellow/orange microbial mat with abundant carbonate-coated gas bubbles and paper-thin rafts

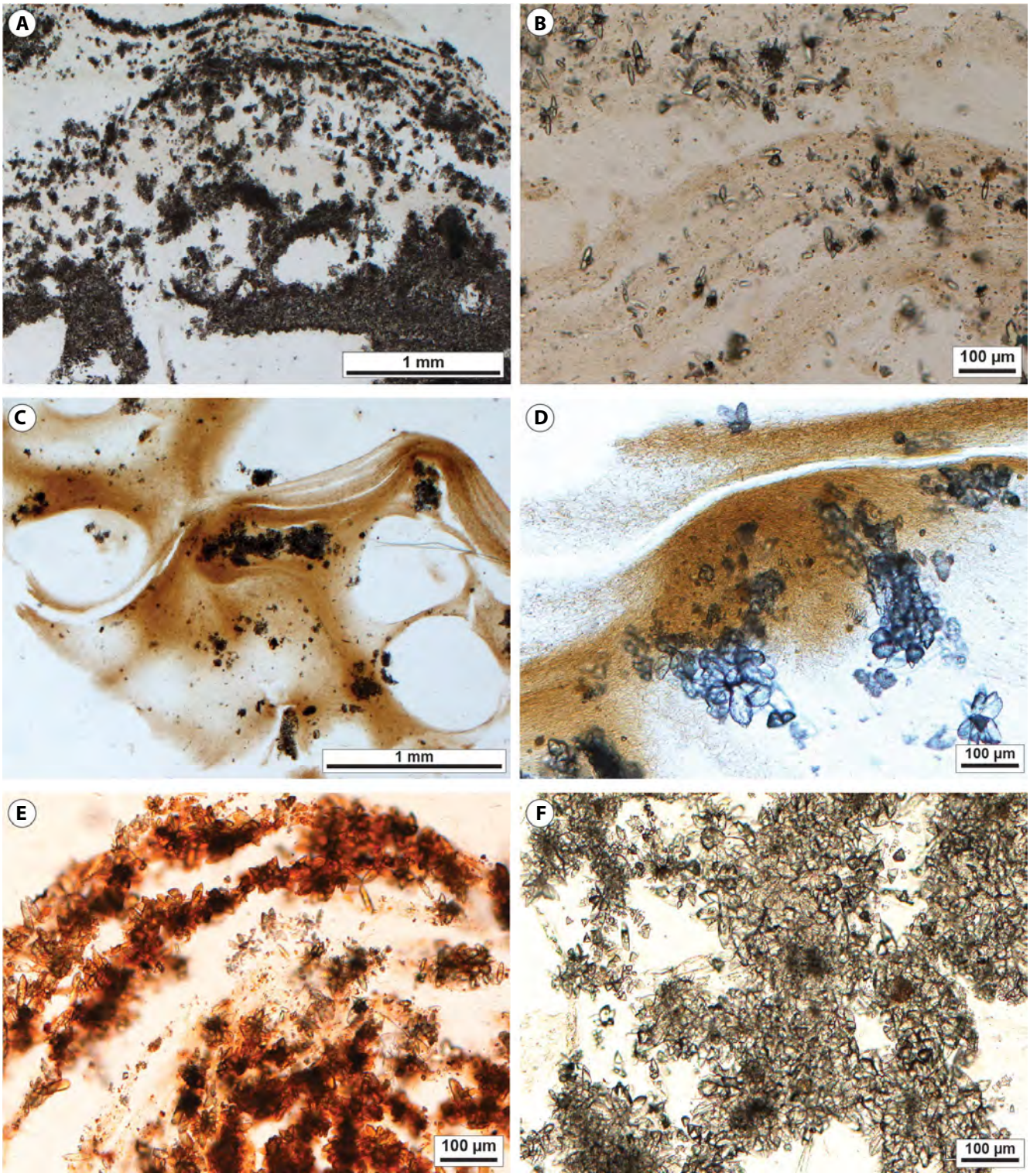

FIGURE 3 Petrographic and SEM images of the Bullicame travertines in the proximal channel centre (from 12.5 m to 55.5 or 60 m from vent). (A) Carbonate precipitates as microsparite/sparite forming radial crystal rosettes within and above organic substrates. The spatial distribution of the carbonate precipitates forming laminae and irregular mosaics is controlled by the framework of the EPS (sample BUL-A-18; 30.5 m from vent). (B) Calcite crystal rosettes embedded within microbial mat following the shape and geometry of the organic substrate (sample BUL-A-9; 21.5 m from vent). (C) Photomicrograph of sample stained with tetracycline. The orange colour-stained material represents the microbial mat EPS and filamentous microbes. Carbonates as microsparite/sparite aggregates precipitated within the organic substrate (sample BUL-A-18; 30.5 m from vent). (D) Close-up view of the tetracycline-stained filamentous microbes and EPS embedding rosettes of radially-oriented prismatic calcite crystals (sample BUL-A-18; 30.5 m from vent). (E) Calcein-stained sample showing that the calcite crystal rosettes mimic the shape and geometry of the organic substrate binding Ca^{2+} forming undulated laminae (sample BUL-A-9; 21.5 m from vent). (F) Photomicrograph of calcite microsparite/sparite mosaic with sparse clots of micrite (sample BUL-2; 30.5 m from vent)

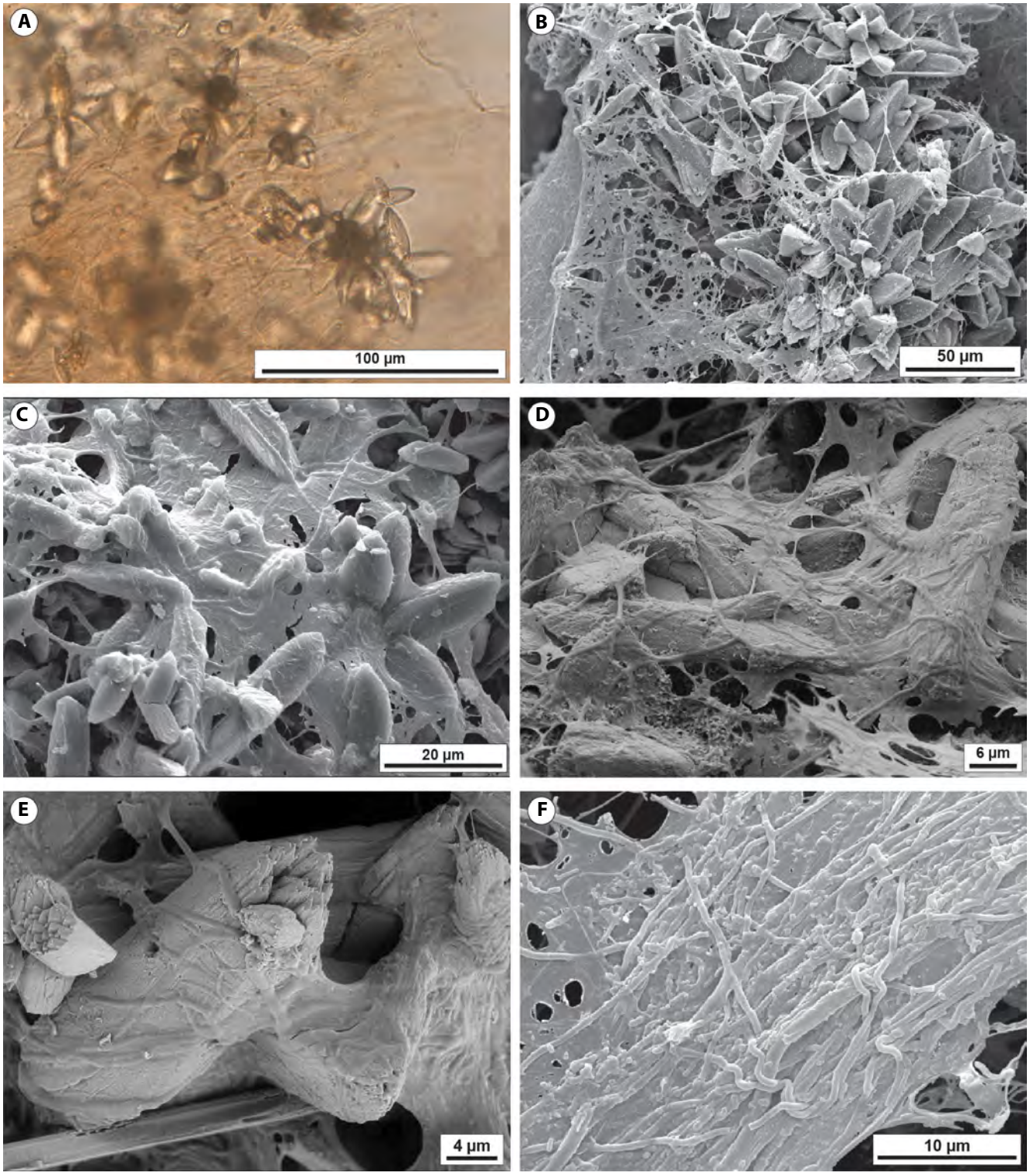

FIGURE 4 Petrographic and SEM images of the Bullicame travertines in the proximal channel centre (from 12.5 m to 55.5 or 60 m from vent). (A) Rosettes consist of euhedral spindle-shaped calcite crystals radially departing from a central micrite nucleus embedded within the filamentous microbes and EPS (sample BUL-A-9; 21.5 m from vent). (B) SEM image showing rosettes of euhedral prismatic calcite crystals embedded in EPS with filamentous microbes (sample BUL-A-18; 30.5 m from vent). (C) SEM image of calcite crystal rosettes embedded within EPS including filamentous microbes (sample BUL-A-9; 21.5 m from vent). (D) Spindle-shaped prismatic calcite crystals within EPS and filamentous microbes using SEM (sample BUL-A-9; 21.5 m from vent). (E) SEM close-up view of prismatic calcite crystals embedded in EPS and filamentous microbes. At the bottom a calcium-phosphate crystal (sample BUL-A-9; 21.5 m from vent). (F) SEM image of microbial mat in the proximal channel consisting of bundles of filamentous microbes. EPS include also rod-shaped microbes (upper left corner) (sample BUL-A-18; 30.5 m from vent)

an average of 50–200 μm and the micrite nuclei reach a diameter of 50–150 μm around 30.5 m from the vent (Figure 3F). Patches of clotted peloidal micrite, with 10–20 μm wide peloids, are embedded in microsparite mosaics (Figure 3F). The EPS and some filaments appear birefringent in crossed polarizers and are enriched in silicon, aluminium, calcium, magnesium, sodium and potassium or calcium and sulphur measured via EDX (Figures S12 and S13). Rare calcium-phosphate crystals (200–300 μm in size) and gypsum crystals are present.

At the proximal channel margin, flat horizontal millimetre-thick carbonate crusts consist of laminae (20–100 μm thick; Figure 5A) made of rosettes (Figure 5B,C) of radially oriented prismatic spindle-shaped crystals (10–50 μm long, 5–20 μm wide) precipitated within EPS, embedding prevalent filamentous, spiral-shaped and rare rod-shaped microbes (Figure 5D through F). Hollow spheres (10–20 μm in diameter) made of fibrous aragonite crystals precede calcite precipitation (Figure 5D). Calcite crystals are coated by granular mucilaginous substances, probably EPS, enriched in silicon and aluminium or phosphorous (Figure 5F) and show tubular perforations from which filamentous microbes emerge (Figure 5D,F).

In the distal channel, >60 m from the vent, precipitated carbonate crusts show abundant coated gas bubbles (Figure 2F), similar to the proximal channel margins, and consist of micrite clots and microsparite mosaics (Figure 6A). At the microscale, calcite crystals are similar to the proximal channel part in terms of shape, size and organisation in radial rosettes (50–300 μm in diameter), often with micrite nuclei (Figure 6A,B). Spindle-crystal rosettes precipitate within EPS embedding filamentous microbes (Figure 6B), which are spiral-shaped or segmented associated with rare coccoid or rod-shaped forms (Figure 6D,E). Calcium-phosphate crystals are draped by filamentous microbes and EPS (Figure 6F; Figure S14).

4.1.2 | Bollore

The Bollore travertine mound consists of a main hydrothermal vent at the centre top of the mound, from which thermal water outflows along a channel, and a second vent in a lower topographic position, at the base of the mound flank (Figure 7; Figure S3). Information about the travertine deposits, measured thermal water parameters and characteristics of the microbial mats is summarised in Table 2 and Supporting Information.

The main vent travertines show bundles (50–500 μm wide) of organic filaments acting as substrates for carbonate precipitation of microsparite/fine sparite and clotted peloidal micrite (Figure 8A,B). Calcite crystals are prismatic euhedral (20–100 μm long, mostly 50–60 μm, 5–20 μm wide) and organised in radial rosettes (50–300 μm in diameter; Figure 8C), in some cases with micrite nuclei (20–150 μm wide) or coating micritic filament, 20 μm wide (Figure 8B). Clotted peloidal micrite occurs in patches (200–300 μm in diameter) embedded in microsparite mosaics (Figure 8B). Calcite crystals are embedded in EPS with filamentous microbes (diameters 0.2–1 μm), some spiral-shaped, associated with 1–2 μm size, rod-shaped microbes (Figure 8D,E; Figure S4). Calcite crystals show square-shaped moulds (Figure 8C) and are coated by EPS, enriched in aluminium, silicon, sulphur, calcium and potassium. Samples proximal to the vent contain fibrous aragonite spherulites, up to 10–200 μm in diameter (Figure 8D,F), precipitated both before and after the adjacent calcite crystals. Calcium-phosphate and euhedral crystals of gypsum, also forming rosettes up to 200 μm in diameter, post-date calcite and aragonite spherulite precipitation (Figure 8F; Figure S11, S15).

At the second Bollore vent, carbonate precipitates are similar: prismatic microsparite/sparite calcite crystals (5–40 μm wide, 30–120 μm long) form rosettes dispersed in EPS associated with fibrous aragonite spherulites and fans, 20–200 μm in size (Figure 9A,B). Filamentous microbes (0.1–1 μm in cross-section), rarely spiral-shaped, are associated with sparse rod-shaped (Figure 9C,D) and coccoid microbes, around 1 μm in size. In the channel 2 m from the vent, spiral-shaped filamentous microbes become common. Aggregates of minerals, with a chemical composition including silicon, aluminium, magnesium and calcium, show a reticulate fabric and might represent authigenic aluminium-silicate minerals (Figure 9C). They occur on the filamentous microbe bundles and calcite crystals (Figure 9C,E,F).

In the proximal channel, within 10 m from the main vent, there are centimetre-size fan-shaped bundles of filamentous microbial mat encrusted by euhedral prismatic calcite crystals (15–80 μm long, 5–30 μm wide but also 5–2 μm in size), sometimes with gothic-arch shape, organised in rosettes with a micrite clot at the nucleus or aligned along micritic filamentous structures (Figure 10A through C). Carbonate precipitates are similar to those at the vent pools with abundant fibrous aragonite spherulites (from 30 to 100 μm to millimetres in diameter), lining the precipitated calcite (Figure 10D). Gypsum crystals (50–80 μm long) form rosettes 100–200 μm in diameter (Figure 10E). Calcium-phosphate post-dates calcite precipitation. All the precipitated crystals are surrounded by EPS and filamentous and rod-shaped microbes (Figure 10C,E,F).

In the distal channel, from 10 to 28 m from the vent (Figure 7), aragonite, gypsum or calcium-phosphate crystals are lacking and precipitated carbonates are dominated by calcite micrite and microsparite crystals (4–20 μm in size, mostly 4–10 μm) forming rosettes 10–50 μm in size (Figure 11A through D). Filamentous microbes, largely spiral-shaped, are abundant (Figure 11E,F; Figure S4).

4.1.3 | Gorello Waterfall

The Gorello Waterfall travertine deposits form a nearly 20 m long terraced slope apron with metre-scale pools at the base of a waterfall at a distance from the vent of approximately 1,170 m (Figure 12; Figure S5). Information about travertine deposits, measured thermal water parameters and characteristics of the microbial mat is summarised in Table 3 and Supporting Information. Travertine laminated boundstone from the pool rims and walls (Figure 12B through D) displays a 0.5–1.5 mm thick superficial microbial mat with only sparse carbonate precipitates, overlying centimetre-thick alternations of carbonate precipitated laminae and organic matter (Figure 13A through C; Figure S6). The microbial mat consists of a network of undulated filamentous microorganisms, oriented mostly upright, perpendicular to the lamination, or prostrated horizontally. Carbonate precipitates form subparallel undulated laminae or a reticulate framework mimicking the spatial distribution and alveolar structure of EPS and filamentous microbes (Figure 13C,D; Supporting Information S6). Pore spaces of the microbial mat framework lack carbonate precipitates, which appear to occur only embedded in EPS following the orientation of filamentous microbes (Figure 13D,E). Carbonate precipitates consist of clotted peloidal micrite and euhedral microsparite to fine sparite crystals (5–100 μm in size; Figures 13E,F and 14A,B). Micrite occurs also as nanometre-scale particles forming aggregates or encrusting filamentous microbes forming tubular envelopes (Figure 14C,D). Microsparite to fine sparite crystals are prismatic to sub-equant with a rhombohedral or trigonal cross-section or dodecahedral shape, often organised in rosettes, with a diameter of 10–200 μm (Figures 13E,F and 14A,B,E,F), and nuclei of peloids and organic matter (5–20 μm in diameter). Rosettes can occur embedded in clotted peloidal micrite or surrounded by erect filamentous microbes and embedded in EPS (Figures 13E and 14A,B,E,F). Filamentous microbes can depart radially from the calcite rosettes (Figure 14A) and emerge from hollows within the crystals as they were entombed during crystal growth (Figure 14B). Filamentous microbes with a diameter of 1 μm are dominant, associated with larger segmented filamentous forms (4–5 μm in diameter) with an outer sheath (Figure 14D; Figure S7), spiral-shaped, segmented and chain-like filamentous microbes (Figure 15A through E), rod-shaped microbes (Figure 15F) and pennate diatoms. Other authigenic minerals observed are calcium-phosphate (Figure 16A; Figure S16), gypsum, framboidal pyrite and aluminium-silicate minerals. These authigenic aluminium-silicates (Figure 16B through D) occur as aggregates among the calcite crystals and as coatings of EPS and filamentous microbes that appear birefringent in crossed polarizers (Figure 16E) and show, as EPS, a chemical composition enriched in silicon, aluminium, potassium, calcium, magnesium, iron or sulphur and calcium (Figures S17 and S18).

The nuclei of oncoids (Figures 12E,F and 16F; Figures S5 and S8) are detrital grains (travertine intraclasts, clasts of substrate rocks, plant stem fragments). The cortex varies from predominantly micritic laminae to an alternation of micrite (4–50 μm thick) and microsparite/sparite (10–200 μm thick) laminae with crystals from equant to bladed, oriented perpendicular to the underlying micritic lamina, forming palisades or crystalline fans adjacent to each other. The micritic laminae can be discontinuous and develop millimetre-size columnar structures. The outer rim of the oncoids and some internal laminae are rich in EPS and filamentous microbes (Figure S8).

4.2 | Travertine stable oxygen and carbon isotopes

The oxygen and carbon stable isotope measurements of the three investigated travertine sites are plotted in Figure 17 and summarised in Table S1. The three travertine sites plot in distinct fields of the $\delta^{13}C$-$\delta^{18}O$ diagram with some overlap between Bullicame and Bollore. All three data sets show a linear positive correlation between $\delta^{13}C$ and $\delta^{18}O$ values (Table S1). Bullicame travertine fabrics are characterised by the highest $\delta^{13}C$ values for the rafts and coated bubbles and coated reeds (average $\delta^{13}C$ 7.3 and 6.7‰, respectively; average $\delta^{18}O$ −9.4‰ for both); the streamer fabric shows lower values of $\delta^{13}C$ (average 5.4‰) and $\delta^{18}O$ (average −11.8‰). The Bollore travertine deposits show carbon and oxygen isotope values lower than Bullicame but the stable isotope signatures partly overlap. Rafts, coated bubbles and dendrites are characterised by higher values of $\delta^{13}C$ and $\delta^{18}O$ (average $\delta^{13}C$ 5.3 and 5.4‰, average $\delta^{18}O$ −12.0‰ and −12.4‰, respectively) with respect to the streamer fabrics (average $\delta^{13}C$ 4.5‰; $\delta^{18}O$ −12.6‰) as observed in Bullicame. The Gorello Waterfall travertines have an isotopic signature characterised by uniform $\delta^{18}O$ values, around −8.5‰, and $\delta^{13}C$ values ranging from 2.2 to 3.5‰.

4.3 | Microbial communities at Bagni San Filippo travertine

At the Bagni San Filippo, Fosso Bianco and Balena Bianca localities, travertine and microbial mat samples were collected on the floor of a creek with flowing thermal water and on the walls of travertine cascades and terraces (Figure S9). Temperatures of the sampling sites varied between 45.8 and 29.0°C; pH varied between 6.4 and 7.7 (Table 4). Samples I4.5 and I4.6 correspond to sites where thermal water mixes with freshwater from

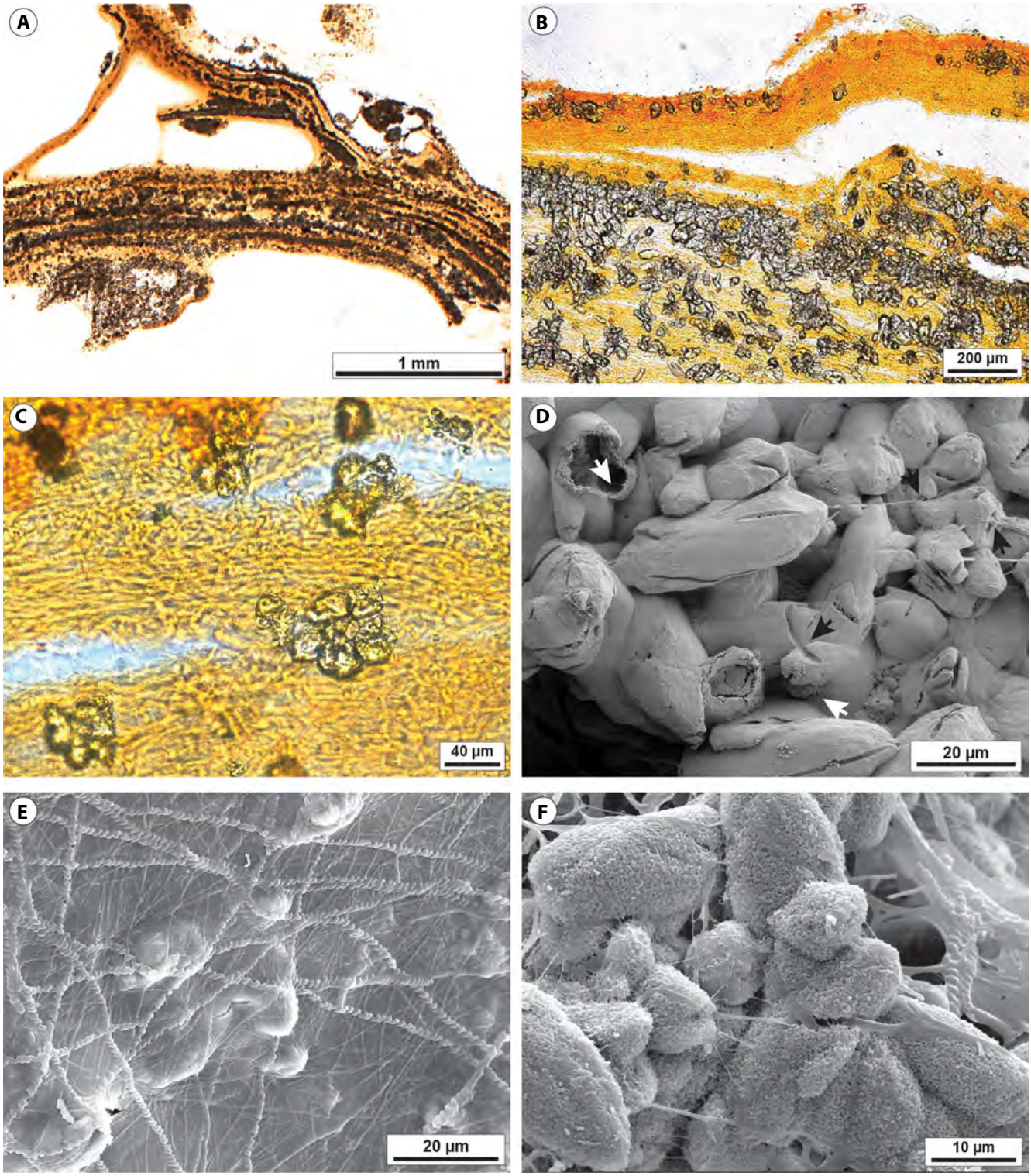

FIGURE 5 Petrographic and SEM images of Bullicame travertine samples from the margin of the proximal channel at 21.5 m from the vent (sample BUL-A-9R channel rim). (A) Tetracycline-stained channel margin crust showing calcite rosettes forming laminae within the microbial mat following the framework structure of the organic substrate. (B) Calcein-stained sample with calcite crystal rosettes precipitated within EPS, spatially distributed following the framework of the organic substrate. (C) Close-up view of calcite crystal rosettes surrounded by EPS and filamentous microbes. (D) SEM image of spindle-shaped microsparite crystals showing tubular perforations probably related to moulds of filamentous microbes entombed during crystal growth with organic filaments emerging from the tubular hollows (black arrows). The image shows also fibrous aragonite hollow spheres (white arrows). (E) SEM image of EPS surrounding the calcite crystals embedding *Spirulina* cyanobacteria and other filamentous microbes. (F) SEM image showing prismatic calcite crystals surrounded by EPS with filamentous microbes, also spiral-shaped, emerging from the crystal as they had been entombed

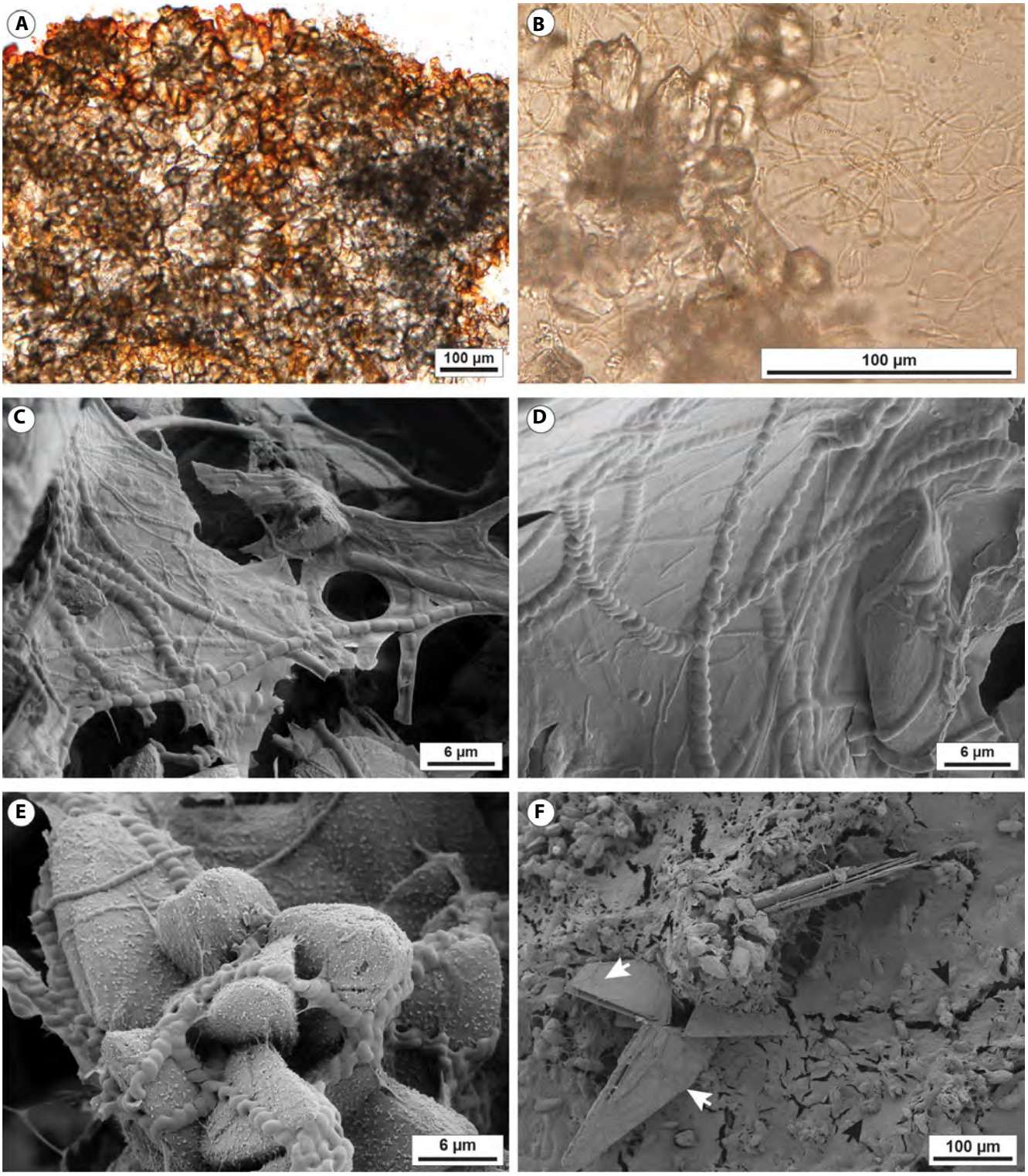

FIGURE 6 Petrographic and SEM images of Bullicame travertine samples from the distal channel from 60 to 83.5 m from the vent (sample BUL-B-12; 60.5 m from vent). (A) Photomicrograph of calcein-stained sample showing the microsparite/sparite mosaic formed by aggregated calcite crystal rosettes and areas with clotted micrite. (B) Close-up view of microsparite crystal rosettes with a micrite nucleus surrounded by EPS embedding filamentous microbes including *Spirulina* cyanobacteria. (C) SEM image of EPS embedding spiral-shaped *Spirulina* and segmented filamentous microbes. (D) SEM image of EPS embedding various filamentous and coccoid microbes and prismatic calcite crystals. (E) SEM image of calcite crystals draped by *Spirulina* cyanobacteria and other filamentous microbes and by a granular mucilaginous organic material. (F) SEM image showing EPS embedding calcite crystals (black arrows) and calcium-phosphate crystals coated by filamentous microbes (white arrows)

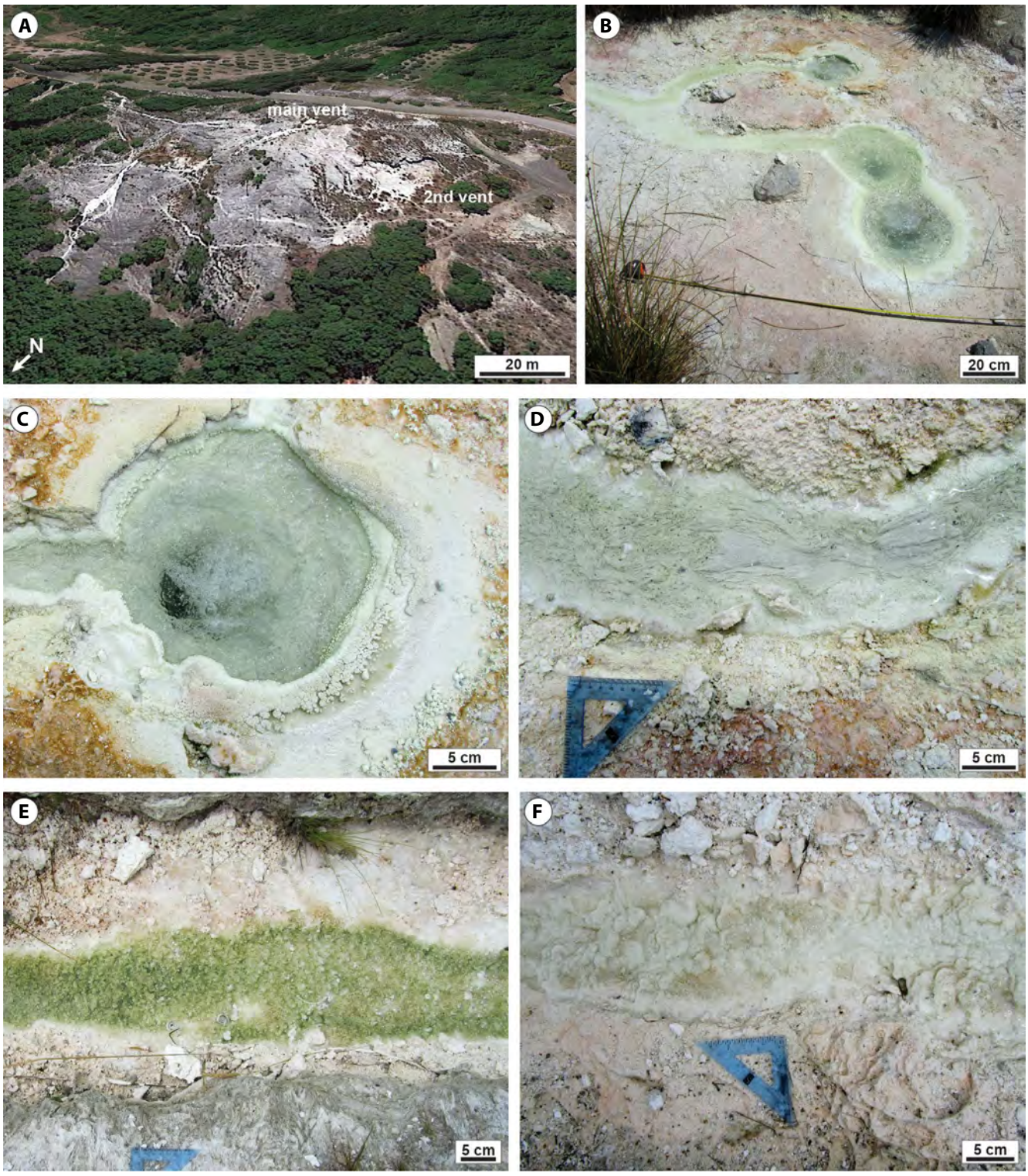

FIGURE 7 Bollore (Bagni San Filippo) active hydrothermal travertine system. (A) Google Earth Pro image showing the Bollore mound and the location of the main vent at the mound top and the second vent at the flank base. (B) Main vent with three orifices and the channel departing on the left side. (C) Close-up view of one of the vent orifices with white carbonate precipitates along the rims and pink to orange microbial mat. (D) Proximal channel 1 m from the vent with white bundles of carbonate-encrusted filaments oriented following the water flow direction (streamers) and margins with pink microbial mat. (E) Distal channel, 10 m from the vent, with the channel floor draped by green microbial mat, light pink margins and with abundant carbonate-coated gas bubbles. The fossil channel margins (lower part of image) consist of lithified bacteria streamer fans. (F) Channel 20 m from the vent where the increase in topographic gradient induces the formation of centimetre-size terraces

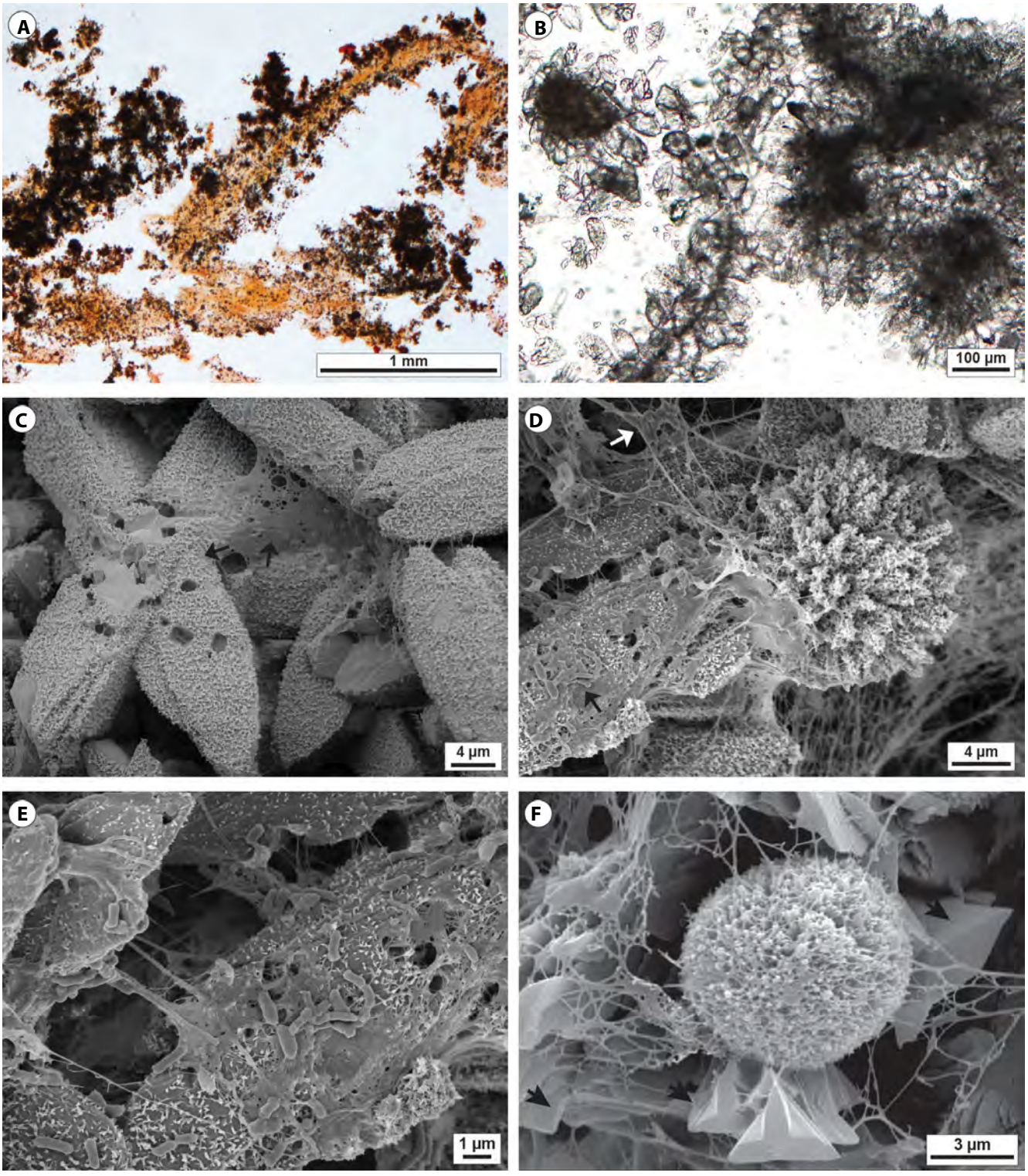

FIGURE 8 Petrographic and SEM images of the Bollore (Bagni San Filippo) travertines at the main vent (sample BF 0.6B). (A) Photomicrograph of sample stained with calcein showing carbonate precipitates draping and embedded within orange colour microbial mat filamentous bundles. (B) Photomicrograph showing the euhedral prismatic microsparite/fine sparite calcite crystals forming radial rosettes with a central micrite nucleus or around elongated micrite filaments. (C) SEM image showing the radial arrangement of the prismatic calcite crystals with squared moulds, coated by EPS (black arrows). (D) SEM image of aragonitic spherulites and calcite crystals embedded in EPS with rod-shaped microbes (black and white arrows). (E) Calcite crystals embedded in EPS and overlain by rod-shaped microbes. (F) SEM image of fibrous aragonite spherulites surrounded by gypsum crystals (black arrows) all draped by EPS

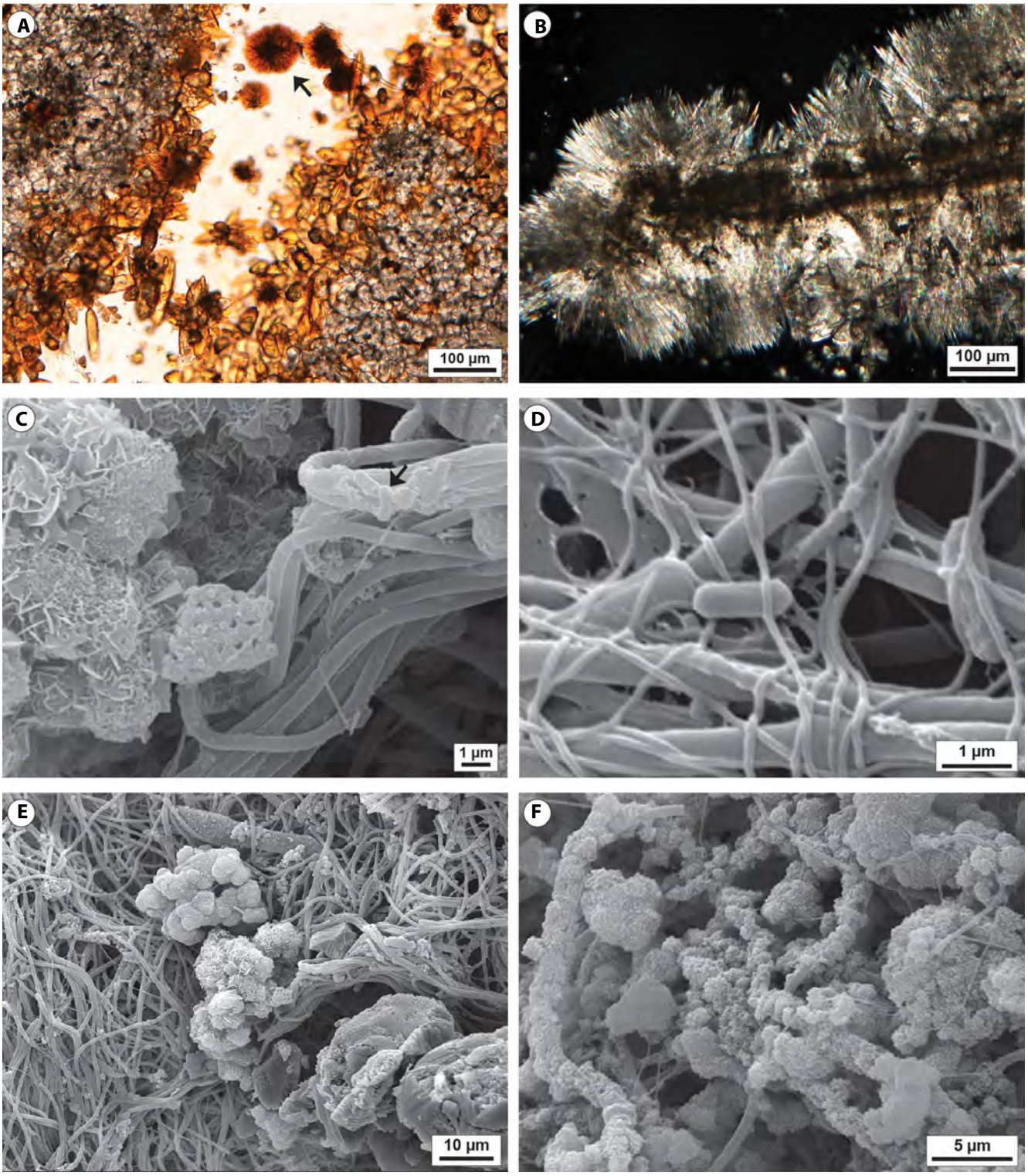

FIGURE 9 Petrographic and SEM images of the Bollore (Bagni San Filippo) travertines at the second vent (samples BF2-0, BF2-2). (A) A mosaic of microsparite/fine sparite crystals forming rosettes or irregular aggregates around micrite clots and aragonite spherulites (black arrow) stained orange by calcein dye reacting with calcium-binding organic matter. (B) Crossed-polarizers image of micritic and microsparitic laminae surrounded by fibrous aragonite crystal fans. (C) SEM image of bundles of filamentous microbes associated with rod-shaped microbes (black arrow). On the left side a reticulate aggregate of authigenic aluminium-silicate mineral, forming on filamentous microbes. (D) SEM image showing entangled filamentous microbes of different diameter in cross-section and rod-shaped microbes. (E) Bundles of filamentous microbes overlain by aggregates of possible authigenic aluminium-silicate mineral. (F) Close-up view of previous image showing the filamentous microbes coated by authigenic aluminium-silicate

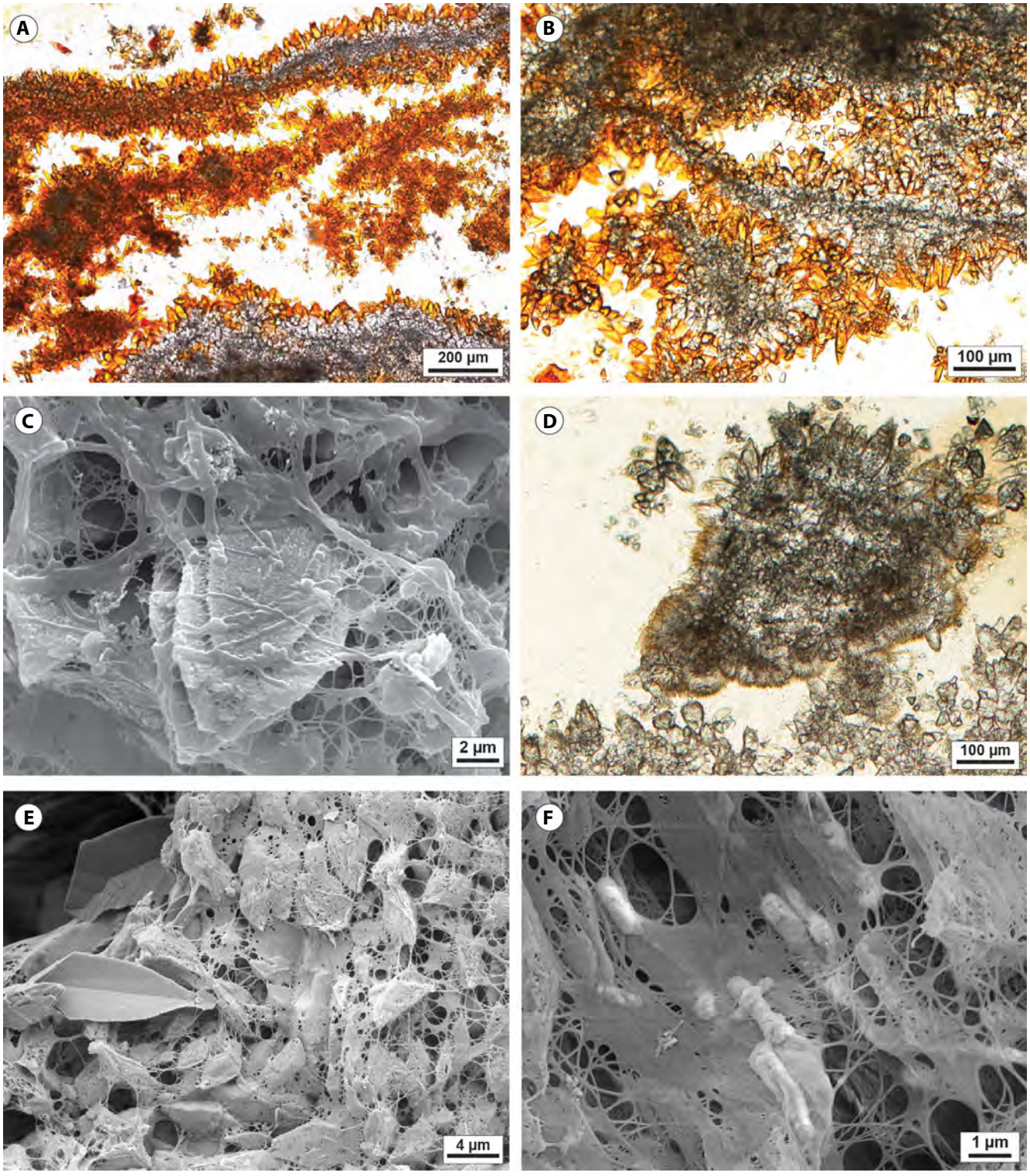

FIGURE 10 Petrographic and SEM images of the Bollore (Bagni San Filippo) travertines at the proximal channel (within 10 m from the main vent; sample BF 1.3, 0.8 m from vent). (A) Carbonate-encrusted bundles of filamentous microbes are characterised by microsparite to fine sparite euhedral crystals coating micrite filaments and peloids. (B) Micrite filaments and clots surrounded by microsparite to fine sparite crystals departing radially from the micritic substrate. Crystals are stained by orange calcein dye as they were coated by organic matter. (C) SEM image of prismatic calcite crystals with gothic-arch shape surrounded by EPS embedding filamentous and rod-shaped microbes. (D) Calcite microsparite and micrite aggregates coated by fibrous aragonite crystal fans. (E) SEM image of EPS embedding micrite calcite crystals and swallow-tail gypsum crystals on the left side. (F) SEM image of EPS embedding rod-shaped microbes

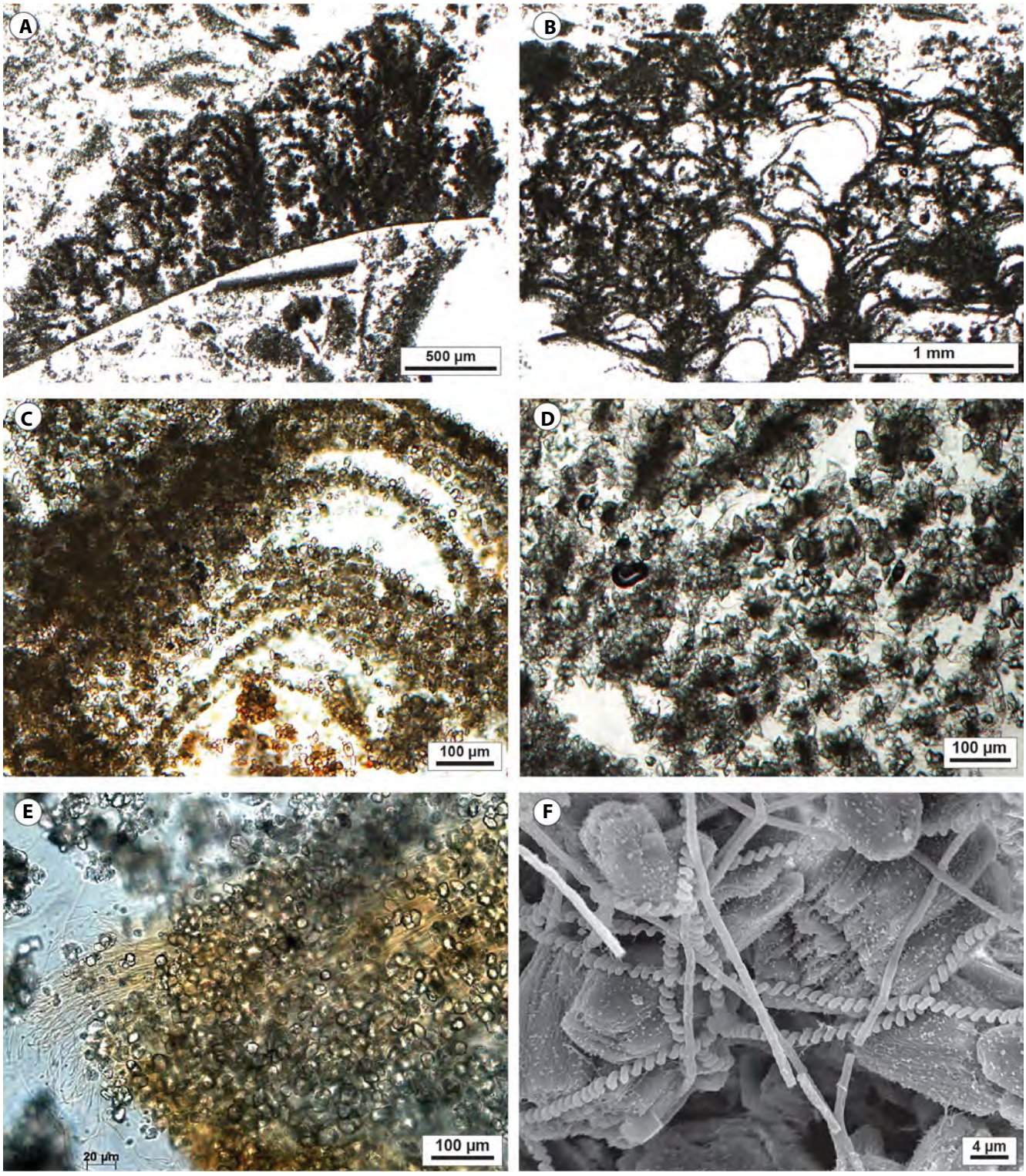

FIGURE 11 Petrographic and SEM images of the Bollore (Bagni San Filippo) travertines at the distal channel (10–28 m from vent; sample BF 14, 14 m from vent). (A) Distal channel carbonate precipitates are characterised by abundant clotted peloidal micrite forming dendritic structures, rafts and coated gas bubbles. (B) Photomicrograph of distal channel coated bubble boundstone made of clotted peloidal micrite. (C) Laminae made of microsparite and micrite supported by EPS and filamentous microbes. (D) Photomicrograph of a framework of aligned calcite crystal rosettes with micrite nuclei; rosettes are embedded in organic matter that must sustain the crystal framework. (E) Microsparite crystals embedded in EPS and filamentous microbes. (F) SEM image of calcite prismatic crystals overlain by filamentous microbes including spiral-shaped *Spirulina* cyanobacteria

FIGURE 12 Gorello Waterfall (Saturnia) active hydrothermal travertine system. (A) Google Earth Pro image of the Gorello Waterfall showing the channel running southward from the thermal spa, the waterfall developing at the break in slope where in the past there was a windmill, the terraced slope and the river to the south. (B) Terraced slope with metre-size pools rimmed by rounded margins with vertical decimetres high walls. (C) The pool rims are coated by an olive green microbial mat. (D) The pool vertical walls are coated by white to dark green filamentous microbial mat. (E) The pool floors include detrital mud and sand, microbial mat and centimetre-size carbonate coated grains (oncoids). (F) Close-up view of the oncoids with the pitted outer surface with green microbial mat (black arrows). On the upper right corner plant fragments are coated by carbonate (white arrow)

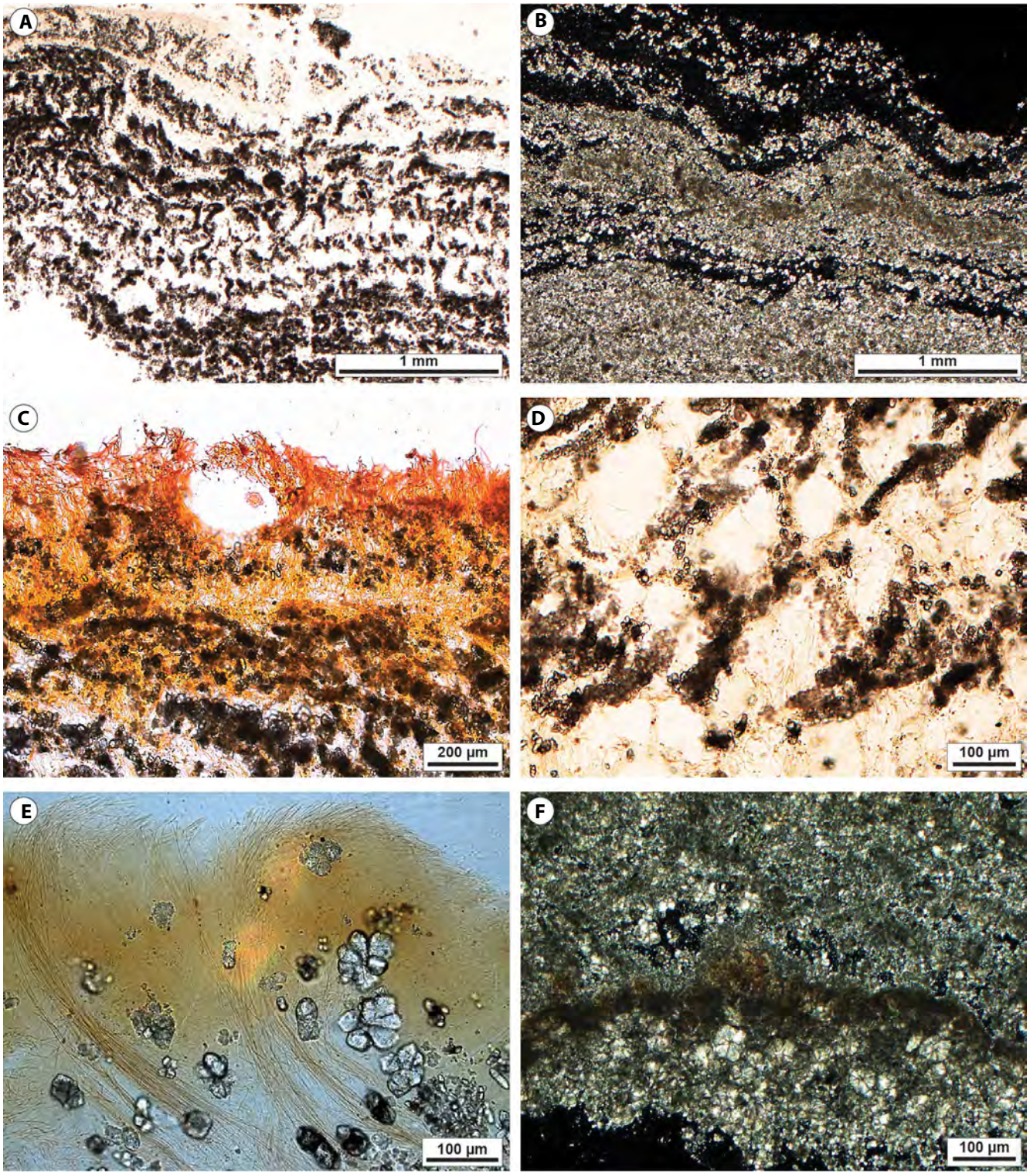

FIGURE 13 Petrographic analysis of the Gorello Waterfall (Saturnia) travertine from the rims and walls of the pools (5–10 m from waterfall, samples Gor 8, Gor 12). (A) Travertine laminated boundstone made of laminae of clotted peloidal micrite and microsparite rosettes alternating with EPS and filamentous microbes. (B) Image in crossed-polarizers of undulated laminated boundstone made of clotted micrite and microsparite rosettes. Carbonate precipitates follow the structure of the organic substrate. (C) Calcein-stained sample showing the outer surface of the laminated boundstone with upright filamentous microbes and clots of micrite/microsparite distributed within the EPS and between erect filamentous microbes. (D) Alveolar framework of microbial filaments and EPS within which calcite crystal rosettes and micrite clots precipitate mimicking the EPS structure. (E) Outer portion of the laminated boundstone with microsparite rosettes embedded between the upright filamentous microbes. (F) Image in crossed-polarizers of a framework of microsparite rosettes and patches and laminae of clotted peloidal micrite

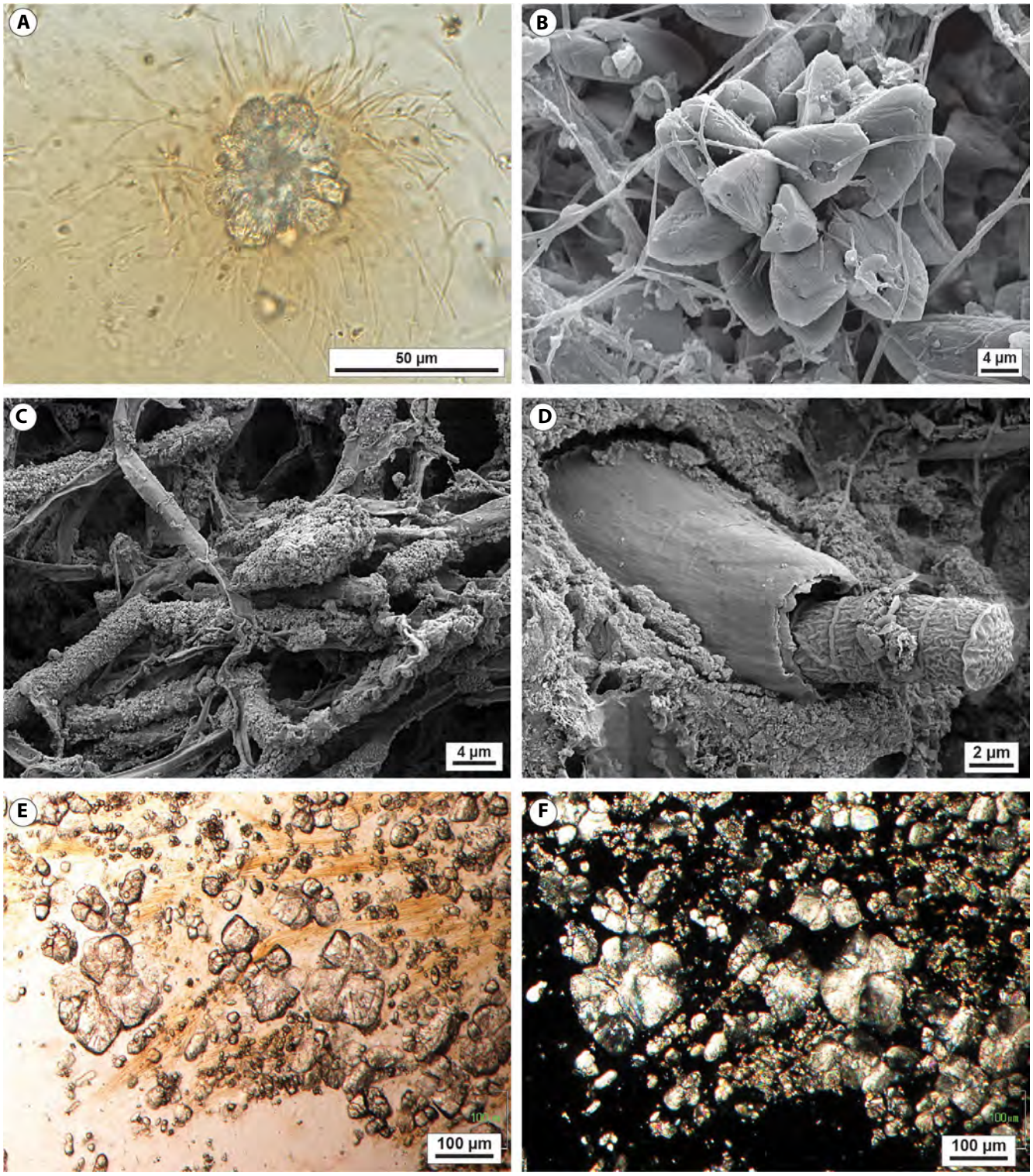

FIGURE 14 Petrographic and SEM images of the Gorello Waterfall (Saturnia) travertines from the rims and walls of the pool of the terraced slope system (5–10 m from waterfall, samples Gor 5, Gor 6, Gor 12). (A) Microsparite rosette with filamentous microbes departing from the radial crystalline structure. (B) SEM image of prismatic calcite crystals radially arranged in a rosette. Filamentous microbes emerge from tubular moulds within the crystals as they were entombed during crystal growth. (C) SEM image of filamentous microbes encrusted by nanometre-scale micrite. (D) Large, segmented cyanobacteria with a thick sheath probably belonging to *Calothrix thermalis* emerging out of a micritic lamina. (E) Microsparite to sparite rosettes floating within filamentous microbes. (F) Crossed-polarizers image of microsparite/sparite rosettes showing the undulose extinction of the fan-shaped calcite crystals

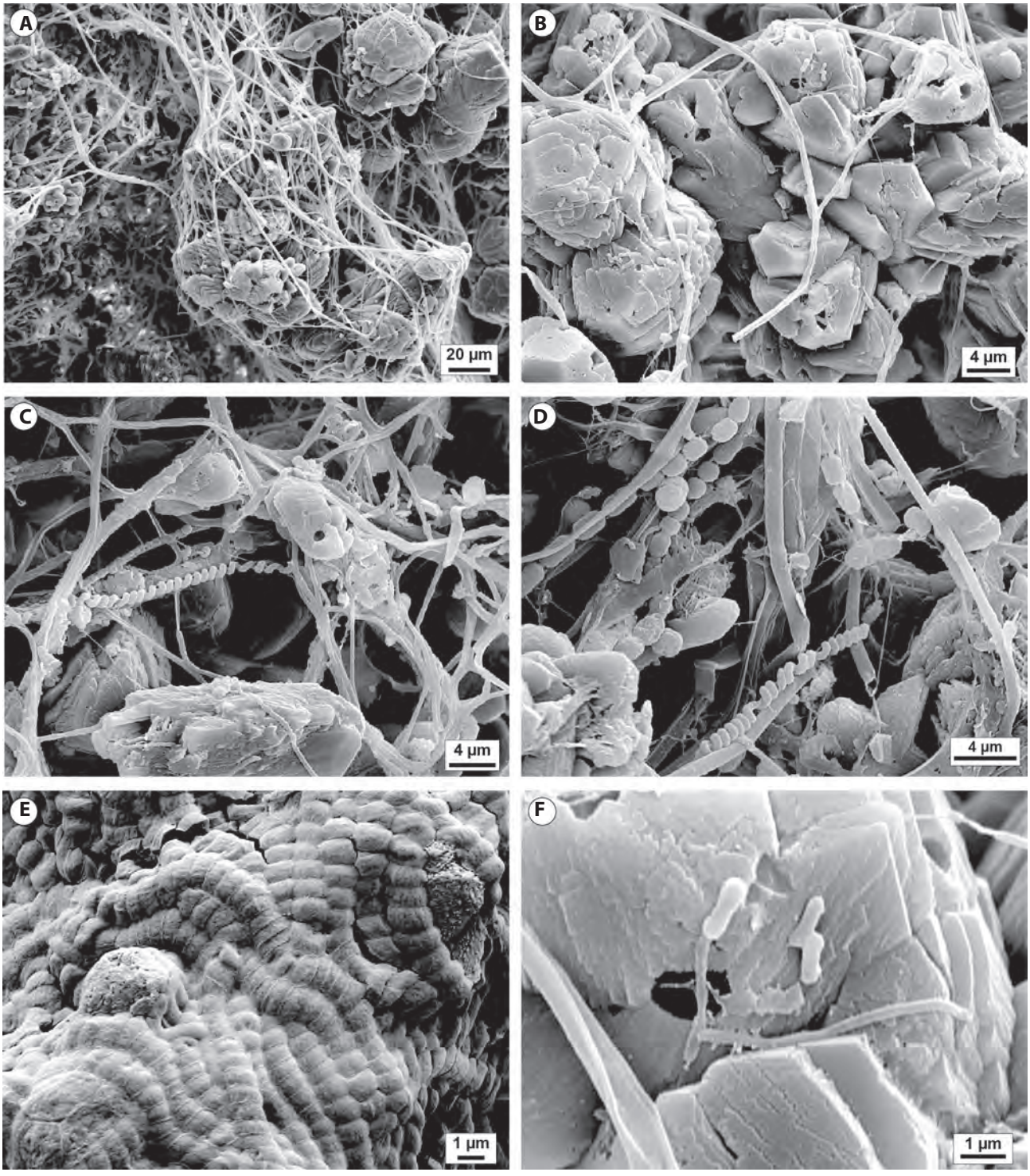

FIGURE 15 Petrographic and SEM images of the Gorello Waterfall (Saturnia) travertines from the rims and walls of the pools of the terraced slope system (5–10 m from waterfall, samples Gor 6, Gor 8, Gor 12). (A) SEM image showing dodecahedral calcite crystals forming aggregates and rosettes surrounded by filamentous microbes. (B) Dodecahedral calcite crystals with tubular moulds related to the entrapped filamentous microbes and rod-shaped microbes. (C) SEM image showing calcite crystals surrounded by filamentous cyanobacteria including *Spirulina*. (D) SEM image showing a diverse community of filamentous microbes including spiral-shaped, segmented and chain-like forms, probably cyanobacteria. (E) Segmented filamentous microbes probably belonging to *Phormidium* or *Oscillatoria* cyanobacteria. (F) Close-up view of rod-shaped microbes with a dumbbell shape

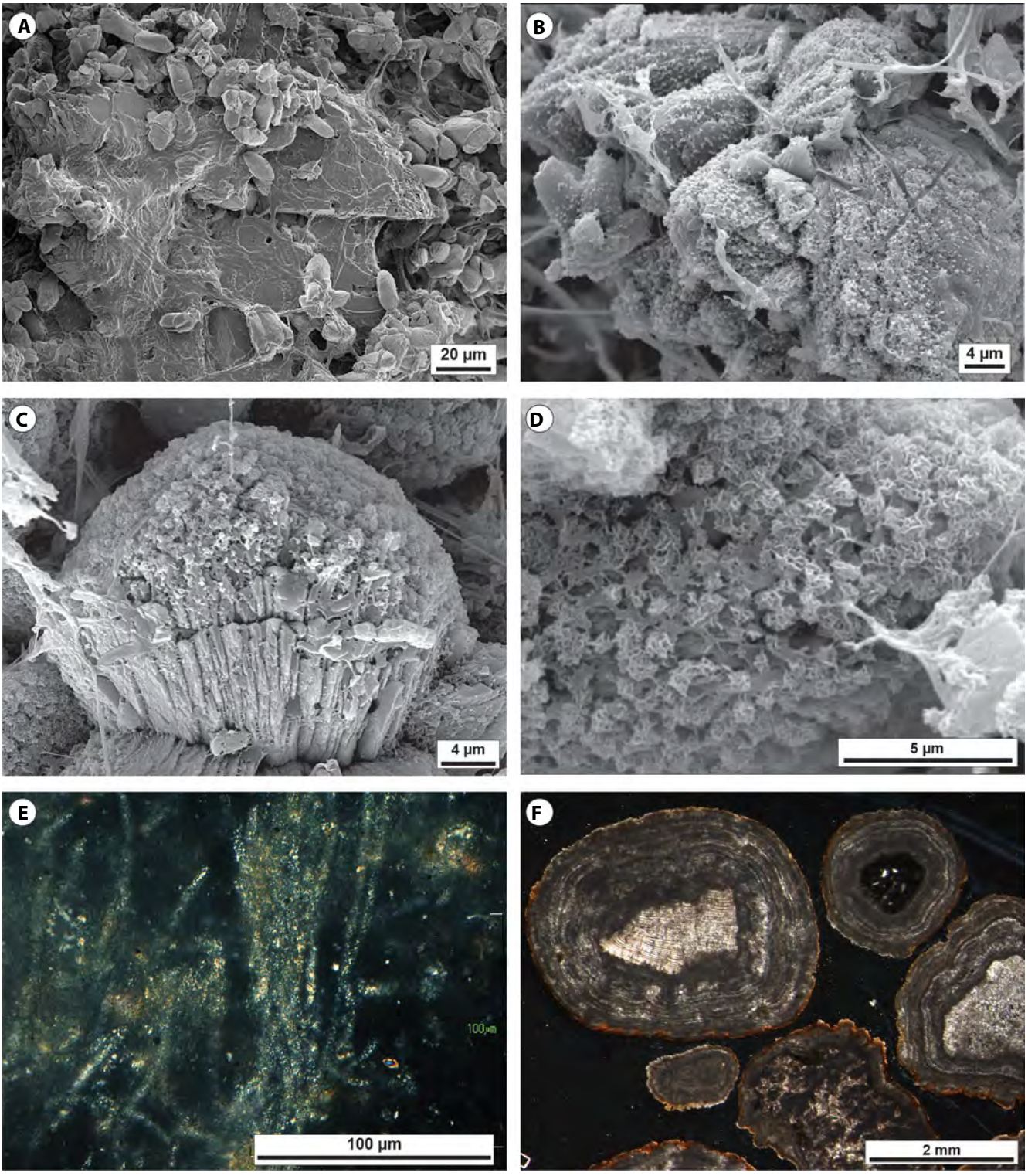

FIGURE 16 Petrographic and SEM images of the Gorello Waterfall (Saturnia) travertines from the rims and walls and pool floor of the terraced slope system (5–10 m from waterfall, samples Gor 6, Gor 8, Gor 12). (A) SEM image showing calcium-phosphate crystals coated by microsparite crystals, EPS and filamentous microbes with *Spirulina*. (B) SEM image of calcite crystals coated by mucilaginous organic matter, probably EPS, with tubular moulds related to the entombed filamentous microbes. (C) Bladed calcite crystals covered by aluminium-silicate minerals. (D) Close-up view of authigenic aluminium-silicate mineral forming on calcite. (E) Crossed-polarizers image of large filamentous microbes probably belonging to the cyanobacteria *Calothrix* that show a birefringent internal filling material that could be an authigenic aluminium-silicate. (F) Crossed-polarizers image of pool floor oncoids with nuclei made of detrital intraclasts or substrate rock extraclasts and cortex consisting of an alternation of micrite and microsparite laminae

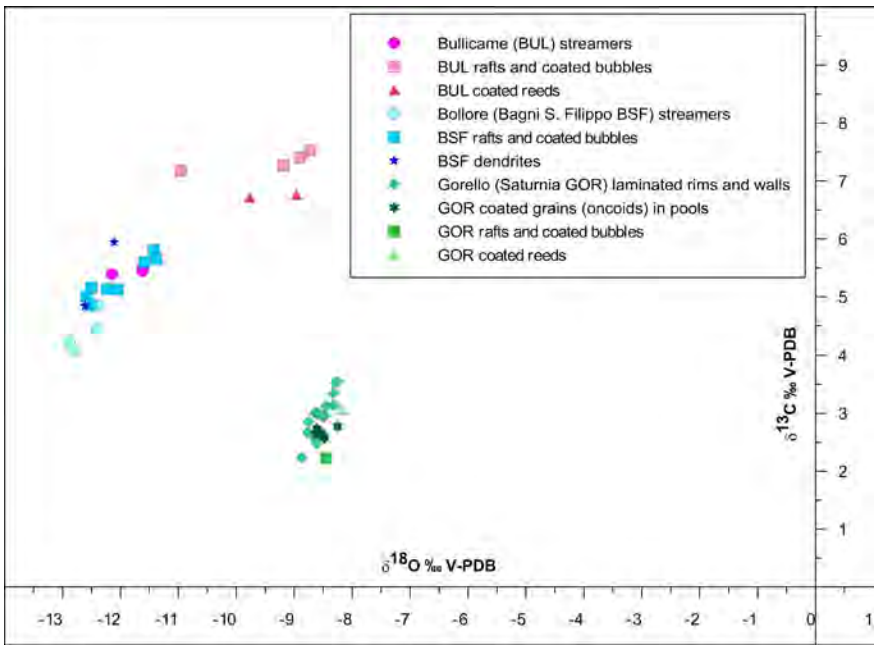

FIGURE 17 Plot of the carbon and oxygen stable isotope measurements of the three analysed case studies

a stream. Samples I4.7-I4.9 are at the base of the Balena Bianca cascade sourced by the discharge from the thermal spa.

Light microscopy on samples from the highest temperature site (45.8–44.8°C, pH 6.4, Table 4) consisting of whitish to pale yellow/greenish streamers on the creek floor revealed the presence of mostly filamentous bacterial morphotypes (mainly Cyanobacteria and Chloroflexi, Figure S10A,C,D), in many cases with loosely attached calcite crystals (Figure S10 B,D through G). In one sample at 41.1°C and pH 6.3 (I4.5), brownish iron oxide-rich precipitates occurred (Figure S10H).

After sequencing and processing, ASVs related to taxa of Bacteria and Eukarya were retrieved (Figures 18 and 19). In some cases, the genus level could be resolved, whereas in other cases only the identifications of higher taxonomic ranks were achieved.

The higher temperature samples (from I4.1 to I4.4; 45.8–44.8°C) from the whitish to pale yellow zone (I4.3; Figure S9C,D) in the centre of the creek floor are dominated by Chloroflexi (Anaerolineaceae, Chloroflexaceae *Oscillochloris*), Desertifilaceae and *Spirulina* Cyanobacteria, Spirochaeta, the Bacteroidetes/Chlorobi *Chlorobaculum* and *Thiofaba* (Figure 18). The greenish zone at the margin of the thermal water creek shows increased abundances in *Spirulina* and *Phormidium* (*Ph.* ETS-05-related) cyanobacteria, *Thiofaba* and slightly less Chloroflexi (Anaerolineaceae). Among eukaryotic organisms (Figure 19), the most abundant in the whitish creek floor centre are: nematodes *Labronema* and *Chronogaster*, amoeba *Hartmannella*, and rotifer (*Brachionus*). Along the margins of the creek, besides *Labronema*, another nematode (*Mesodorylaimus*) becomes more abundant, the annelid *Pristina* and the gastrotrich *Chaetonotus* occur in one sample and diatoms (*Navicula*) increase in abundance. The ciliate *Oxytricha* is particularly abundant in sample I4.1.

The lower temperature samples (from I4.5 to I4.9; 41.1–29°C) show distinct microbial communities. Sample I4.5 (temperature 41.1°C, pH 6.3), a brownish mat formed by iron oxide-hydroxide precipitates (Figure S9E), differs from the other samples due to peak abundances of Patescibacteria, *Nitrospira*, *Streptomyces* and *Sulfuritalea* (Figure 18). The iron oxidizing environment is reflected by the presence of Gallionellaceae ASVs. Some of the abundant bacteria at higher temperature (*Thiofaba*, *Spirulina*) are missing. In the other three samples with temperatures moderately above ambient temperature (*ca* 29–30°C, pH 7.7), the Chloroflexi (Anaerolineaceae), being highly abundant in the higher temperature sites, are much less common (less than 10% of all retrieved sequences). The cyanobacteria *Spirulina*, *Tychonema*, and *Pseudanabaena* or unclassified cyanobacteria may become abundant, but *Phormidium* ETS-05-related OTUs decrease. Proteobacterial Thiotrichaceae as well as two groups of Chloroflexi increase. Among the Eukarya (Figure 19), the nematode *Labronema* is absent in samples at around 30°C water temperature; among diatoms, several groups increase (*Pauliella*) or decrease (*Navicula cryptocephala*) gradually.

5 | INTERPRETATION AND DISCUSSION

The three investigated travertine sites are characterised by thermal water with distinct physico-chemical properties but supersaturated with respect to carbonate minerals (Tables 1 through 3; Minissale, 2004; Pentecost, 1995a) and different microbial mat compositions associated with similar microscale carbonate precipitates. The macroscale travertine facies vary according to local water temperature, flow velocity,

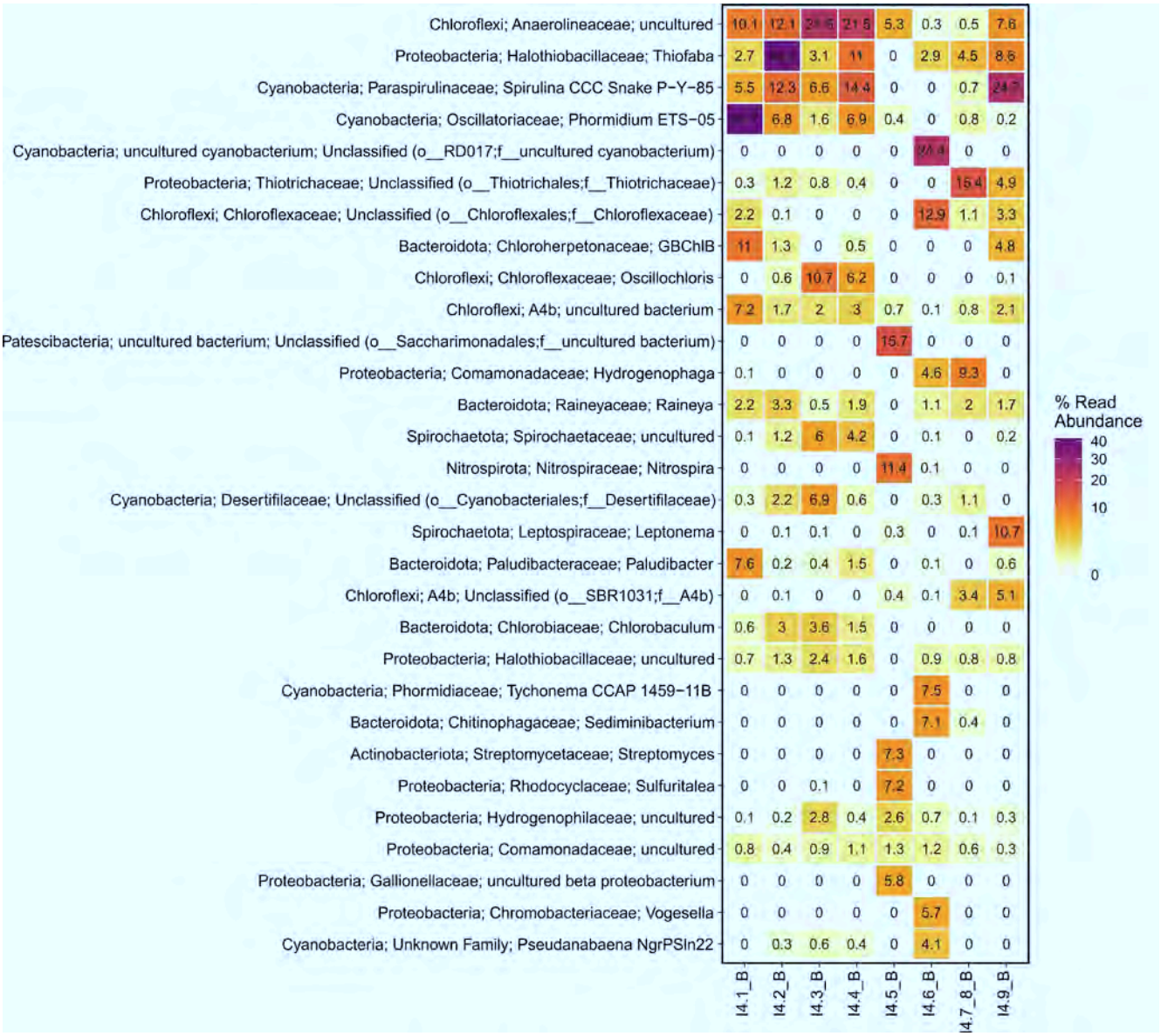

FIGURE 18 Heatmap depicting relative abundance of the top 30 bacterial taxa from Bagni San Filippo (Fosso Bianco and Balena Bianca) nine sampling sites. Squares point out the percentage of reads (amplicon sequence variants ASVs) in a sample assigned to a specific bacterial taxon (left). Sampling sites are indicated in the horizontal axis at the bottom; samples I4.7 and I4.8 were combined

turbulence, topographic gradients (cf. Capezzuoli et al., 2014; Della Porta, 2015; Della Porta et al., 2017a, 2017b; Gandin & Capezzuoli, 2014 and references therein) and organic substrate for carbonate precipitation, whereas, at the microscale, carbonate precipitates appear similar, with only some differences with respect to carbonate mineralogy, crystal size and shape (Figure 20).

5.1 | Crystal morphology and arrangement

At the microscale, calcite and aragonite crystals are similarly organised in radial structures such as rosettes and spherulites precipitating on the microbial mat surface and embedded in EPS. The prismatic and spindle-shape of travertine calcite crystals must be influenced by concentrations of magnesium, phosphate or sulphate, high fluid supersaturation with respect to calcium carbonate and the presence of microbial biofilms (cf. Bosak & Newman, 2005; Di Benedetto et al., 2011; Folk, 1993, 1994; Folk et al., 1985; Jones, 2017a; Jones & Peng, 2014a; Tracy et al., 1998). Numerous experimental studies on the precipitation of carbonate minerals confirm that crystal morphology is affected by the presence of impurities, hydrogels, polymers and various organic molecules (Bosak & Newman, 2005; Chekroun et al., 2004; Cölfen, 2003; Falini et al., 2000; Gower & Tirrell, 1998; Kato et al., 2002; Keller & Plank, 2013; Kosanović et al., 2017; Meldrum & Hyde, 2001; Oaki

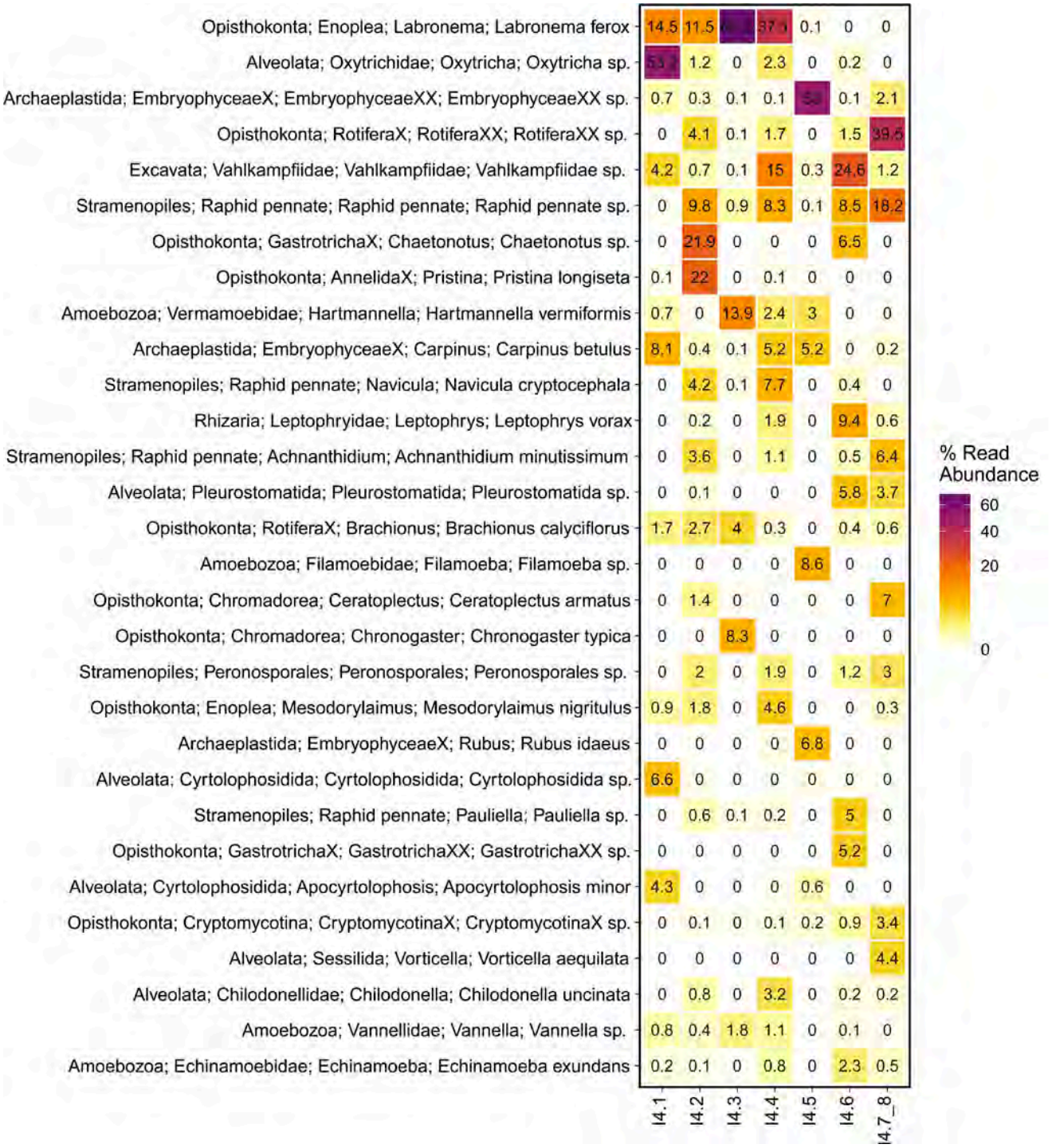

FIGURE 19 Heatmap depicting relative abundance of the top 30 eukaryote taxa from Bagni San Filippo (Fosso Bianco and Balena Bianca) sampling sites. Squares point out the percentage of reads (amplicon sequence variants ASVs) in a sample assigned to a specific bacterial taxon (left). Sampling sites are indicated in the horizontal axis at the bottom; samples I4.7 and I4.8 were combined

& Imai, 2003; Sand et al., 2011; Tobler et al., 2014; Tong et al., 2004). Calcite crystal morphology changes from scalenohedral to rhombo-scalenohedral elongated crystals and crystal size decreases at increasing organic compound concentrations (Konopacka-Lyskawa et al., 2017). The amount of dissolved silica seems also to affect crystal shape and size (Lakshtanov & Stipp, 2010). It is proposed that at hydrothermal springs, carbonate minerals precipitate in conditions far from equilibrium and develop a wide spectrum of morphologies ranging from monocrystals, mesocrystals, skeletal crystals, dendrites and spherulites at increasing disequilibrium conditions and non-classical crystal growth patterns (Jones,

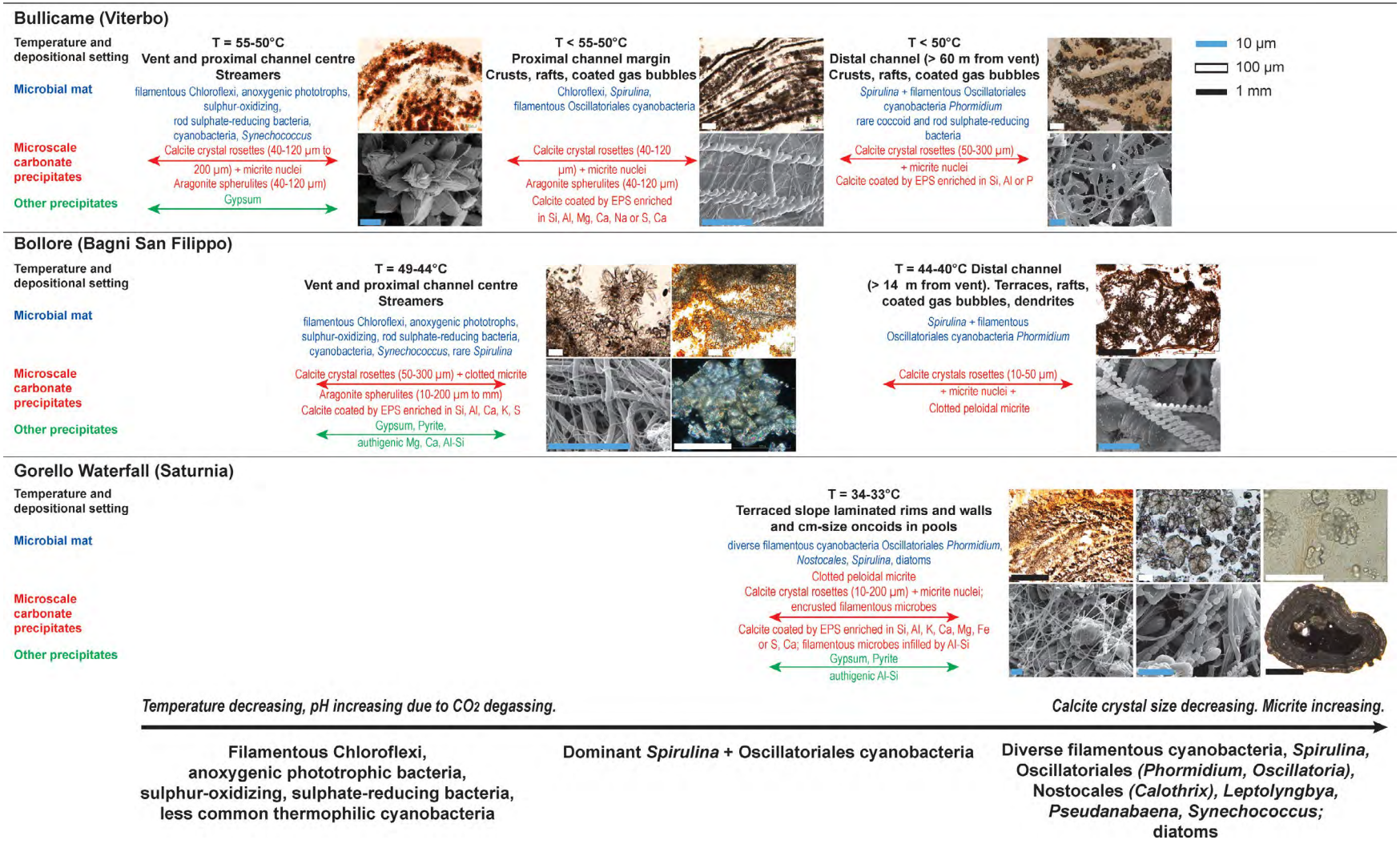

FIGURE 20 Diagram summarising the main features of carbonate and other mineral precipitates and associated microbial mats in the three study sites at thermal water decreasing temperature

2017a; Jones & Renaut, 1995). Non-classical crystal growth produces mesocrystals that are mesoscopically structured crystals made of nanocrystals or ACC (amorphous calcium carbonate), arranged into an isooriented crystal via oriented attachment, which shows birefringent properties of a single crystal (Cölfen & Antonietti, 2005; Jones, 2017a; Meldrum & Cölfen, 2008; Rodriguez-Navarro et al., 2015). The development of ACC in spring carbonates may be widespread and may play a critical, but transitory role, in the development of crystalline calcium carbonate at high temperature (Jones & Peng, 2012, 2014a, 2014b, 2016; Peng & Jones, 2013), but also, in ambient temperature environments (Pedley, 2014; Pedley et al., 2009). In the studied travertines, SEM observations did not provide ubiquitous evidence of mesocrystal formation through the aggregation of nanometre-scale particles in the higher temperature Bullicame and Bollore calcites probably due to the transitory nature of this mechanism of crystal formation. At Bollore, in some cases fibrous aragonite crystals departing from the spherulite micritic nucleus appear to result from aggregation of nanometre-size carbonate particles. In the lower temperature Gorello Waterfall travertines, nanometre-scale precipitates are present but mesocrystals, derived from the aggregation of nanoparticles, comparable to published examples (cf. Jones & Peng, 2014a; Pedley, 2014; Pedley et al., 2009), were not clearly identified.

In travertines, aragonite generally precipitates at sites with water temperature >40°C or Mg/Ca >1 (Folk, 1993, 1994). The Bullicame and Bollore thermal water is supersaturated with respect to both calcite and aragonite (Tables 1 and 2; Minissale, 2004; Pentecost, 1995a; Piscopo et al., 2006). The collected samples show evidence of fibrous aragonite spherulites in the proximal areas at temperatures >44°C confirming that the major controls on aragonite formation are abiotic factors. Jones (2017b) suggested that aragonite may precipitate either due to physicochemical parameters (e.g. rapid carbon dioxide degassing, high Mg/Ca ratio) but also due to the presence of different micro-domains within microbial biofilms. In fact, precipitation of different carbonate polymorphs could also be controlled by the acidic EPS organic matrix. The distances of the COO-groups initiate the nucleation via the 001 plane of the carbonate crystal and determine the type of mineral (e.g. 4.99 Å = calcite, 4.96Å = aragonite, 4.13Å = vaterite; Addadi & Weiner, 1985). However, often the COO-groups are not at the right distance and the initial carbonate phase is amorphous (ACC) and, in later stages, the better ordered crystal nanostructure can form euhedral crystal faces (cf. Gong et al., 2012; Ma & Feng, 2015; Rodriguez-Navarro et al., 2015).

Calcite and aragonite crystals arranged in spherulites have been observed in various travertine, lacustrine and soil settings and attributed to microbial mediation, EPS-influenced mineralization, presence of organic acids (Arp et al., 2012; Dupraz et al., 2009; Folk, 1993; Guo & Riding, 1992; Kirkham & Tucker, 2018; Mercedes Martin et al., 2016, 2017; Rogerson et al., 2017; Verrecchia et al., 1995), or abiotic precipitation within silica gels (Tosca & Wright, 2018; Wright & Barnett, 2015). Spherulites are polycrystals commonly linked to high supersaturation levels and far from equilibrium precipitation (Jones, 2017a, 2017b; Jones & Renaut, 1995). Spherulites seem to form due to increased supersaturation and slow diffusion in a viscous gel media (Oaki & Imai, 2003; Sanchez-Navas et al., 2009; Tracy et al., 1998). The presence of impurities, such as additives, polymers, organic molecules, magnesium and sulphate ions, may be responsible for spherulitic growth (Davis et al., 2000; Fernández-Díaz et al., 1996; Sanchez-Navas et al., 2009; Shtukenberg et al., 2011; Tracy et al., 1998). However, Andreassen et al. (2012) suggested that spherulites may also form without additives. Chekroun et al. (2004) proposed that spherulitic and dipyramid crystals in natural mucilaginous biofilms are linked to biologically induced mineralization. Braissant et al. (2003) demonstrated, through laboratory experiments, that calcium carbonate polymorphs (calcite and vaterite) form spherulites at increasing concentrations of EPS and amino-acid acidity, which enhance sphere formation. The morphology of calcite crystals evolves from rhombohedral to needle-shape due to stretching along the c axis as the amino-acid changes from glutamine to aspartic acid and as the medium is progressively enriched in EPS (Braissant et al., 2003). These numerous studies linking spherulitic structures and radial arrangement of precipitated carbonate crystals to the presence of organic molecules and biofilm EPS might explain why in the described travertines both calcite and aragonite crystals embedded within EPS are arranged in radial spherulitic structures.

There is no conclusive explanation for the formation of calcium-phosphate in the three investigated sites. Calcium-phosphate might be a fixation artefact because PBS was used with the fixative. However, calcium-phosphate crystals are observed draped by EPS and microbes and might represent authigenic precipitates (Figures 6F and 16A). Gypsum crystals might be related to the high concentration of sulphate and hydrogen sulphide in thermal water related to the Triassic evaporite succession in the subsurface (Minissale, 2004). In fact, thermal water in Bullicame and Bollore is supersaturated with respect to gypsum, which represents the 1.7%–4.1% of authigenic precipitates in the investigated thermal springs (Pentecost, 1995a). Hydrogen sulphide must be oxidized to elemental sulphur and sulphate either due to atmospheric oxygen or microbial activity. Authigenic calcium and magnesium aluminium-silicates occur as aggregates on calcite crystals, EPS and as coatings or fillings of filamentous microbes (Figures 9C,E

and 16C through E). The impregnation of EPS with silicon, aluminium, calcium, magnesium, potassium and iron, and the formation of amorphous silica or authigenic aluminium-silicate minerals have been observed in various hydrothermal and lacustrine case studies and attributed to biologically induced or influenced mineralization (Allen et al., 2000; Arp et al., 2003; Jones & Peng, 2012, 2014a, 2014b, 2015, 2016; Konhauser et al., 2001; Kremer et al., 2019; Lalonde et al., 2005; Pace et al., 2016; Peng & Jones, 2013; Pentecost, 2005).

5.2 | Microbial mats associated with travertine deposits

The identification of microbial communities based on morphologies observed utilising SEM is tentative because microbe morphologic characteristics do not reflect phenotypic characteristics and it is difficult to ascribe metabolism based on morphology (cf. Giovannoni et al., 1987; Reysenbach & Cady, 2001). However, form-taxa based upon morphological characters provide a useful general overview (Pentecost, 2003). Morphological observations on the three sampled sites (Bullicame, Bollore and Gorello; Figure 20; Tables 1 through 3) have been integrated with information from published literature and analysis of environmental DNA from the thermal water cascade and creek in Bagni San Filippo (Figures 18 and 19; Table 4). All the investigated sites show that there is a temperature control on the composition of the microbial mats and within the same system from proximal to distal settings, confirming the significant influence of water temperature on the composition of microbial communities in hydrothermal terrestrial settings (Cady & Farmer, 1996; Des Marais & Walter, 2019; Di Benedetto et al., 2011; Djokic et al., 2017; Dunckel et al., 2009; Farmer, 2000; Gong et al., 2020; Sanchez-Garcia et al., 2019). At Bagni San Filippo, combined microscopic observations and analysis of environmental DNA show a temperature gradient in the composition of the microbial mats dominated by filamentous Chloroflexi and Cyanobacteria. Chloroflexi and *Thiofaba* associated with *Phormidium* and *Spirulina* cyanobacteria colonise the higher temperature creek floor, whereas diverse cyanobacteria, still intermixed with Chloroflexi, colonise lower water temperature sites at the margins of the thermal water creek or the distal terraces and pools. Filamentous eukaryotes or typical filamentous algae are missing even at moderate temperatures; pennate diatoms are present, in particular at lower water temperature.

Chloroflexi include anoxygenic photoautotrophic green non-sulphur bacteria (genus *Chloroflexus*), often associated with other anoxygenic phototrophs, such as purple sulphur bacteria. Under fully aerobic conditions *Chloroflexus* bacteriochlorophyll synthesis is repressed and the organism grows chemoheterotrophically and the colour changes from dull green to orange (Dunckel et al., 2009; Konhauser, 2007; Norris et al., 2002). This may suggest that the orange to red/purple microbial mats observed in the Bullicame and Bagni San Filippo proximal channel floor might be related to Chloroflexi. *Thiofaba tepidiphila* is a chemolithoautotrophic sulphur-oxidizing bacterium of the Gammaproteobacteria, family Halothiobacillaceae, isolated from a thermal spring in Japan at a temperature of 45°C and pH 7.0 (Mori & Suzuki, 2008).

5.2.1 | Bullicame

In the three Bullicame sampling sites (i.e. proximal channel centre and margins, distal channel), at the microscale the predominant carbonate precipitates similarly consist of microsparite to fine sparite prismatic spindle-shaped calcite crystals forming radial rosettes, despite the fact that the different macroscale carbonate fabrics vary from streamers in the proximal channel to rafts and coated gas bubbles in the distal channel. Carbonate precipitation occurs exclusively on the surface or embedded within the organic substrates provided by the microbial mats that appear to control the spatial distribution of the precipitated travertines. Calcite crystals show numerous perforations as tubular pores from which filamentous microbes emerge, probably formed by entombment of microbes during fast crystal growth rather than borings of endolithic microorganisms. Aragonite spherulites occur only in the proximal location of the channel centre and margins, where temperature is higher than 50°C. The proximal channel centre (50–55°C) is dominated by filamentous streamers and purple microbial mat associated with rod-shaped bacteria. These streamers might be formed by carbonate precipitating on filamentous mats of Chloroflexi (Anaerolineaceae, Chloroflexaceae), green non-sulphur anoxygenic photoautotroph bacteria (*Chloroflexus*) and/or sulphur-oxidizing bacteria as suggested by the DNA analysis at Bagni San Filippo and reported in various travertine settings (Allen et al., 2000; Farmer, 2000; Folk, 1993; Fouke, 2011; Fouke et al., 2000; Pentecost, 2003; Pentecost & Coletta, 2007; Valeriani et al., 2018).

Valeriani et al. (2018) performed metagenomics analysis of the Bullicame microbial mat sampled at 54°C. Water was dominated by the sulphur-oxidizing bacteria *Thiofaba*, which was very rare in the channel mat; sulphate-reducing bacteria were common in both water and microbial mat. The anoxygenic phototrophs *Chloroflexus* and *Roseiflexus* were present both in water and mat (Valeriani et al., 2018). In the channel microbial mat, the phyla identified were Proteobacteria (40%), Cyanobacteria (13%), Chloroflexi (11%), Firmicutes (7%), Thermotogae (6%), Bacteroidetes (3%), Acidobacteria and Chlorobi (2%). The most represented genera were: cyanobacteria *Leptolyngbya* (8%), aerobic heterotroph

Chondromyces (7%), sulphur-reducing/anoxygenic heterotroph *Marinitoga* (5%), anoxygenic phototrophs *Gloeotrichia* and *Roseiflexus*, *Oscillochloris*, aerobic chemoheterotrophic *Sphingomonas*, sulphate-reducing *Desulfobacca*, hydrogen-oxidizing *Hydrogenophilus* and sulphur-oxidizing *Thiofaba* (1%) (Valeriani et al., 2018).

In the Bullicame and Bagnaccio (nearly 6 km north of Bullicame) hydrothermal vents at temperatures of 56–64°C, Folk (1993) indicated the presence of anoxygenic photosynthetic microbes (green sulphur *Chlorobium*, purple sulphur *Chromatium*, green non-sulphur *Chloroflexus*), *Thiobacillus* (sulphur-oxidizing proteobacteria) and *Oscillatoria* cyanobacteria. At Le Zitelle vent (nearly 1 km north-west of Bullicame), at temperatures of 61–50°C, the filamentous mat was attributed to *Chloroflexus* associated with the sulphur-reducing bacterium *Desulfovibrio thermophilus*, whereas at temperatures <50°C the microbial mat was dominated by the cyanobacteria *Spirulina* and *Synechococcus elongatus* (Allen et al., 2000; Folk, 1994; Pentecost & Coletta, 2007).

At Mammoth Hot Springs, Yellowstone, the filamentous microbes forming streamers were identified as belonging to the thermophilic Aquificales sulphide-oxidizing bacteria group (Farmer, 2000; Fouke, 2011; Fouke et al., 2000, 2003; Reysenbach & Cady, 2001; Reysenbach et al., 2000; Veysey et al., 2008). They occur at the vent, apron and channel facies at temperatures of 73–60°C (Fouke, 2011; Fouke et al., 2000). The Aquificales bacterium *Sulfurihydrogenibium yellowstonensis* is a chemolithoautotrophic microbe fixing carbon dioxide via sulphur oxidation (Fouke, 2011; Fouke et al., 2003). Aquificales are rod-shaped and this contrasts with the travertine filamentous streamers. Nevertheless, according to the environmental conditions and permanent water flow, Aquificales can develop macroscopic filaments or aggregates (Alain et al., 2003; Eder & Huber, 2002). The intermediate temperature settings of the pond facies are dominated by the filamentous *Chloroflexus*, associated with cyanobacteria (*Oscillatoria*, *Spirulina*, *Synechococcus*), green sulphur bacteria (*Chlorobium*) and β-proteobacteria (Farmer, 2000; Fouke et al., 2000, 2003). *Chloroflexus aurantiacus* occurs at temperatures of 65–55°C with the purple sulphur anoxygenic phototrophic bacterium *Thermochromatium tepidum* (Fouke, 2011; Giovannoni et al., 1987; Madigan, 2003). In the proximal slope facies (63–35°C), the presence of sulphate-reducing bacteria is confirmed by clones of *Desulfovibrio*, associated with green non-sulphur bacteria (*Heliothrix*), cyanobacteria (*Pseudanabaena*, *Spirulina*, *Synechococcus*), *Thermus-Deinococcus* and *Chlorobium* green sulphur bacteria (Fouke, 2011; Fouke et al., 2003). Giovannoni et al. (1987) determined a 20% decrease in night time sulphate concentrations in the pond water indicative of enhanced rates of sulphate reduction. The distal slope environments (44–28°C) are characterised by a high diversity of microorganisms with dominant cyanobacteria (*Spirulina*, *Calothrix*, *Synechococcus*), diatoms, algae and plants (Farmer, 2000; Fouke, 2011; Fouke et al., 2000, 2003). The Yellowstone silica depositing thermal springs (Cady & Farmer, 1996) are characterised by *Chloroflexus* and cyanobacteria *Synechococcus* at temperatures of 60–73°C, whereas cyanobacteria *Phormidium* and *Spirulina* occur at 59–35°C and the association of *Phormidium* and *Calothrix* cyanobacteria thrives at temperatures less than 35°C.

The sulphide-oxidizing Aquificales microbes forming the streamers at Yellowstone hot springs at temperature higher than 60°C seem to have a broad niche and a wide range of environmental tolerance (40–70°C; Flores et al., 2008; Fouke, 2011; Nakagawa et al., 2005), but they were not identified in the lower temperature (50–55°C) conditions of the Bullicame channel (Valeriani et al., 2018) and in the Bagni San Filippo DNA analysis (Figure 18).

The inferred microbial mat composition for the Bullicame proximal channel based on morphological features, published studies and the DNA analysis of the microbial communities from Bagni San Filippo suggest that the microbial mats at Bullicame contain moderate thermophiles similar to those identified in the intermediate temperature conditions at Yellowstone, whereas those thermophiles adapted to higher temperatures (around 70°C) as identified at Yellowstone are absent, rare or could not be retrieved. In Bagni San Filippo DNA analysis, few OTUs (0.03%) could be assigned to members of the *Deinococcus-Thermus* group and Aquificales are missing. Cyanobacteria and Chloroflexi, instead, are major representatives of the community. Besides the abundant Cyanobacteria *Phormidium* and *Spirulina*, many other cyanobacterial OTUs were present in minor amounts.

Hence, the proximal channel streamers at Bullicame might be formed by carbonate precipitation encrusting a microbial mat of filamentous Chloroflexi anoxygenic phototrophs (Allen et al., 2000; Folk, 1994; Pentecost & Coletta, 2007) or the sulphur-oxidizing *Thiofaba* (Valeriani et al., 2018) or an association of both. The sparse rod-shaped microbes observed could be sulphate-reducing bacteria as identified through geomicrobiological analyses (Allen et al., 2000; Valeriani et al., 2018). The rod-shaped thermophilic cyanobacteria *Synechococcus* might occur as reported in numerous travertine microbial mats (Pentecost, 2003). Kubo et al. (2011) observed that, at the Nakabusa hot spring in Japan at 65°C, three thermophilic bacteria groups (sulphide-oxidizers, anoxygenic phototrophs, sulphate-reducers) occur spatially distributed controlling the sulphur cycle in the microbial mat. The aerobic chemolithotrophic sulphide-oxidizing *Sulfurihydrogenibium* dominated near the mat surface, while the filamentous anoxygenic photosynthetic *Chloroflexus* was in deeper layers. Sulphide was produced by the anaerobic sulphate-reducing *Thermodesulfobacterium*/*Thermodesulfatator* under anoxic-dark conditions, while sulphide was consumed by the *Chloroflexus* anoxygenic photosynthetic bacteria under

anoxic-light conditions and strong sulphide oxidation occurred following activity by the chemolithotrophic members of the Aquificales under oxic-dark conditions (Kubo et al., 2011). Kubo et al. (2011) proposed the intimate association between rod-shaped sulphide-oxidizers and filamentous anoxygenic phototrophs where Aquificales act as highly efficient scavengers of oxygen from the spring water, creating a favourable anoxic environment for *Chloroflexus* and sulphate-reducers in deeper layers.

The channel margins and distal channel, at temperatures <50°C, are characterised by filamentous microbes, dominated by spiral-shaped forms attributed to *Spirulina labyrinthiformis* (Pentecost, 2003), associated with filamentous segmented cyanobacteria that could belong to *Lyngbya limnetica*, *Phormidium* (cf. Di Benedetto et al., 2011), *Leptolyngbya* (cf. Gong et al., 2020; Valeriani et al., 2018) or to *Pseudanabaena* corresponding to the retrieved cyanobacterial ASVs from Bagni San Filippo analysed samples (Figure 18). At the Le Zitelle vent, Pentecost and Coletta (2007) identified *S. labyrinthiformis* as the most abundant cyanobacterium at temperatures <54°C, associated with *Fischerella laminosus*, *Oscillatoria* cf. *geminata* and *Phormidium laminosum*. Diatoms were present only occasionally and the desmid green alga *Cosmarium leave* was found at temperatures below 50°C (Pentecost & Coletta, 2007). The cyanobacterium *F. laminosus* seems to live at temperatures of 47–35°C, whereas *Oscillatoria formosa* and *P. laminosum* occur at 56–40°C (Pentecost, 2003). Di Benedetto et al. (2011) at the Bullicame 3 vent, located half way between Bullicame mound and Le Zitelle spring, determined cyanobacteria associations varying as a function of water temperature: (1) at high temperature (57°C) cyanobacteria *Synechococcus eximius*, *Chroococcus* cf. *yellowstonensis*; (2) at intermediate temperature (47°C) *S. eximius*, *L. limnetica*, *Phormidium*; (3) at 37°C *S. eximius*, *Oscillatoria*, diatoms and Chlorophyta *Dyctiospherium*, *Scenedesmus acuminata*; (4) at coolest temperature (27°C) cyanobacteria *Nostoc commune*, *Anabaena circinalis*, *Oscillatoria*, diatoms and green algae.

5.2.2 | Bollore

At Bollore, travertine facies vary downstream at the macroscale with streamers at the vent and proximal channel (49–44°C), and centimetre-size terraced coated gas bubbles, dendrites, laminae and rafts in the distal channel (44–40°C). These distal channel facies are characteristic of numerous fossil travertine deposits (cf. Chafetz & Folk, 1984; Della Porta et al., 2017a, 2017b; Gandin & Capezzuoli, 2014; Guo & Riding, 1998). As for Bullicame, at the microscale, the carbonate precipitates are similar from proximal to distal settings with microsparite/fine sparite calcite radial rosettes embedded within and overlying the microbial mat. The EPS act as a substrate for crystal nucleation controlling the spatial distribution of calcite crystals and influencing the morphology of carbonate fabrics. Fibrous aragonite spherulites only occur in the highest temperature proximal setting (>44°C), as in Bullicame, and crystal size decreases distally. At Bollore, the high temperature (49–44°C) microbial mat includes filamentous, rod-shaped and coccoid microbes and rare *Spirulina* cyanobacteria, whereas the low temperature (44–40°C) assemblage shows dominant *Spirulina* and other filamentous forms. Similarly to Bullicame, the Bollore filamentous streamers might be formed by an association of sulphur-oxidizing microbes and Chloroflexi anoxygenic phototrophs (cf. Kubo et al., 2011). In the samples from Fosso Bianco at temperatures of 46–44°C, the ASVs retrieved are related to anaerobic heterotrophic Anaerolineaceae (Chloroflexi) and photoautotrophic sulphur-oxidizing *Oscillochloris* (Chloroflexaceae), *Thiofaba* (chemolithotrophic sulphur-oxidizing) and to diverse sulphate-reducing bacteria (in total up to 2% of all retrieved sequences). These findings suggest that a sulphur-cycling model similar to the Nakabusa hot spring microbial mat as proposed by Kubo et al. (2011) could be possible. The identified rod-shaped microbes can represent sulphate-reducing bacteria and/or the cyanobacterium *Synechococcus*, which tolerates the highest temperature conditions (73°C) for oxygenic photosynthesis (Cady & Farmer, 1996; Pentecost, 2003). The lower temperature, distal channel microbial mat is dominated by *Spirulina* and other filamentous cyanobacteria, possibly *Phormidium*, *Oscillatoria*, *Leptolyngbya* and *Pseudanabaena* as shown by the environmental DNA analysis of the lower temperature samples (29–41°C) performed in this study. Pentecost (2003) identified at temperatures of 40–38°C the filamentous cyanobacteria *Schizothrix perforans* and the coccoid *Aphanocapsa thermalis*. At the Bagno Vignoni hydrothermal system (nearly 17 km from Bollore), the cyanobacteria identified at temperatures of 43–34°C were *S. labyrinthiformis*, *P. laminosum*, *Lyngbya* sp., *Pseudanabaena* and *S. elongatus* (Pentecost, 1994, 2003).

5.2.3 | Gorello Waterfall

The lower temperature (33–34°C) Gorello Waterfall carbonate precipitates consist of microsparite to fine sparite crystals forming radial rosettes as at Bullicame and Bollore but micron to nanometre-scale micritic precipitates are common and aragonite is absent. Calcite rosettes precipitate exclusively on the microbial organic substrates, spatially distributed in an alveolar or laminated framework. In this lower alkalinity setting filamentous microbes are also encrusted by micrite (Figure 14C; cf. Arp et al., 2001). The microbial community includes filamentous cyanobacteria with various trichome sizes. Bazzichelli

et al. (1978) identified, at the thermal spring, cyanobacteria (*Pseudanabaena ulula*, *Oscillatoria boryana*, *S. eximius*) and sulphur bacteria. In addition to *S. labyrinthiformis*, the filamentous microbes with a diameter of 1 μm might belong to *Oscillatoria*, *Phormidium* or *Schizothrix* following the diagnostic criteria proposed by Pentecost (2003). The wide filamentous microbes (4–5 μm in diameter; Figure S7) might belong to cyanobacteria *Phormidium* or *Calothrix*. The chain-like forms resemble the cyanobacteria *Pseudanabaena* (cf. Pentecost, 2003) as identified by Bazzichelli et al. (1978). Some of these inferred cyanobacteria forms have been identified by the environmental DNA analysis of the lower temperature samples of Bagni San Filippo performed in this study; all these cyanobacteria genera have been recorded in various moderate to low temperature (20–50°C) hydrothermal systems associated with diatoms (Gong et al., 2020; Pentecost, 2003; Shiraishi et al., 2019). In particular, *Calothrix thermalis* was described in various vents with temperatures of 20–40°C (Cady & Farmer, 1996; Farmer, 2000; Jones & Peng, 2015; Pentecost, 2003, 2005).

5.3 | Travertine oxygen and carbon stable isotope signature

The measured $\delta^{18}O$ and $\delta^{13}C$ values (Figure 17) fall within the field of stable isotope signatures for hydrothermal travertine in Central Italy (Della Porta, 2015; Della Porta et al., 2017a, 2017b; Gandin & Capezzuoli, 2008; Kele et al., 2015; Minissale, 2004; Minissale et al., 2002a, 2002b). Travertine $\delta^{18}O$ and $\delta^{13}C$ values reflect the isotopic composition of thermal water, water temperature, the origin of the DIC from decarbonation of Mesozoic limestone and kinetic fractionation due to carbon dioxide degassing and fast carbonate precipitation rates (Della Porta, 2015; Della Porta et al., 2017a, 2017b; Fouke et al., 2000; Kele et al., 2015; Minissale, 2004; Pentecost, 2005 and references therein). The Bullicame and Bollore streamers record the lowest $\delta^{18}O$ and $\delta^{13}C$ values probably because streamer fabrics precipitate in the proximal setting, where water temperature is higher and degassing of carbon dioxide, removing light ^{12}C carbon dioxide, has not been prolonged. An alternative explanation is that the travertine $\delta^{13}C$ is affected by microbial metabolism, with sulphur oxidation, anoxygenic photosynthesis or microbial respiration influencing the stable isotope signatures in proximal settings, while photosynthesis is more significant in distal settings, as suggested for some travertine case studies (Fouke et al., 2000; Guo et al., 1996; Reysenbach & Cady, 2001; Zhang et al., 2004). Nevertheless, this effect of microbial metabolism on the stable isotopes seems improbable because the physico-chemical processes (carbon dioxide degassing and water cooling) would produce isotopic shifts of larger magnitude than any possible microbial influence on the DIC and fractionation of carbon stable isotopes (cf. Della Porta, 2015; Fouke, 2011; Fouke et al., 2000 and references therein). In addition, carbonate precipitation influenced by EPS acting as substrate for crystal nucleation does not produce enzymatic fractionation (Reitner, 1993; Reitner et al., 1995, 2000).

5.4 | Travertine microbial mats and EPS-mediated mineralization

This study describes three temperature-controlled travertine facies and associated microbial mats (Figure 20): (a) relatively higher temperature (50–55°C in Bullicame, 44–49°C in Bagni San Filippo) streamers with probable associations of filamentous photosynthetic and non-photosynthetic Chloroflexi, sulphur-oxidizing bacteria and possible sulphate-reducing bacteria and less common filamentous and rod-shaped cyanobacteria with possible *Synechococcus*; (b) intermediate temperature (<50°C in Bullicame, 40–44°C in Bagni San Filippo) crystalline and clotted peloidal micrite dendrites, rafts and coated bubbles with cyanobacteria dominated by *Spirulina*, *Synechococcus* and possible cyanobacteria *Oscillatoria*, *Phormidium* and *Pseudanabaena*; (c) low temperature (34–33°C in Gorello Waterfall) laminated boundstone and coated grains with a high diversity of filamentous cyanobacteria (possible Oscillatoriales as *Oscillatoria*, *Phormidium*, *Lyngbya*, and *Leptolyngbya*, *Pseudanabaena*) associated with *Spirulina*, possible Nostocales (*Calothrix*), and diatoms as similarly observed in numerous studies about hydrothermal terrestrial spring deposits (Norris & Castenholz, 2006; Norris et al., 2002; Okumura et al., 2013; Pentecost, 2003; Pentecost et al., 1997; Pentecost & Tortora, 1989; Roeselers et al., 2007; Roy et al., 2014; Shiraishi et al., 2019; Smythe et al., 2016; Sompong et al., 2005; Sugihara et al., 2016; Ward et al., 1998). These temperature-controlled microbial associations are similar to those proposed by various authors for the intermediate to low temperature hydrothermal settings in the Yellowstone National Park (Cady & Farmer, 1996; Des Marais & Walter, 2019; Farmer, 2000; Fouke, 2011). Farmer (2000) proposed that the three temperature-controlled geomicrobiological facies from Yellowstone reflect the inferred sequence of evolutionary events implied by the RNA universal phylogenetic tree with chemolithoautotrophic Aquificales sulphide-oxidizers, anoxygenic phototroph *Chloroflexus* and the oxygenic cyanobacteria (*Synechococcus*, *Spirulina*) followed by cyanobacteria as *Calothrix* and eukaryotes with diatoms at the lowest temperature.

In the studied travertine sites, the temperature influence on the composition of the microbial mats is paralleled by a change in facies at the macroscale and mesoscale with proximal higher temperature streamers to distal lower temperature laminated boundstone, rafts, coated gas bubbles and clotted peloidal micrite dendrites (Figure 20). In contrast, at the microscale the carbonate precipitates similarly consist of prismatic calcite crystal rosettes with sparse to absent aragonite spherulites

nucleated on and within the biofilm EPS, independent of the microbial community composition and dominant metabolic pathways. It appears that in the studied hydrothermal settings, microbial mats exert an influence on carbonate precipitates by acting as substrates for mineral nucleation rather than inducing carbonate mineral precipitation through microbial metabolism. Carbonate supersaturation is achieved through physico-chemical processes, primarily carbon dioxide degassing of near neutral pH and high alkalinity waters, whereas biofilm EPS provide passive substrates for crystal nucleation and influence the characteristics of travertine fabrics controlling the spatial distribution of carbonate crystals. Crystals, arranged in radial spherulitic structures, are distributed in ordered reticulate and laminated frameworks mimicking the organic template that acts as a substrate for crystal nucleation. This suggests that carbonate precipitation in the investigated hydrothermal travertines is the result of EPS-mediated mineralization (cf. Arp et al., 1999, 2003, 2012; Défarge & Trichet, 1995; Ionescu et al., 2014; Reitner, 1993; Reitner et al., 1995, 2001).

6 | CONCLUSIONS

The investigated present-day hydrothermal travertine settings differ for morphology, facies, water chemistry and temperature. At the microscale, however, carbonate precipitates are dominated by microsparite/fine sparite crystals organised in radial rosettes and spherulitic structures within or at the surface of microbial organic substrates. Despite a similarity of the microscale carbonate precipitates, the microbial communities vary with water temperature and from proximal to distal. Three microbial mat associations can be distinguished: (a) a proximal higher temperature association (55–44°C) of filamentous Chloroflexi bacteria and sulphur-oxidizing bacteria forming streamer fabrics associated with less common cyanobacteria; (b) an intermediate temperature (44–40°C) association dominated by *Spirulina* cyanobacteria with rafts, dendrites and coated gas bubble fabrics, (c) lower temperature (40–33°C) microbial mats of diverse filamentous Oscillatoriales, Nostocales and *Spirulina* cyanobacteria and diatoms occurring in travertine laminated boundstone and coated grains. Calcite is the predominant mineralogy, whereas aragonite occurs only at temperatures >44°C. Gypsum, authigenic aluminium-silicate minerals and enrichment of EPS chemical composition in silicon, aluminium, calcium, magnesium, phosphorous or sulphur can occur. Stable oxygen and carbon isotope values are similar to other travertines in Central Italy and reflect the isotopic composition of thermal water, temperature, the source of inorganic carbon and the distance from the vent due to progressive carbon dioxide degassing, cooling and carbonate precipitation.

This study confirms that microbial mat composition in terrestrial hydrothermal travertine systems varies as a function of water temperature. However, the microscale precipitates similarly consist of carbonate crystals forming radial rosettes and spherulites distributed in an ordered framework that reflects the organic substrate template, despite the different temperature-dependent microbial communities. This evidence suggests that microbial metabolism does not play a relevant role in controlling the type of microscale carbonate precipitates and that calcium carbonate precipitation in hydrothermal settings, driven by thermal water physico-chemical processes increasing carbonate supersaturation (e.g. carbon dioxide degassing), is influenced by the microbial biofilm EPS acting as a low-energy substrate for crystal nucleation (EPS-mediated mineralization), controlling the spatial distribution of carbonate crystals and influencing the travertine fabrics.

ACKNOWLEDGMENTS

The DAAD (Deutscher Akademischer Austauschdient) funded the research stay of Giovanna Della Porta at the Geobiology, Göttingen Centre of Geosciences, Georg-August-University Göttingen (Germany). Joachim Reitner received financial support from the Research Council (DFG) DFG-For 571 "Geobiology of Organo- and Biofilms". Wolfgang Dröse is warmly thanked for all the assistance in sample preparation at the Geobiology Laboratory of the University Göttingen. Dorothea Hause-Reitner and Agostino Rizzi are warmly thanked for the assistance in the SEM analyses at the University of Göttingen and University of Milan, respectively. Elena Ferrari is thanked for support in the stable isotope analyses at the Earth Sciences Department of the University of Milan, Miriam Ascagni for the confocal laser scanning microscope analyses at the laboratories Unitech of the University of Milan. Enrico Capezzuoli is thanked for fundamental help during fieldwork and stimulating discussions. The authors warmly thank two anonymous reviewers and editors for their comments that helped to improve the manuscript.

CONFLICT OF INTEREST

The authors declare no conflict of interest.

DATA AVAILABILITY STATEMENT

The authors confirm that the data supporting the findings of this study are available within the article and its supplementary information files; additional data are available from the corresponding author upon request.

ORCID

Giovanna Della Porta https://orcid.org/0000-0003-3479-0592

REFERENCES

Addadi, L. & Weiner, S. (1985) Interactions between acidic proteins and crystals: stereochemical requirements in biomineralization. *Proceedings of the National Academy of Sciences*, *82*, 4110–4114.

Alain, K., Rolland, S., Crassous, P., Lesongeur, F., Zbinden, M., le Gall, C., Godfroy, A., Page, A., Juniper, S.K., Cambon-Bonavita, M.-A., Duchiron, F. & Querellou, J. (2003) *Desulfurobacterium crinifex* sp. nov., a novel thermophilic, pinkish-streamer forming, chemolithoautotrophic bacterium isolated from a Juan de Fuca Ridge hydrothermal vent and amendment of the genus *Desulfurobacterium*. *Extremophiles*, *7*, 361–370. https://doi.org/10.1007/s00792-003-0329-4

Allen, C.C., Albert, F.G., Chafetz, H.S., Combie, J., Graham, C.R., Kieft, T.L., Kivett, S.J., McKay, D.S., Steele, A., Taunton, A.E. & Taylor, M.R. (2000) Microscopic physical biomarkers in carbonate hot springs: implications in the search for life on Mars. *Icarus*, *147*, 49–67. https://doi.org/10.1006/icar.2000.6435

Allwood, A.C., Walter, M.R., Kamber, B.S., Marshall, C.P. & Burch, I.W. (2006) Stromatolite reef from the Early Archean era of Australia. *Nature*, *441*, 714–718. https://doi.org/10.1038/nature04764

Andreassen, J.P., Beck, R. & Nergaard, M. (2012) Biomimetic type morphologies of calcium carbonate grown in absence of additives. *Faraday Discussions*, *159*, 247–261. https://doi.org/10.1039/c2fd20056b

Andres, M.S., Sumner, D.Y., Reid, R.P. & Swart, P.K. (2006) Isotopic fingerprints of microbial respiration in aragonite from Bahamian stromatolites. *Geology*, *34*(11), 973–976. https://doi.org/10.1130/G22859A.1

Arp, G., Bissett, A., Brinkmann, N., Cousin, S., De Beer, D., Friedl, T., Mohr, K.I., Neu, T.R., Reimer, A., Shiraishi, F. & Stackebrandt, E. (2010) Tufa-forming biofilms of German karstwater streams: microorganisms, exopolymers, hydrochemistry and calcification. In: Pedley, H.M. & Rogerson, M. (Eds.) *Tufas and speleothems: unravelling the microbial and physical controls*. *Geological Society, London, Special Publications, 336*, 83–118. https://doi.org/10.1144/SP336.6

Arp, G., Helms, G., Karlinska, K., Schumann, G., Reimer, A., Reitner, J. & Trichet, J. (2012) Photosynthesis versus exopolymer degradation in the formation of microbialites on the atoll of Kiritimati, Republic of Kiribati, Central Pacific. *Geomicrobiology Journal*, *29*, 29–65. https://doi.org/10.1080/01490451.2010.521436

Arp, G., Reimer, A. & Reitner, J. (2001) Photosynthesis-induced biofilm calcification and calcium concentrations in Phanerozoic oceans. *Science*, *292*(5522), 1701–1704. https://doi.org/10.1126/science.1057204

Arp, G., Reimer, A. & Reitner, J. (2002) Calcification of cyanobacterial filaments: *Girvanella* and the origin of lower Paleozoic lime mud: comment. *Geology*, *30*, 579–580. https://doi.org/10.1130/0091-7613(2002)030<0579:COCFGA>2.0.CO;2

Arp, G., Reimer, A. & Reitner, J. (2003) Microbialite formation in seawater of increased alkalinity, Satonda Crater Lake, Indonesia. *Journal of Sedimentary Research*, *73*, 105–127.1527-1404/03/073-105/$03.00

Arp, G., Thiel, V., Reimer, A., Michaelis, W. & Reitner, J. (1999) Biofilm exopolymers control microbialites formation at thermal springs discharging into the alkaline Pyramid Lake, Nevada, USA. *Sedimentary Geology*, *126*, 159–176. https://doi.org/10.1016/S0037-0738(99)00038-X

Baumgartner, L.K., Reid, R.P., Dupraz, C., Decho, A.W., Buckley, D.H., Spear, J.R., Przekop, K.M. & Visscher, P.T. (2006) Sulfate reducing bacteria in microbial mats: changing paradigms, new discoveries. *Sedimentary Geology*, *185*(3–4), 131–145. https://doi.org/10.1016/j.sedgeo.2005.12.008

Bazzichelli, G., Abdelhad, N., Florenzano, G. & Tomaselli, L. (1978) Contributo alla conoscenza delle comunità fototrofiche delle Terme di Saturnia (Toscana). *Annali Botanica*, *37*, 203–238.

Bigi, G., Cosentino, D., Parotto, M., Sartori, R. & Scandone, P. (1990) Structural model of Italy 1: 500,000. *La Ricerca Scientifica, Quaderni, C.N.R. 114* (3)

Bissett, A., de Beer, D., Schoon, R., Shiraishi, F., Reimer, A. & Arp, G. (2008) Microbial mediation of stromatolite formation in karst-water creeks. *Limnology and Oceanography*, *53*, 1159–1168. https://doi.org/10.4319/lo.2008.53.3.1159

Bosak, T. & Newman, D.K. (2005) Microbial kinetic controls on calcite morphology in supersaturated solutions. *Journal of Sedimentary Research*, *75*, 190–199. https://doi.org/10.2110/jsr.2005.015

Braissant, O., Cailleau, G., Dupraz, C. & Verrecchia, E.P. (2003) Bacterially induced mineralization of calcium carbonate in terrestrial environments: the role of exopolysaccharides and amino acids. *Journal of Sedimentary Research*, *73*, 485–490. https://doi.org/10.1306/111302730485

Braissant, O., Decho, A.W., Dupraz, C., Glunk, C., Przekop, K.M. & Visscher, P.T. (2007) Exopolymeric substances of sulfate-reducing bacteria: interactions with calcium at alkaline pH and implication for formation of carbonate minerals. *Geobiology*, *5*, 401–411. https://doi.org/10.1111/j.1472-4669.2007.00117.x

Braissant, O., Decho, A.W., Przekop, K.M., Gallagher, K.L., Glunk, C., Dupraz, C. & Visscher, P.T. (2009) Characteristics and turnover of exopolymeric substances in a hypersaline microbial mat. *FEMS Microbiology Ecology*, *67*(2), 293–307. https://doi.org/10.1111/j.1574-6941.2008.00614.x

Brasier, A.T. (2011) Searching for travertines, calcretes and speleothems in deep time: processes, appearances, predictions and the impact of plants. *Earth-Science Reviews*, *104*, 213–239. https://doi.org/10.1016/j.earscirev.2010.10.007

Brogi, A. & Capezzuoli, E. (2009) Travertine deposition and faulting: the fault-related travertine fissure ridge at Terme S. Giovanni, Rapolano Terme (Italy). *International Journal of Earth Sciences*, *98*, 931–947. https://doi.org/10.1007/s00531-007-0290-z

Brogi, A. & Fabbrini, L. (2009) Extensional and strike-slip tectonics across the Monte Amiata-Monte Cetona transect (Northern Apennines, Italy) and seismotectonic implications. *Tectonophysics*, *476*, 195–209. https://doi.org/10.1016/j.tecto.2009.02.020

Brogi, A., Liotta, D., Ruggieri, G., Capezzuoli, E., Meccheri, M. & Dini, A. (2016) An overview on the characteristics of geothermal carbonate reservoirs in southern Tuscany. *Italian Journal of Geosciences*, *135*, 17–29. https://doi.org/10.3301/IJG.2014.41

Cady, S.L. & Farmer, J.D. (1996) Fossilization processes in siliceous thermal springs: trends in preservation along thermal gradients. In: Bock, G.R. & Goode, G.A. (Eds.) *Evolution of hydrothermal ecosystems on Earth (and Mars?)*. *Ciba Foundation Symposium*, 202. Chichester: Wiley, pp. 150–173.

Cady, S.L. & Noffke, N. (2009) Geobiology: evidence for early life on Earth and the search for life on other planets. *GSA Today*, *19*(11), 4–10. https://doi.org/10.1130/GSATG62A.1

Cady, S.L.S., Skok, J.R., Gulick, V.G., Berger, J.A. & Hinman, N.W. (2018) Siliceous hot spring deposits: why they remain key astrobiologial targets. In:Cabrol, N.A. & Grin, E.A. (Eds.) *From habitability to life on Mars*. Edmond, OK: Elsevier Science, pp. 179–210.

Callahan, B.J., McMurdie, P.J. & Holmes, S.P. (2017) Exact sequence variants should replace operational taxonomic units in marker-gene data analysis. *The ISME Journal*, *11*, 2639–2643. https://doi.org/10.1038/ismej.2017.119

Campbell, K.A., Guido, D.M., Gautret, P., Foucher, F., Ramboz, C. & Westall, F. (2015) Geyserite in hot-spring siliceous sinter: window

on Earth's hottest terrestrial (paleo) environment and its extreme life. *Earth-Science Reviews*, *148*, 44–64. https://doi.org/10.1016/j.earscirev.2015.05.009

Capezzuoli, E., Gandin, A. & Pedley, M. (2014) Decoding tufa and travertine (fresh water carbonates) in the sedimentary record: the state of the art. *Sedimentology*, *61*, 1–21. https://doi.org/10.1111/sed.12075

Carminati, E. & Doglioni, C. (2012) Alps vs. Apennines: the paradigm of a tectonically asymmetric Earth. *Earth-Science Reviews*, *112*, 67–96. https://doi.org/10.1016/j.earscirev.2012.02.004

Castanier, S., Le Métayer-Levrel, G. & Perthuisot, J.P. (1999) Ca-carbonates precipitation and limestone genesis – the microbiogeologist point of view. *Sedimentary Geology*, *126*, 9–23. https://doi.org/10.1016/S0037-0738(99)00028-7

Chafetz, H.S. & Buczynski, C. (1992) Bacterially induced lithification of microbial mats. *Palaios*, *7*, 277–293.

Chafetz, H.S. & Folk, R.L. (1984) Travertines: depositional morphology and the bacterially constructed constituents. *Journal of Sedimentary Petrology*, *54*, 289–316. https://doi.org/10.1306/212F8404-2B24-11D7-8648000102C1865D

Chafetz, H.S. & Guidry, S.A. (1999) Bacterial shrubs, crystal shrubs, and ray-rystal shrubs: bacterial vs. abiotic precipitation. *Sedimentary Geology*, *126*, 57–74. https://doi.org/10.1016/S0037-0738(99)00032-9

Chekroun, K.B., Rodríguez-Navarro, C., González-Muñoz, M.T., Arias, J.M., Cultrone, G. & Rodríguez-Gallego, M. (2004) Precipitation and growth morphology of calcium carbonate induced by *Myxococcus xanthus*: implications for recognition of bacterial carbonates. *Journal of Sedimentary Research*, *74*, 868–876. https://doi.org/10.1306/050504740868

Cölfen, H. (2003) Precipitation of carbonates: recent progress in controlled production of complex shapes. *Current Opinion Colloid Interface Science*, *8*, 23–31. https://doi.org/10.1016/S1359-0294(03)00012-8

Cölfen, H. & Antonietti, M. (2005) Mesocrystals: inorganic superstructures made by highly parallel crystallization and controlled alignment. *Angewandte Chemie International Edition*, *44*, 5576–5591. https://doi.org/10.1002/anie.200500496

Croci, A., Della Porta, G. & Capezzuoli, E. (2016) Depositional architecture of a mixed travertine-terrigenous system in a fault-controlled continental extensional basin (Messinian, Southern Tuscany, Central Italy). *Sedimentary Geology*, *332*, 13–39. https://doi.org/10.1016/j.sedgeo.2015.11.007

Davis, K.J., Dove, P.M. & De Yoreo, J.J. (2000) The role of Mg^{2+} as an impurity in calcite growth. *Science*, *290*, 1134–1137. https://doi.org/10.1126/science.290.5494.1134

Decho, A.W. (2010) Overview of biopolymer-induced mineralization: what goes on in biofilms? *Ecological Engineering*, *36*, 137–144. https://doi.org/10.1016/j.ecoleng.2009.01.003

Decho, A. & Gutierrez, T. (2017) Microbial extracellular polymeric substances (EPSs) in ocean systems. *Frontiers in Microbiology*, *8*, 922. https://doi.org/10.3389/fmicb.2017.00922

Défarge, C., Gautret, P., Reitner, J., & Trichet, J. Defining organominerals: comment on 'Defining biominerals and organominerals: direct and indirect indicators of life' by Perry et al. 2007, Sedimentary Geology, 201, 157–179. *Sedimentary Geology*, *213*, 152–155. https://doi.org/10.1016/j.sedgeo.2008.04.002

Défarge, C. & Trichet, J. (1995) From biominerals to "organominerals": the example of the modern lacustrine calcareous stromatolites from Polynesian atolls. *Bulletin de l'Institut océanographique Monaco, Special Issue*, *14*, 265–271.

Défarge, C., Trichet, J., Jaunet, A.-M., Robert, M., Tribble, J. & Sansone, F.J. (1996) Texture of microbial sediments revealed by cryo-scanning electron microscopy. *Journal of Sedimentary Research*, *66*, 935–947. https://doi.org/10.1306/D4268446-2B26-11D7-8648000102C1865D

Della Porta, G., Capezzuoli, E. & De Bernardo, A. (2017a) Facies character and depositional architecture of hydrothermal travertine slope aprons (Pleistocene, Acquasanta Terme, Central Italy). *Marine and Petroleum Geology*, *87*, 171–187. https://doi.org/10.1016/j.earscirev.2003.09.001

Della Porta, G. (2015) Carbonate build-ups in lacustrine, hydrothermal and fluvial settings: comparing depositional geometry, fabric types and geochemical signature. In: Bosence, D.W.J., Gibbons, K.A., Le Heron, D.P., Morgan, W.A., Pritchard, T. & Vining, B.A. (Eds.) *Microbial carbonates in space and time: implications for global exploration and production*. *Geological Society London, Special Publications*, *418*, 17-68. DOI: https://doi.org/10.1144/SP418.4

Della Porta, G., Croci, A., Marini, M. & Kele, S. (2017b) Depositional architecture, facies character and geochemical signature of the Tivoli travertines (Pleistocene, Acque Albule Basin, Central Italy). *RIPS Rivista Italiana Paleontologia Stratigrafia*, *123*, 487–540. https://doi.org/10.13130/2039-4942/9148

Des Marais, D.J. & Walter, M.R. (2019) Terrestrial hot spring systems: introduction. *Astrobiology*, *19*(12), 1419–1432. https://doi.org/10.1089/ast.2018.1976

Di Benedetto, F., Montegrossi, G., Minissale, A., Pardi, L.A., Romanelli, M., Tassi, F., Delgado Huertas, A., Pampin, E.M., Vaselli, O. & Borrini, D. (2011) Biotic and inorganic control on travertine deposition at Bullicame 3 spring (Viterbo, Italy): a multidisciplinary approach. *Geochimica Cosmochimica Acta*, *75*, 4441–4455. https://doi.org/10.1016/j.gca.2011.05.011

Djokic, T., Van Kranendonk, M.J., Campbell, K.A., Walter, M.R. & Ward, C.R. (2017) Earliest signs of life on land preserved in ca. 3.5 Ga hot spring deposits. *Nature Communications*, *8*, 1–9. https://doi.org/10.1038/ncomms15263

Doglioni, C. (1991) A proposal for the kinematic modelling of W-dipping subductions – possible applications to the Tyrrhenian-Apennines system. *Terra Nova*, *3*, 423–434. https://doi.org/10.1111/j.1365-3121.1991.tb00172.x

Dunckel, A.E., Cardenas, M.B., Sawyer, A.H. & Bennett, P.C. (2009) High-resolution in-situ thermal imaging of microbial mats at El Tatio Geyser, Chile shows coupling between community color and temperature. *Geophysical Research Letters*, *36*, L23403. https://doi.org/10.1029/2009GL041366

Dupraz, C., Reid, R.P., Braissant, O., Decho, A.W., Norman, R.S. & Visscher, P.T. (2009) Processes of carbonate precipitation in modern microbial mats. *Earth-Science Reviews*, *96*, 141–162. https://doi.org/10.1016/j.earscirev.2008.10.005

Dupraz, C. & Visscher, P.T. (2005) Microbial lithification in marine stromatolites and hypersaline mats. *Trends in Microbiology*, *13*, 429–438. https://doi.org/10.1016/j.tim.2005.07.008

Dupraz, C., Visscher, P.T., Baumgartner, L.K. & Reid, R.P. (2004) Microbe-mineral interactions: early carbonate precipitation in a hypersaline lake (Eleuthera Island, Bahamas). *Sedimentology*, *51*, 745–765. https://doi.org/10.1111/j.1365-3091.2004.00649.x

Eder, W. & Huber, R. (2002) New isolates and physiological properties of the Aquificales and description of *Thermocrinis albus* sp. nov. *Extremophiles*, *6*, 309–318. https://doi.org/10.1007/s00792-001-0259-y

Erthal, M.M., Capezzuoli, E., Mancini, A., Claes, H., Soete, J. & Swennen, R. (2017) Shrub morpho-types as indicator for the water

flow energy – Tivoli travertine case (Central Italy). *Sedimentary Geology*, *347*, 79–99. https://doi.org/10.1016/j.sedgeo.2016.11.008

Eymard, I., Alvarez, M.D.P., Bilmes, A., Vasconcelos, C. & Ariztegui, D. (2020) Tracking organomineralization processes from living microbial mats to fossil microbialites. *Minerals*, *10*, 605. https://doi.org/10.3390/min10070605

Faccenna, C., Soligo, M., Billi, A., De Filippis, L., Funiciello, R., Rossetti, C. & Tuccimei, P. (2008) Late Pleistocene depositional cycles of the *Lapis Tiburtinus* travertine (Tivoli, central Italy): possible influence of climate and fault activity. *Global and Planetary Change*, *63*, 299–308. https://doi.org/10.1016/j.gloplacha.2008.06.006

Falini, G., Fermani, S., Gazzano, M. & Ripamonti, A. (2000) Polymorphism and architectural crystal assembly of calcium carbonate in biologically inspired polymeric matrices. *Journal Chemical Society, Dalton Transactions*, *21*, 3983–3987. https://doi.org/10.1039/B003334K

Farmer, J. (1998) Thermophiles, early biosphere evolution, and the origin of life on Earth: implications for the exobiological exploration of Mars. *Journal Geophysical Research Planets*, *103*(E12), 28457–28461. https://doi.org/10.1029/98JE01542

Farmer, J.D. (2000) Hydrothermal systems: doorways to early biosphere evolution. *GSA Today*, *10*, 1–9.

Fernàndez-Díaz, L., Putnis, A., Prieto, M. & Putnis, C.V. (1996) The role of magnesium in the crystallization of calcite and aragonite in a porous medium. *Journal of Sedimentary Research*, *66*, 482–491. https://doi.org/10.1306/D4268388-2B26-11D7-8648000102C1865D

Flores, G.E., Liu, Y., Ferrera, I., Beveridge, T.J. & Reysenbach, A.L. (2008) *Sulfurihydrogenibium kristjanssonii* sp. nov., a hydrogen-and sulfur-oxidizing thermophile isolated from a terrestrial Icelandic hot spring. *International Journal of Systematic and Evolutionary Microbiology*, *58*, 1153–1158. https://doi.org/10.1099/ijs.0.65570-0

Folk, R.L. (1993) SEM imaging of bacteria and nannobacteria in carbonate sediments and rocks. *Journal of Sedimentary Research*, *63*, 990–999. https://doi.org/10.1306/D4267C67-2B26-11D7-8648000102C1865D

Folk, R. (1994) Interaction between bacteria, nannobacteria, and mineral precipitation in hot springs of central Italy. *Géographie Physique Quaternaire*, *48*, 233–246. https://doi.org/10.7202/033005ar

Folk, R.L., Chafetz, H.S. & Tiezzi, P.A. (1985) Bizarre forms of depositional and diagenetic calcite in hot-spring travertines, central Italy. In: Schneidermann, N. & Harris, P.M. (Eds.) *Carbonate cements*. *SEPM Special Publications*, *36*, 349–369.

Fouke, B.W. (2011) Hot-spring systems geobiology: abiotic and biotic influences on travertine formation at mammoth hot springs, Yellowstone National Park, USA. *Sedimentology*, *58*, 170–199. https://doi.org/10.1111/j.1365-3091.2010.01209.x

Fouke, B.W., Bonheyo, G.T., Sanzenbacher, B. & Frias-Lopez, J. (2003) Partitioning of bacterial communities between travertine depositional facies at Mammoth Hot Springs, Yellowstone National Park, USA. *Canadian Journal Earth Sciences*, *40*, 1531–1548. https://doi.org/10.1139/e03-067

Fouke, B.W., Farmer, J.D., Des Marais, D.J., Pratt, L., Sturchio, N.C., Burns, P.C. & Discipulo, M.K. (2000) Depositional facies and aqueos-solid geochemistry of Travertine-depositing hot spring (Angel Terrace, Mammoth hot spring, Yellowstone National Park, U.S.A.). *Journal of Sedimentary Research*, *70*, 202–207. https://doi.org/10.1306/2DC40929-0E47-11D7-8643000102C1865D

Fox, E., Meyer, E., Panasiak, N. & Taylor, A.R. (2018) Calcein staining as a tool to investigate coccolithophore calcification. *Frontiers in Marine Science*, *5*, 326. https://doi.org/10.3389/fmars.2018.00326

Franchi, F. & Frisia, S. (2020) Crystallization pathways in the Great Artesian Basin (Australia) spring mound carbonates: implications for life signatures on Earth and beyond. *Sedimentology*, *67*, 2561–2595. https://doi.org/10.1111/sed.12711

Gandin, A. & Capezzuoli, E. (2008) Travertine vs. calcareous tufa: distinctive petrologic features and stable isotope signatures. *Italian Journal of Quaternary Sciences*, *21*, 125–136.

Gandin, A. & Capezzuoli, E. (2014) Travertine: distinctive depositional fabrics of carbonates from thermal spring systems. *Sedimentology*, *61*, 264–290. https://doi.org/10.1111/sed.12087

Giovannoni, S.J., Revsbech, N.P., Ward, D.M. & Castenholz, R.W. (1987) Obligately phototrophic *Chloroflexus*: primary production in anaerobic hot spring microbial mats. *Archives of Microbiology*, *147*, 80–87. https://doi.org/10.1007/BF00492909

Glunk, C., Dupraz, C., Braissant, O., Gallagher, K.L., Verrecchia, E.P. & Visscher, P.T. (2011) Microbially mediated carbonate precipitation in a hypersaline lake, Big Pond (Eleuthera, Bahamas). *Sedimentology*, *58*(3), 720–736. https://doi.org/10.1111/j.1365-3091.2010.01180.x

Golubic, S., Seong-Joo, L. & Browne, K.M. (2000) Cyanobacteria: architects of sedimentary structures. In: Riding, R.E. & Awramik, S.M. (Eds.) *Microbial sediments*. Berlin, Heidelberg: Springer-Verlag, pp. 57–67.

Gong, J., Myers, K.D., Munoz-Saez, C., Homann, M., Rouillard, J., Wirth, R., Schreiber, A. & van Zuilen, M.A. (2020) Formation and preservation of microbial palisade fabric in silica deposits from El Tatio, Chile. *Astrobiology*, *20*(4), 500–524. https://doi.org/10.1089/ast.2019.2025

Gong, Y.U., Killian, C.E., Olson, I.C., Appathurai, N.P., Amasino, A.L., Martin, M.C., Holt, L.J., Wilt, F.H. & Gilbert, P.U.P.A. (2012) Phase transitions in biogenic amorphous calcium carbonate. *Proceedings of the National Academy of Sciences*, *109*(16), 6088–6093. https://doi.org/10.1073/pnas.1118085109

Gower, L.A. & Tirrell, D.A.J. (1998) Calcium carbonate films and helices grown in solutions of poly (aspartate). *Journal of Crystal Growth*, *191*, 153–160. https://doi.org/10.1016/S0022-0248(98)00002-5

Guo, L., Andrews, J., Riding, R., Dennis, P. & Dresser, Q. (1996) Possible microbial effects on stable carbon isotopes in hot-spring travertines. *Journal Sedimentary Research*, *66*, 468–473. https://doi.org/10.1306/D4268379-2B26-11D7-8648000102C1865D

Guo, L. & Riding, R. (1992) Aragonite laminae in hot water travertine crusts, Rapolano Terme, Italy. *Sedimentology*, *39*, 1067–1079. https://doi.org/10.1111/j.1365-3091.1992.tb01997.x

Guo, L. & Riding, R. (1994) Origin and diagenesis of Quaternary travertine shrub fabrics, Rapolano Terme, central Italy. *Sedimentology*, *41*, 499–520. https://doi.org/10.1111/j.1365-3091.1994.tb02008.x

Guo, L. & Riding, R. (1998) Hot-spring travertine facies and sequences, Late Pleistocene, Rapolano Terme, Italy. *Sedimentology*, *45*, 163–180. https://doi.org/10.1046/j.1365-3091.1998.00141.x

Guo, L. & Riding, R. (1999) Rapid facies changes in Holocene fissure ridge hot spring travertines, Rapolano Terme, Italy. *Sedimentology*, *46*, 1145–1158. https://doi.org/10.1046/j.1365-3091.1999.00269.x

Hoffmann, F., Janussen, D., Dröse, W., Arp, G. & Reitner, J. (2003) Histological investigation of organisms with hard skeletons: a case study of siliceous sponges. *Biotechnic & Histochemistry*, *78*, 191–199. https://doi.org/10.1080/10520290310001613042

Ionescu, D., Spitzer, S., Reimer, A., Schneider, D., Daniel, R., Reitner, J., de Beer, D. & Arp, G. (2014) Calcium dynamics in microbialite-forming exopolymer-rich mats on the atoll of Kiritimati, Republic of Kiribati, Central Pacific. *Geobiology*, *13*(2), 170–180. https://doi.org/10.1111/gbi.12120

Jones, B. (2017a) Review of calcium carbonate polymorph precipitation in spring systems. *Sedimentary Geology*, *353*, 64–75. https://doi.org/10.1016/j.sedgeo.2017.03.006

Jones, B. (2017b) Review of aragonite and calcite crystal morphogenesis in thermal spring systems. *Sedimentary Geology*, *354*, 9–23. https://doi.org/10.1016/j.sedgeo.2017.03.012

Jones, B. & Peng, X. (2012) Amorphous calcium carbonate associated with biofilms in hot spring deposits. *Sedimentary Geology*, *269*, 58–68. https://doi.org/10.1016/j.sedgeo.2012.05.019

Jones, B. & Peng, X. (2014a) Signatures of biologically influenced $CaCO_3$ and Mg–Fe silicate precipitation in hot springs: case study from the Ruidian geothermal area, western Yunnan Province, China. *Sedimentology*, *61*, 56–89. https://doi.org/10.1111/sed.12043

Jones, B. & Peng, X. (2014b) Hot spring deposits on a cliff face: a case study from Jifei, Yunnan Province, China. *Sedimentary Geology*, *302*, 1–28. https://doi.org/10.1016/j.sedgeo.2013.12.009

Jones, B. & Peng, X. (2015) Laminae development in opal-A precipitates associated with seasonal growth of the form-genus *Calothrix* (Cyanobacteria), Rehai geothermal area, Tengchong, Yunnan Province, China. *Sedimentary Geology*, *319*, 52–68. https://doi.org/10.1016/j.sedgeo.2015.01.004

Jones, B. & Peng, X. (2016) Mineralogical, crystallographic, and isotopic constraints on the precipitation of aragonite and calcite at Shiqiang and other hot springs in Yunnan Province, China. *Sedimentary Geology*, *345*, 103–125. https://doi.org/10.1016/j.sedgeo.2016.09.007

Jones, B. & Renaut, R.W. (1995) Noncrystallographic calcite dendrites from hot-spring deposits at Lake Bogoria, Kenya. *Journal of Sedimentary Research*, *65*, 154–169. https://doi.org/10.1306/D4268059-2B26-11D7-8648000102C1865D

Jones, B. & Renaut, R.W. (2010) Calcareous spring deposits in continental settings. In: Alonso-Zarza, A.M. & Tanner, L.H. (Eds.) *Carbonates in continental settings: facies, environments and processes*. *Developments in Sedimentology*, *61*, 177–224.

Jones, B. & Renaut, R.W. (2011) Hot springs and Geysers. In: Reitner, J. & Thiel, V. (Eds.) *Encyclopedia of geobiology*. Heidelberg: Springer, Berlin, pp. 447–451.

Kamennaya, N.A., Ajo-Franklin, C.M., Northen, T. & Jansson, C. (2012) Cyanobacteria as biocatalysts for carbonate mineralization. *Minerals*, *2*(4), 338–364. https://doi.org/10.3390/min2040338

Kamran, A., Sauter, K., Reimer, A., Wacker, T., Reitner, J. & Hoppert, M. (2021) Cyanobacterial mats in calcite-precipitating serpentinite-hosted alkaline springs of the Voltri Massif, Italy. *Microorganisms*, *9*, 62. https://doi.org/10.3390/microorganisms9010062

Kato, T., Sugawara, A. & Hosoda, N. (2002) Calcium carbonate-organic hybrid materials. *Advanced Materials*, *14*, 869–877. https://doi.org/10.1002/1521-4095(20020618)14:12<869:AID-ADMA869>3.0.CO;2-E

Kele, S., Breitenbach, S.F.M., Capezzuoli, E., Meckler, A.N., Ziegler, M., Millan, I.M., Kluge, T., Deák, J., Hanselmann, K., John, C.M., Yan, H., Liu, Z. & Bernasconi, S.M. (2015) Temperature dependence of oxygen-and clumped isotope fractionation in carbonates: a study of travertines and tufas in the 6–95°C temperature range. *Geochimica Cosmochimica Acta*, *168*, 172–192. https://doi.org/10.1016/j.gca.2015.06.032

Keller, H. & Plank, J. (2013) Mineralisation of $CaCO_3$ in the presence of polycarboxylate comb polymers. *Cement Concrete Research*, *54*, 1–11. https://doi.org/10.1016/j.cemconres.2013.06.017

Kirkham, A. & Tucker, M.E. (2018) Thrombolites, spherulites and fibrous crusts (Holkerian, Purbeckian, Aptian): context, fabrics and origins. *Sedimentary Geology*, *374*, 69–84. https://doi.org/10.1016/j.sedgeo.2018.07.002

Knorre, H.V. & Krumbein, W.E. (2000) Bacterial calcification. In: Riding, R.E. & Awramik, S.M. (Eds.) *Microbial sediments*. Berlin Heidelberg: Springer-Verlag, pp. 23–31.

Konhauser, K. (2007) *Introduction to geomicrobiology*. Singapore: Blackwell Publishing, 425 p.

Konhauser, K.O., Phoenix, V.R., Bottrell, S.H., Adams, D.G. & Head, I.M. (2001) Microbial-silica interactions in Icelandic hot spring sinter: possible analogues for some Precambrian siliceous stromatolites. *Sedimentology*, *48*, 415–433. https://doi.org/10.1046/j.1365-3091.2001.00372.x

Konopacka-Łyskawa, D., Kościelska, B. & Karczewski, J. (2017) Controlling the size and morphology of precipitated calcite particles by the selection of solvent composition. *Journal of Crystal Growth*, *478*, 102–110. https://doi.org/10.1016/j.jcrysgro.2017.08.033

Kosanović, C., Fermani, S., Falini, G. & Kralj, D. (2017) Crystallization of calcium carbonate in alginate and xanthan hydrogels. *Crystals*, *7*, 355–370. https://doi.org/10.3390/cryst7120355

Kremer, B., Kaźmierczak, J. & Kempe, S. (2019) Authigenic replacement of cyanobacterially precipitated calcium carbonate by aluminium-silicates in giant microbialites of Lake Van (Turkey). *Sedimentology*, *66*, 285–304. https://doi.org/10.1111/sed.12529

Kubo, K., Knittel, K., Amann, R., Fukui, M. & Matsuura, K. (2011) Sulfur-metabolizing bacterial populations in microbial mats of the Nakabusa hot spring, Japan. *Systematic and Applied Microbiology*, *34*, 293–302. https://doi.org/10.1016/j.syapm.2010.12.002

Lakshtanov, L.Z. & Stipp, S.L.S. (2010) Interaction between dissolved silica and calcium carbonate: 1. Spontaneous precipitation of calcium carbonate in the presence of dissolved silica. *Geochimica Cosmochimica Acta*, *74*, 2655–2664. https://doi.org/10.1016/j.gca.2010.02.009

Lalonde, S.V., Konhauser, K.O., Reysenbach, A.L. & Ferris, F.G. (2005) The experimental silicification of Aquificales and their role in hot spring sinter formation. *Geobiology*, *3*, 41–52. https://doi.org/10.1111/j.1472-4669.2005.00042.x

Lowenstam, H.A. & Weiner, S. (1989) *On biomineralization*. New York, Oxford: Oxford University Press, 324 p.

Ma, Y. & Feng, Q. (2015) A crucial process: organic matrix and magnesium ion control of amorphous calcium carbonate crystallization on β-chitin film. *CrystEngComm*, *17*(1), 32–39. https://doi.org/10.1039/C4CE01616E

Madigan, M.T. (2003) Anoxygenic phototrophic bacteria from extreme environments. *Photosynthesis Research*, *76*, 157–171. https://doi.org/10.1023/A:1024998212684

Malinverno, A. & Ryan, W.B.F. (1986) Extension in the Tyrrhenian Sea and shortening in the Apennines as result of arc migration driven by sinking of the lithosphere. *Tectonics*, *5*, 227–254. https://doi.org/10.1029/TC005i002p00227

Mancini, A., Capezzuoli, E., Erthal, M. & Swennen, R. (2019) Hierarchical approach to define travertine depositional systems: 3D conceptual morphological model and possible applications. *Marine and Petroleum Geology*, *103*, 549–563. https://doi.org/10.1016/j.marpetgeo.2019.02.021

Meldrum, F.C. & Cölfen, H. (2008) Controlling mineral morphologies and structures in biological and synthetic systems. *Chemical Reviews*, *108*, 4332–4432. https://doi.org/10.1021/cr8002856

Meldrum, F.C. & Hyde, S.T. (2001) Morphological influence of magnesium and organic additives on the precipitation of calcite. *Journal of Crystal Growth*, *231*, 544–558. https://doi.org/10.1016/S0022-0248(01)01519-6

Melezhik, V.A. & Fallick, A.E. (2001) Palaeoproterozoic travertines of volcanic affiliation from a ^{13}C-rich rift lake environment. *Chemical Geology*, *173*, 293–312. https://doi.org/10.1016/S0009-2541(00)00281-3

Mercedes-Martín, R., Brasier, A.T., Rogerson, M., Reijmer, J.J., Vonhof, H. & Pedley, M. (2017) A depositional model for spherulitic carbonates associated with alkaline, volcanic lakes. *Marine and Petroleum Geology*, *86*, 168–191. https://doi.org/10.1016/j.marpetgeo.2017.05.032

Mercedes-Martín, R., Rogerson, M.R., Brasier, A.T., Vonhof, H.B., Prior, T.J., Fellows, S.M., Reijmer, J.J.G., Billing, I. & Pedley, H.M. (2016) Growing spherulitic calcite grains in saline, hyperalkaline lakes: experimental evaluation of the effects of Mg-clays and organic acids. *Sedimentary Geology*, *335*, 93–102. https://doi.org/10.1016/j.sedgeo.2016.02.008

Merz, M.U.E. (1992) The biology of carbonate precipitation by cyanobacteria. *Facies*, *26*, 81–102. https://doi.org/10.1007/BF02539795

Merz-Preiß, M. (2000) Calcification in cyanobacteria. In: Riding, R.E. & Awramik, S.M. (Eds.) *Microbial sediments*. Berlin, Heidelberg: Springer-Verlag, pp. 50–56.

Merz-Preiß, M. & Riding, R. (1999) Cyanobacterial tufa calcification in two freshwater streams: ambient environment, chemical thresholds and biological processes. *Sedimentary Geology*, *126*, 103–124. https://doi.org/10.1016/S0037-0738(99)00035-4

Minissale, A. (2004) Origin, transport and discharge of CO_2 in central Italy. *Earth-Science Reviews*, *66*, 89–141. https://doi.org/10.1016/j.earscirev.2003.09.001

Minissale, A., Kerrick, D.M., Magro, G., Murrell, M.T., Paladini, M., Rihs, S., Sturchio, N.C., Tassi, F. & Vaselli, O. (2002a) Geochemistry of Quaternary travertines in the region north of Rome (Italy): structural, hydrologic and paleoclimatic implications. *Earth Planetary Science Letters*, *203*, 709–728. https://doi.org/10.1016/S0012-821X(02)00875-0

Minissale, A., Vaselli, O., Tassi, F., Magro, G. & Grechi, G.P. (2002b) Fluid mixing in carbonate aquifers near Rapolano (central Italy): chemical and isotopic constraints. *Applied Geochemistry*, *17*, 1329–1342. https://doi.org/10.1016/S0883-2927(02)00023-9

Mori, K. & Suzuki, K.I. (2008) *Thiofaba tepidiphila* gen. nov., sp. nov., a novel obligately chemolithoautotrophic, sulfur-oxidizing bacterium of the Gammaproteobacteria isolated from a hot spring. *International Journal of Systematic and Evolutionary Microbiology*, *58*, 1885–1891. https://doi.org/10.1099/ijs.0.65754-0

Nakagawa, S., Shtaih, Z., Banta, A., Beveridge, T.J., Sako, Y. & Reysenbach, A.L. (2005) *Sulfurihydrogenibium yellowstonense* sp. nov., an extremely thermophilic, facultatively heterotrophic, sulfur-oxidizing bacterium from Yellowstone National Park, and emended descriptions of the genus *Sulfurihydrogenibium*, *Sulfurihydrogenibium subterraneum* and *Sulfurihydrogenibium azorense*. *International Journal of Systematic and Evolutionary Microbiology*, *55*, 2263–2268. https://doi.org/10.1099/ijs.0.63708-0

Neuweiler, F., Gautret, P., Thiel, V., Lange, R., Michaelis, W. & Reitner, J. (1999) Petrology of Lower Cretaceous carbonate mud mounds (Albian, N. Spain): insights into organomineralic deposits of the geological record. *Sedimentology*, *46*, 837–859. https://doi.org/10.1046/j.1365-3091.1999.00255.x

Norris, T.B. & Castenholz, R.W. (2006) Endolithic photosynthetic communities within ancient and recent travertine deposits in Yellowstone National Park. *FEMS Microbiology Ecology*, *57*, 470–483. https://doi.org/10.1111/j.1574-6941.2006.00134.x

Norris, T.B., McDermott, T.R. & Castenholz, R.W. (2002) The long-term effects of UV exclusion on the microbial composition and photosynthetic competence of bacteria in hot-spring microbial mats. *FEMS Microbiology Ecology*, *39*, 193–209. https://doi.org/10.1111/j.1574-6941.2002.tb00922.x

Oaki, Y. & Imai, H. (2003) Experimental demonstration for the morphological evolution of crystals grown in gel media. *Crystal Growth Design*, *3*, 711–716. https://doi.org/10.1021/cg034053e

Obst, M., Dynes, J.J., Lawrence, J.R., Swerhone, G.D.W., Benzerara, K., Karunakaran, C., Kaznatcheev, K., Tyliszczak, T. & Hitchcock, A.P. (2009) Precipitation of amorphous $CaCO_3$ (aragonite-like) by cyanobacteria: a STXM study of the influence of EPS on the nucleation process. *Geochimica Cosmochimica Acta*, *73*, 4180–4198. https://doi.org/10.1016/j.gca.2009.04.013

Okumura, T., Takashima, C. & Kano, A. (2013) Textures and processes of laminated travertines formed by unicellular cyanobacteria in Myoken hot spring, southwestern Japan. *Island Arc*, *22*, 410–426. https://doi.org/10.1111/iar.12034

Pace, A., Bourillot, R., Bouton, A., Vennin, E., Galaup, S., Bundeleva, I., Patrier, P., Dupraz, C., Thomazo, C., Sansjofre, P., Yokoyama, Y., Franceschi, M., Anguy, Y., Pigot, L., Virgone, A. & Visscher, P.T. (2016) Microbial and diagenetic steps leading to the mineralisation of Great Salt Lake microbialites. *Scientific Reports*, *6*(1), 1–12. https://doi.org/10.1038/srep31495

Parkhurst, D.L. & Appelo, C.A.J. (1999) User's guide to PHREEQC (version 2): a computer program for speciation, batch reaction,one-dimensional transport and inverse geochemical calculations. Water Resources Investigations Report 95–4259, US Geological Survey, Denver, CO. WEB-PHREEQ, a WWW implementation of the aqueous geochemical modeling program PHREEQC by David Parkhurst of the U.S.G.S.

Pedley, H.M. (1990) Classification and environmental models of cool freshwater tufas. *Sedimentary Geology*, *68*, 143–154. https://doi.org/10.1016/0037-0738(90)90124-C

Pedley, H.M., Rogerson, M. & Middleton, R. (2009) Freshwater calcite precipitates from in vitro mesocosm flume experiments: a case for biomediation of tufas. *Sedimentology*, *56*, 511–527. https://doi.org/10.1111/j.1365-3091.2008.00983.x

Pedley, M. (2014) The morphology and function of thrombolytic calcite precipitating biofilms: a universal model derived from freshwater mesocosm experiments. *Sedimentology*, *61*, 22–40. https://doi.org/10.1111/sed.12042

Peng, X. & Jones, B. (2013) Patterns of biomediated $CaCO_3$ crystal bushes in hot spring deposits. *Sedimentary Geology*, *294*, 105–117. https://doi.org/10.1016/j.sedgeo.2013.05.009

Pentecost, A. (1994) Formation of laminate travertines at Bagno Vignone, Italy. *Geomicrobiology Journal*, *12*, 239–251. https://doi.org/10.1080/01490459409377992

Pentecost, A. (1995a) Geochemistry of carbon dioxide in six travertine-depositing waters of Italy. *Journal of Hydrology*, *167*, 263–278. https://doi.org/10.1016/0022-1694(94)02596-4

Pentecost, A. (1995b) The Quaternary travertine deposits of Europe and Asia Minor. *Quaternary Science Reviews*, *14*, 1005–1028. https://doi.org/10.1016/0277-3791(95)00101-8

Pentecost, A. (2003) Cyanobacteria associated with hot spring travertines. *Canadian Journal of Earth Sciences*, *40*, 1447–1457. https://doi.org/10.1139/e03-075

Pentecost, A. (2005) *Travertine*. Berlin Heidelberg: Springer, 445 p.

Pentecost, A., Bayari, S. & Yesertener, C. (1997) Phototrophic microorganisms of the Pamukkale travertine Turkey: their distribution and influence on travertine deposition. *Geomicrobiology Journal*, *14*, 269–283. https://doi.org/10.1080/01490459709378052

Pentecost, A. & Coletta, P. (2007) The role of photosynthesis and CO_2 evasion in travertine formation: a quantitative investigation at an important travertine-depositing hot spring, Le Zitelle, Lazio, Italy. *Journal Geological Society*, *164*, 843–853. https://doi.org/10.1144/0016-76492006-037

Pentecost, A. & Riding, R. (1986) Calcification of cyanobacteria. In: Leadbeater, B.S.C. & Riding, R. (Eds.) *Biomineralization in lower plants and animals*. *Systematic Association, Special Volume 30*, 73–90.

Pentecost, A. & Tortora, P. (1989) Bagni di Tivoli, Lazio: a modern travertine-depositing site and its associated microorganisms. *Bollettino Società Geologica Italiana*, *108*, 315–324.

Piscopo, V., Barbieri, M., Monetti, V., Pagano, G., Pistoni, S., Ruggi, E. & Stanzione, D. (2006) Hydrogeology of thermal waters in Viterbo area, central Italy. *Hydrogeology Journal*, *14*, 1508–1521. https://doi.org/10.1007/s10040-006-0090-8

Plée, K., Pacton, M. & Ariztegui, D. (2010) Discriminating the role of photosynthetic and heterotrophic microbes triggering low-Mg calcite precipitation in freshwater biofilms (Lake Geneva, Switzerland). *Geomicrobiology Journal*, *27*, 391–399. https://doi.org/10.1080/01490450903451526

Rainey, D.K. & Jones, B. (2009) Abiotic v. biotic controls on the development of the Fairmont Hot Springs carbonate deposit, British Columbia, Canada. *Sedimentology*, *56*, 1832–1857. https://doi.org/10.1111/j.1365-3091.2009.01059.x

Reinhardt, M., Goetz, W., Duda, J.P., Heim, C., Reitner, J. & Thiel, V. (2019) Organic signatures in Pleistocene cherts from Lake Magadi (Kenya) - implications for early Earth hydrothermal deposits. *Biogeosciences*, *16*(12), 2443–2465. https://doi.org/10.5194/bg-16-2443-2019

Reitner, J. (1993) Modern cryptic microbialite/metazoan facies from Lizard Island (Great Barrier Reef, Australia): formation and Concept. *Facies*, *29*, 3–40. https://doi.org/10.1007/BF02536915

Reitner, J. (2004) Organomineralization: a clue to the understanding of meteorite related “bacteria-shaped” carbonate particles. In: Seckbach, J. (Ed.) *Origins. Genesis, evolution and diversity of life*. Dordrecht, The Netherlands: Kluwer Academic Publishers, pp. 195–212.

Reitner, J., Arp, G., Thiel, V., Gautret, P., Galling, U. & Michaelis, W. (1997) Organic matter in Great Salt Lake ooids (Utah, USA) – first approach to a formation of organic matrices. *Facies*, *36*, 210–219.

Reitner, J. & Gautret, P. (1996) Skeletal formation in the modern but ultraconservative chaetetid sponge *Spirastrella* (*Acanthochaetetes*) wellsi (Demospongiae, Porifera). *Facies*, *34*(1), 193–207. https://doi.org/10.1007/BF02546164

Reitner, J., Gautret, P., Marin, F. & Neuweiler, F. (1995a) Automicrites in a modern marine microbialite. Formation model via organic matrices (Lizard Island, Great Barrier Reef, Australia). *Bulletin de l'Institut océanographique de Monaco, Spec Issue*, *14*, 237–263.

Reitner, J., Hoffmann, F. & Dröse, W. (2004) Workshop Geohistologie. In: Reitner, J., Reich, M. & Schmidt, G. (Eds.) *Geobiologie 2, 74. Jahrestagung der Paläontologischen Gesellschaft in Göttingen 02. Bis 08*. Oktober 2004, Exkursionen und Workshops, pp. 211–226.Göttingen: Universitätsdrucke.

Reitner, J., Neuweiler, F. & Gautret, P. (1995b) Modern and fossil automicrites: implications for mud mound genesis. In: Reitner, J. & Neuweiler, F. (Coords) *A polygenetic spectrum of fine-grained carbonate buildups*. *Facies*, *32*, 4–17.

Reitner, J., Paul, J., Arp, G. & Hause-Reitner, D. (1996) Lake Thetis domal microbialites – a complex framework of calcified biofilms and organomicrites (Cervantes, Western Australia). In: Reitner, J., Neuweiler, F. & Gunkel, F. (Eds.) *Reef evolution*. Research Reports. *Göttinger Arbeiten zur Geologie und Paläontologie*, *Sb2*, 85–89.

Reitner, J., Thiel, V., Zankl, H., Michaelis, W., Wörheide, G. & Gautret, P. (2000) Organic and biogeochemical patterns in cryptic microbialites. In: Riding, R.E. & Awramik, S.M. (Eds.) *Microbial sediments*. Berlin, Heidelberg: Springer-Verlag, pp. 149–160.

Reitner, J., Wörheide, G., Lange, R. & Schumann-Kindel, G. (2001) Coralline Demosponges - A geobiological portrait. In: Mori, K., Ezaki, Y. & Sorauf, J. (Eds.) *Proceedings of the 8th international symposium on Fossil Cnidaria and Porifera, September 1999, Sendai*. *Bulletin of the Tohoku University Museum*, *1*, 219–235.

Reysenbach, A.L. & Cady, S.L. (2001) Microbiology of ancient and modern hydrothermal systems. *Trends in Microbiology*, *9*, 79–86. https://doi.org/10.1016/S0966-842X(00)01921-1

Reysenbach, A.L., Ehringer, M. & Hershberger, K. (2000) Microbial diversity at 83°C in Calcite Springs, Yellowstone National Park: another environment where the Aquificales and "Korarchaeota" coexist. *Extremophiles*, *4*, 61–67. https://doi.org/10.1007/s007920050008

Reysenbach, A.L., Seitzinger, S., Kirshtein, J. & McLaughlin, E. (1999) Molecular constraints on a high-temperature evolution of early life. *The Biological Bulletin*, *196*, 367–372. https://doi.org/10.2307/1542972

Reysenbach, A.L. & Shock, E. (2002) Merging genomes with geochemistry in hydrothermal ecosystems. *Science*, *296*, 1077–1082. https://doi.org/10.1126/science.1072483

Riding, R. (2000) Microbial carbonates: the geological record of calcified bacterial-algal mats and biofilms. *Sedimentology*, *47*, 179–214. https://doi.org/10.1046/j.1365-3091.2000.00003.x

Riding, R. (2008) Abiogenic, microbial and hybrid authigenic carbonate crusts: components of Precambrian stromatolites. *Geologia Croatica*, *61*, 73–103.

Robbins, L.L. & Blackwelder, P.L. (1992) Biochemical and ultrastructural evidence for the origin of whitings: a biologically induced calcium carbonate precipitation mechanism. *Geology*, *20*, 464–468. https://doi.org/10.1130/0091-7613(1992)020<0464:BAUEFT>2.3.CO;2

Rodriguez-Navarro, C., Kudłacz, K., Cizer, Ö. & Ruiz-Agudo, E. (2015) Formation of amorphous calcium carbonate and its transformation into mesostructured calcite. *CrystEngComm*, *17*, 58–72. https://doi.org/10.1039/c4ce01562b

Roeselers, G., Norris, T.B., Castenholz, R.W., Rysgaard, S., Glud, R.N., Kühl, M. & Muyzer, G. (2007) Diversity of phototrophic bacteria in microbial mats from Arctic hot springs (Greenland). *Environmental Microbiology*, *9*, 26–38. https://doi.org/10.1111/j.1462-2920.2006.01103.x

Rogerson, M., Mercedes-Martín, R., Brasier, A.T., McGill, R.A., Prior, T.J., Vonhof, H., Fellows, S.M., Reijmer, J.J.G., McClymont, E., Billingh, I., Matthews, A. & Pedley, H.M. (2017) Are spherulitic lacustrine carbonates an expression of large-scale mineral carbonation? A case study from the East Kirkton Limestone, Scotland. *Gondwana Research*, *48*, 101–109. https://doi.org/10.1016/j.gr.2017.04.007

Romeis, B. (1989) *Mikroskopische Technik* (ed by P. Böck). 17. Aufl. München: Urban & Schwarzenberg.

Ronchi, P. & Cruciani, F. (2015) Continental carbonates as a hydrocarbon reservoir, an analog case study from the travertine of Saturnia, Italy. *AAPG Bulletin*, *99*, 711–734. https://doi.org/10.1306/10021414026

Rothschild, L.J. & Mancinelli, R.L. (2001) Life in extreme environments. *Nature*, *409*, 1092–1101. https://doi.org/10.1038/35059215

Roy, S., Debnath, M. & Ray, S. (2014) Cyanobacterial flora of the geothermal spring at Panifala, West Bengal, India. *Phykos*, *44*, 1–8.

Ruff, S.W. & Farmer, J.D. (2016) Silica deposits on Mars with features resembling hot spring biosignatures at El Tatio in Chile. *Nature Communications*, *7*(1), 1–10. https://doi.org/10.1038/ncomms13554

Salminen, P.E., Brasier, A.T., Karhu, J.A. & Melezhik, V.A. (2014) Travertine precipitation in the Paleoproterozoic Kuetsjärvi Sedimentary Formation, Pechenga Greenstone Belt, NE Fennoscandian Shield. *Precambrian Research*, *255*, 181–201. https://doi.org/10.1016/j.precamres.2014.09.023

Sanchez-Garcia, L., Fernandez-Martinez, M.A., García-Villadangos, M., Blanco, Y., Cady, S.L., Hinman, N., Bowden, M.E., Pointing, S.B., Lee, K.C., Warren-Rhodes, K., Lacap-Bugler, D., Cabrol, N.A., Parro, V. & Carrizo, D. (2019) Microbial biomarker transition in high-altitude sinter mounds from El Tatio (Chile) through different stages of hydrothermal activity. *Frontiers in Microbiology*, *9*, 3350. https://doi.org/10.3389/fmicb.2018.03350

Sánchez-Navas, A., Martín-Algarra, A., Rivadeneyra, M.A., Melchor, S. & Martín-Ramos, J.D. (2009) Crystal-growth behavior in Ca-Mg carbonate bacterial spherulites. *Crystal Growth Design*, *9*, 2690–2699. https://doi.org/10.1021/cg801320p

Sand, K.K., Rodriguez-Blanco, J.D., Makovicky, E., Benning, L.G. & Stipp, S.L.S. (2011) Crystallization of $CaCO_3$ in water-alcohol mixtures: spherulitic growth, polymorph stabilization, and morphology change. *Crystal Growth Design*, *12*, 842–853. https://doi.org/10.1021/cg2012342

Schulz, G., Schneider, D., Brinkmann, N., Edy, N., Daniel, R., Polle, A., Scheu, S. & Krashevska, V. (2019) Changes in trophic groups of protists with conversion of rainforest into rubber and oil palm plantations. *Frontiers in Microbiology*, *10*, 240. https://doi.org/10.3389/fmicb.2019.00240

Scott, J.E. & Dorling, J. (1965) Differential staining of acid glycosaminoglycans (mucopolysaccharides) by Alcian blue in salt solutions. *Histochemie*, *5*, 221–233.

Shiraishi, F., Eno, Y., Nakamura, Y., Hanzawa, Y., Asada, J. & Bahniuk, A.M. (2019) Relative influence of biotic and abiotic processes on travertine fabrics, Satono-yu hot spring, Japan. *Sedimentology*, *66*, 459–479. https://doi.org/10.1111/sed.12482

Shtukenberg, A.G., Punin, Y.O., Gunn, E. & Kahr, B. (2011) Spherulites. *Chemical Reviews*, *112*, 1805–1838. https://doi.org/10.1021/cr200297f

Smythe, W.F., McAllister, S.M., Hager, K.W., Hager, K.R., Tebo, B.M. & Moyer, C.L. (2016) Silica biomineralization of *Calothrix*-dominated biofacies from Queen's Laundry Hot-Spring, Yellowstone National Park, USA. *Frontiers in Environmental Science*, *4*, article 40, 1–11. DOI: https://doi.org/10.3389/fenvs.2016.00040

Sompong, U., Hawkins, P.R., Besley, C. & Peerapornpisal, Y. (2005) The distribution of cyanobacteria across physical and chemical gradients in hot springs in northern Thailand. *FEMS Microbiology Ecology*, *52*, 365–376. https://doi.org/10.1016/j.femsec.2004.12.007

Sugihara, C., Yanagawa, K., Okumura, T., Takashima, C., Harijoko, A. & Kano, A. (2016) Transition of microbiological and sedimentological features associated with the geochemical gradient in a travertine mound in northern Sumatra, Indonesia. *Sedimentary Geology*, *343*, 85–98. https://doi.org/10.1016/j.sedgeo.2016.07.012

Tobler, D.J., Blanco, J.R., Dideriksen, K., Sand, K.K., Bovet, N., Benning, L.G. & Stipp, S.L.S. (2014) The effect of aspartic acid and glycine on amorphous calcium carbonate (ACC) structure, stability and crystallization. *Procedia Earth and Planetary Science*, *10*, 143–148. https://doi.org/10.1016/j.proeps.2014.08.047

Tong, H., Ma, W., Wang, L., Wan, P., Hu, J. & Cao, L. (2004) Control over the crystal phase, shape, size and aggregation of calcium carbonate via a L-aspartic acid inducing process. *Biomaterials*, *25*, 3923–3929. https://doi.org/10.1016/j.biomaterials.2003.10.038

Tosca, N.J. & Wright, V.P. (2018) Diagenetic pathways linked to labile Mg-clays in lacustrine carbonate reservoirs: a model for the origin of secondary porosity in the Cretaceous pre-salt Barra Velha Formation, offshore Brazil. In: Armitage, P.J., Butcher, A.R., Churchill, J.M., Csoma, A.E., Hollis, C., Lander, R.H., Omma, J.E. & Worden, R.H. (Eds.) *Reservoir quality of clastic and carbonate rocks: analysis, modelling and prediction*. *Geological Society London, Special Publications*, *435*, 33–46. https://doi.org/10.1144/SP435.1

Tracy, S.L., Williams, D.A. & Jennings, H.M. (1998) The growth of calcite spherulites from solution: II. Kinetics of formation. *Journal of Crystal Growth*, *193*, 382–388. https://doi.org/10.1016/S0022-0248(98)00521-1

Trichet, J. & Défarge, C. (1995) Non-biologically supported organomineralisation. *Bulletin de l'Institut océanographique de Monaco*, Special Issue, *14*, 203–236.

Valeriani, F., Crognale, S., Protano, C., Gianfranceschi, G., Orsini, M., Vitali, M. & Romano Spica, V. (2018) Metagenomic analysis of bacterial community in a travertine depositing hot spring. *New Microbiologica*, *41*, 126–135.

Verrecchia, E.P., Freytet, P., Verrecchia, K.E. & Dumont, J.L. (1995) Spherulites in calcrete laminar crusts: biogenic $CaCO_3$ precipitation as a major contributor to crust formation. *Journal of Sedimentary Research*, *65*, 690–700. https://doi.org/10.1306/D426819E-2B26-11D7-8648000102C1865D

Veysey, J., Fouke, B.W., Kandianis, M.T., Schickel, T.J., Johnson, R.W. & Goldenfeld, N. (2008) Reconstruction of water temperature, pH, and flux of ancient hot springs from travertine depositional facies. *Journal of Sedimentary Research*, *78*, 69–76. https://doi.org/10.2110/jsr.2008.013

Viehmann, S., Reitner, J., Tepe, N., Hohl, S.V., Van Kranendonk, M., Hofmann, T., Koeberl, C. & Meister, P. (2020) Carbonates and cherts as archives of seawater chemistry and habitability on a carbonate platform 3.35 Ga ago: insights from Sm/Nd dating and trace element analysis from the Strelley Pool Formation, Western Australia. *Precambrian Research*, *344*, 105742. https://doi.org/10.1016/j.precamres.2020.105742

Visscher, P.T., Reid, R.P. & Bebout, B.M. (2000) Microscale observations of sulfate reduction: correlation of microbial activity with lithified micritic laminae in modern marine stromatolites. *Geology*, *28*(10), 919–922. https://doi.org/10.1130/0091-7613(2000)28<919:MOOSRC>2.0.CO;2

von Hoyningen-Huene, A.J.E., Schneider, D., Fussmann, D., Reimer, A., Arp, G. & Daniel, R. (2019) Bacterial succession along a sediment porewater gradient at Lake Neusiedl in Austria. *Scientific Data*, *6*, 163. https://doi.org/10.1038/s41597-019-0172-9

Ward, D.M., Ferris, M.J., Nold, S.C. & Bateson, M.M. (1998) A natural view of microbial biodiversity within hot spring cyanobacterial mat communities. *Microbiology and Molecular Biology Reviews*, *62*, 1353–1370. https://doi.org/10.1128/MMBR.62.4.1353-1370.1998

Westall, F., Steele, A., Toporski, J., Walsh, M., Allen, C., Guidry, S., McKay, D., Gibson, E. & Chafetz, H. (2000) Polymeric substances and biofilms as biomarkers in terrestrial materials: implications for extraterrestrial samples. *Journal of Geophysical Research Planets*, *105*(E10), 24511–24527. https://doi.org/10.1029/2000JE001250

Wingender, J., Neu, T.R. & Flemming, H.C. (Eds) (1999) *Microbial extracellular polymeric substances*. Berlin: Springer-Verlag, 251 p.

Wright, V.P. & Barnett, A. (2015) An abiotic model for the development of textures in some South Atlantic early Cretaceous lacustrine carbonates. In: Bosence, D.W.J., Gibbons, K.A., Le Heron, D.P., Morgan, W.A., Pritchard, T. & Vining, B.A. (Eds.) *Microbial carbonates in space and time: implications for global exploration and production*. *Geological Society London*, Special Publications, *418*, 209–219. https://doi.org/10.1144/SP418.3

Zhang, C.L., Fouke, B.W., Bonheyo, G.T., Peacock, A.D., White, D.C., Huang, Y. & Romanek, C.S. (2004) Lipid biomarkers and carbon-isotopes of modern travertine deposits (Yellowstone National Park, USA): implications for biogeochemical dynamics in hot-spring systems. *Geochimica Cosmochimica Acta*, *68*, 3157–3169. https://doi.org/10.1016/j.gca.2004.03.005

SUPPORTING INFORMATION

Additional supporting information may be found online in the Supporting Information section.

How to cite this article: Della Porta G, Hoppert M, Hallmann C, Schneider D, Reitner J. The influence of microbial mats on travertine precipitation in active hydrothermal systems (Central Italy). *Depositional Rec*. 2022;8:165–209. https://doi.org/10.1002/dep2.147

SUPPORTING INFORMATION

The influence of microbial mats on travertine precipitation in active hydrothermal systems (Central Italy)

Giovanna Della Porta[1], Michael Hoppert[2], Christine Hallmann[2], Dominik Schneider[2] and Joachim Reitner[3]

[1] Earth Sciences Department, University of Milan, via Mangiagalli 34, 20133 Milan, Italy. Orcid 0000-0003-3479-0592
[2] Institute of Microbiology and Genetics, Georg-August-University Göttingen, Grisebachstr. 8, 37077 Göttingen, Germany
[3] Geobiology, Göttingen Centre of Geosciences, Georg-August-University Göttingen, Goldschmidtstr. 3, 37077 Göttingen, Germany

*e-mail: giovanna.dellaporta@unimi.it

1. TRAVERTINE DEPOSITIONAL SETTING, THERMAL WATER AND MICROBIAL MAT FEATURES

1.1 Bullicame (Viterbo)

Bullicame is a Holocene travertine mound with a thickness up to 5-10 m, a diameter of at least 220 m and gentle flank dips, with a central orifice from which thermal water is radially flowing and precipitating carbonates (Figure 2, S1). The vent circular pool (8 m wide) is surrounded by a fence (Figure 2A-B) limiting sampling only in a channel (20-40 cm wide) departing from the vent. The channel is accessible at a distance of 12.5 m from the centre of the vent orifice (Figure 2A-C), where measured water temperature (Table 1) is 55°C, cooling down to 50°C at a distance of 48.5-60.5 m from the vent and to 48.2°C at a distance of 83.5 m; pH values gradually increase along the channel from 6.7 to 7.4. Alkalinity decreases from 15.6 meq/l to 14.5 meq/l along the channel. The 1-4 cm deep channel has a laminar flow of water. For the first 25 m (12.5-37.5 m from the vent), the channel centre is draped by a dark orange/purple colour microbial mat changing into a green mat overlain by centimetre-size bundles of white carbonate-encrusted filaments oriented with the flow direction; the channel sides are draped by orange/yellow to green microbial mat with embedded sparse millimetre-size gas bubbles not coated by carbonate (Figure 2C-E). The bundles of filaments are poorly to non-calcified in the proximal areas close to the vent and become distally progressively calcified (Figure 2C-D) resembling the travertine bacterial streamer fabric described by Farmer (2000) [Farmer, J.D. Hydrothermal systems: doorways to early biosphere evolution. GSA Today 2000, 10, 1-9] in the Mammoth Hot Spring (Yellowstone National Park, Wyoming, USA). The channel floor colour gradually changes becoming dark green below the carbonate-encrusted white fans of filamentous microbes (Figure 2D-E, S1). Nearly 60.5 m from the vent the channel becomes progressively dominated by light green to yellow microbial mat with abundant gas bubbles, some of which coated by carbonates (Figure 2F, S1H). The centimetre-size levees at the sides of the channel are light orange to green and draped by microbial mat with calcified gas bubbles, carbonate crusts and paper-thin rafts (Figure 2C-F). The Holocene fossil travertines surrounding the active vent show calcified filamentous bundles comparable to the bacterial streamer fabric.

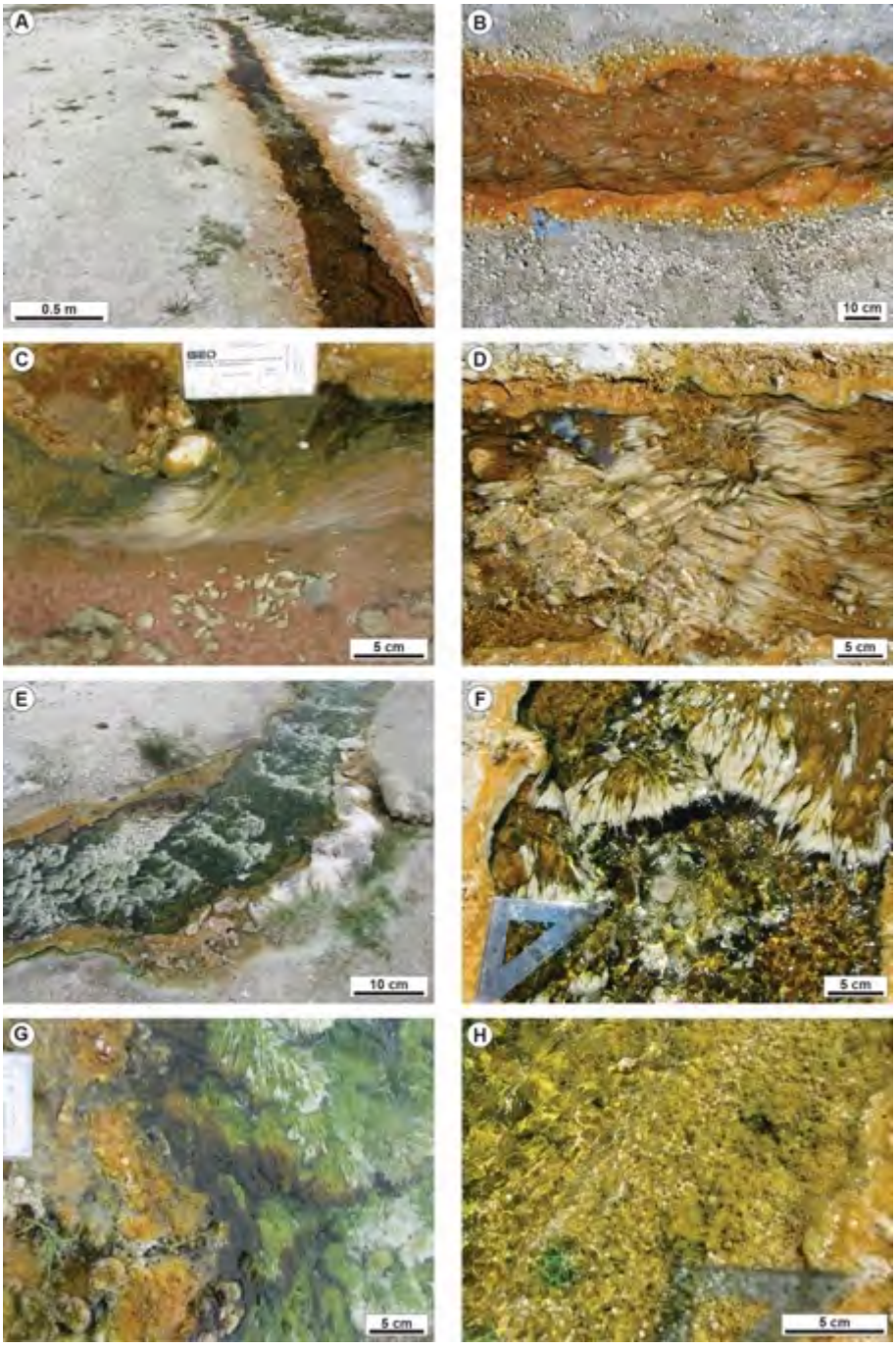

Figure S1. Bullicame (Viterbo) active hydrothermal travertine system. (A, B, C) Proximal channel, from 12.5 m to 20 m from the vent centre, draped by dark orange/purple microbial mat in the centre, with sparse bundles of white filaments oriented according to the current flow direction and with orange/yellow to green microbial mat on the channel margin. (D, E, F) Proximal channel in the stretch from 20 m to 40 m from the vent centre with abundant bundles of carbonate-coated filaments, the channel floor draped by microbial mat that changes in colour from orange/purple to green while the channel margins are orange/yellow to green in colour with gas bubbles. (G) Proximal channel at 30 m from the vent with channel margin characterized by yellow/orange microbial mats with coated gas bubbles and the channel centre rich of white filamentous bundles coated by green to brown microbial mat. (H) Distal channel at 60 m from the vent centre, with centre and margin draped by orange/yellow to green microbial mat with abundant carbonate-coated gas bubbles and rafts.

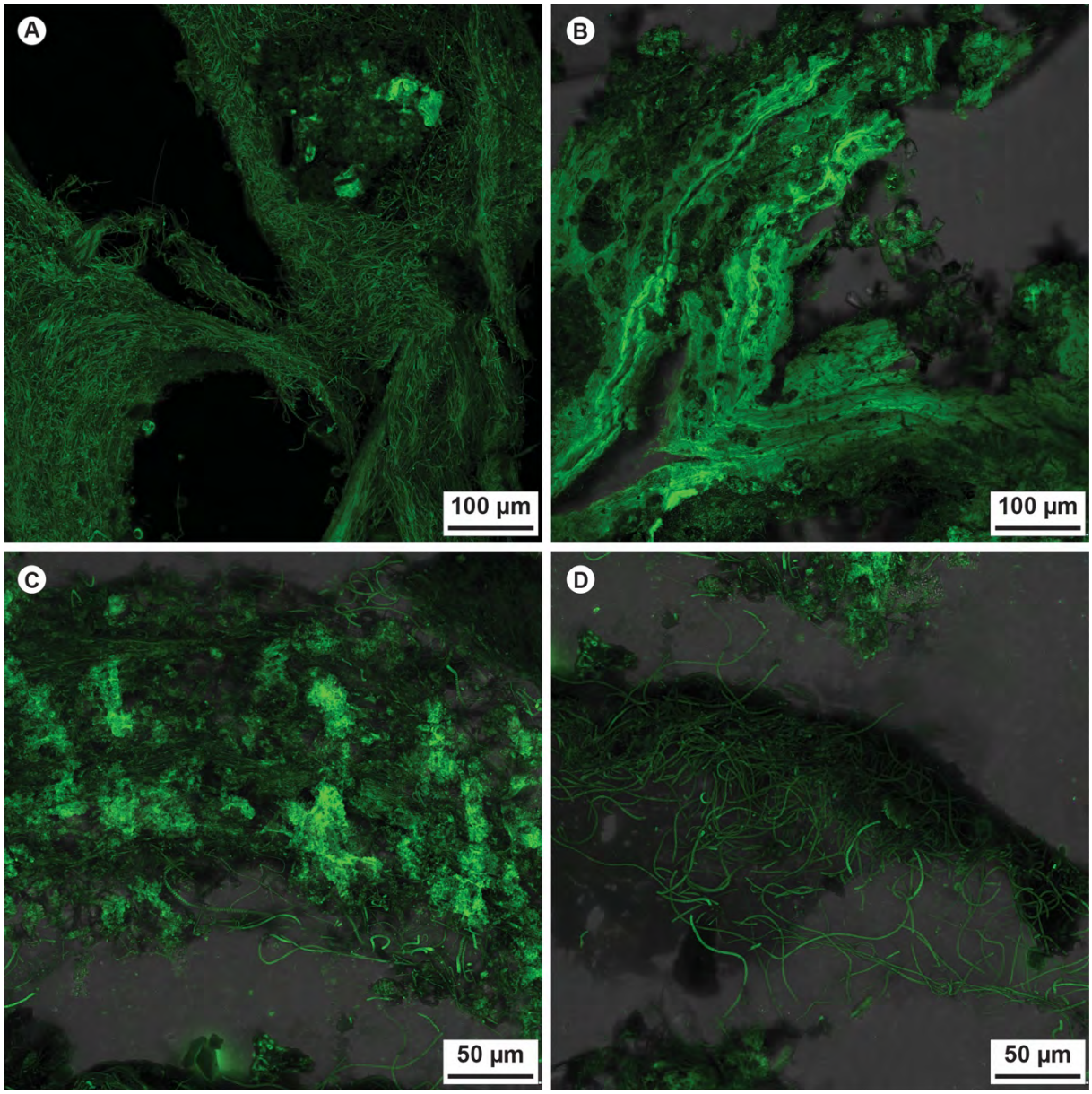

Figure S2. Confocal laser scanning microscope images of samples stained with calcein from Bullicame proximal (A, 30.5 m from vent, sample Bul A 18) and distal channel (B-D, 60.5 m from vent, sample B 12). Calcein, which can be transported through the cell membrane into living cells, is able to chelate calcium within the cell, resulting in green fluorescence. (A, B) Sample from the Bullicame proximal channel showing the bundles of filamentous microbes forming the streamers, possible Chloroflexi and sulphur-oxidizing bacteria. (C, D) Sample from the Bullicame distal channel with abundant EPS and *Spirulina* filamentous cyanobacteria.

1.2 Bollore (Bagni San Filippo)

The travertine deposits of the Bollore hydrothermal vent form an asymmetric mound, approximately 10 m thick and 100 m wide (Figure 7, S3). The main vent at the mound top consists of a circular pool with three orifices (20-50 cm in diameter) from which thermal water outflows into a 15-40 cm wide channel, following the main topographic gradient towards the North (Figure 7A-B).

The maximum water temperature is 49.5°C from one orifice, while for the other two orifices temperature is 46.1-46.5°C (Table 2). The values of pH are 6.5-6.6 at the vent and 7.5 nearly 24.5 m from the orifices where temperature drops to 36.4°C. Alkalinity decreases from 31.7 meq/l to 21.6 meq/l 14 m along the channel.

At the rims of the vent orifices and in the first 8 m of the channel, the channel floor is draped by light orange/pink microbial mat with white filamentous bundles encrusted by carbonate form bacterial streamer fans 1-3 cm wide and 5-8 cm long (Figure 7C-D) oriented with the water flow direction. These carbonate-encrusted filamentous fans can be observed also as fossil travertine streamer deposits on the channel sides (Figure 7E). Around the vent pool, travertines are coated by white to light orange-pink microbial mat, while decimetre-size stagnant pools with a few millimetres water depth and the sides of the channel are covered by white, submillimetre-thick paper-thin rafts with underlying adherent dark green microbial mat. From nearly 8 m from the vent, where temperature drops to 44-41°C (Table 2), light green microbial mat drapes the channel floor and is associated with millimetre-size carbonate coated gas bubbles and rafts (Figure 7E). At 20 to 25 m from the vent, the topographic gradient increases and the light pink to green channel floor is characterized by centimetre-size terraces and pools with coated gas bubbles, coated grains and dendrites (Figure 7F). The main vent and channel at Bollore visited during the humid winter season (January) had a different appearance thriving with green to brown/pink coloured microbial mat and abundant carbonate-encrusted filamentous bundles (Figure S3).

A second vent is present at the Bollore mound (Figure 7A, S3) in a lower topographic position, at the base of the mound flank. Here the temperature measured is 49.3 °C and pH 6.5. The decimetre-wide channel departing from this second vent is draped by carbonate-encrusted filamentous bundles. The channel floor and margins are stained by bright yellow sulphur precipitates and the carbonate and detrital sediments appear black stained by sulphide coatings.

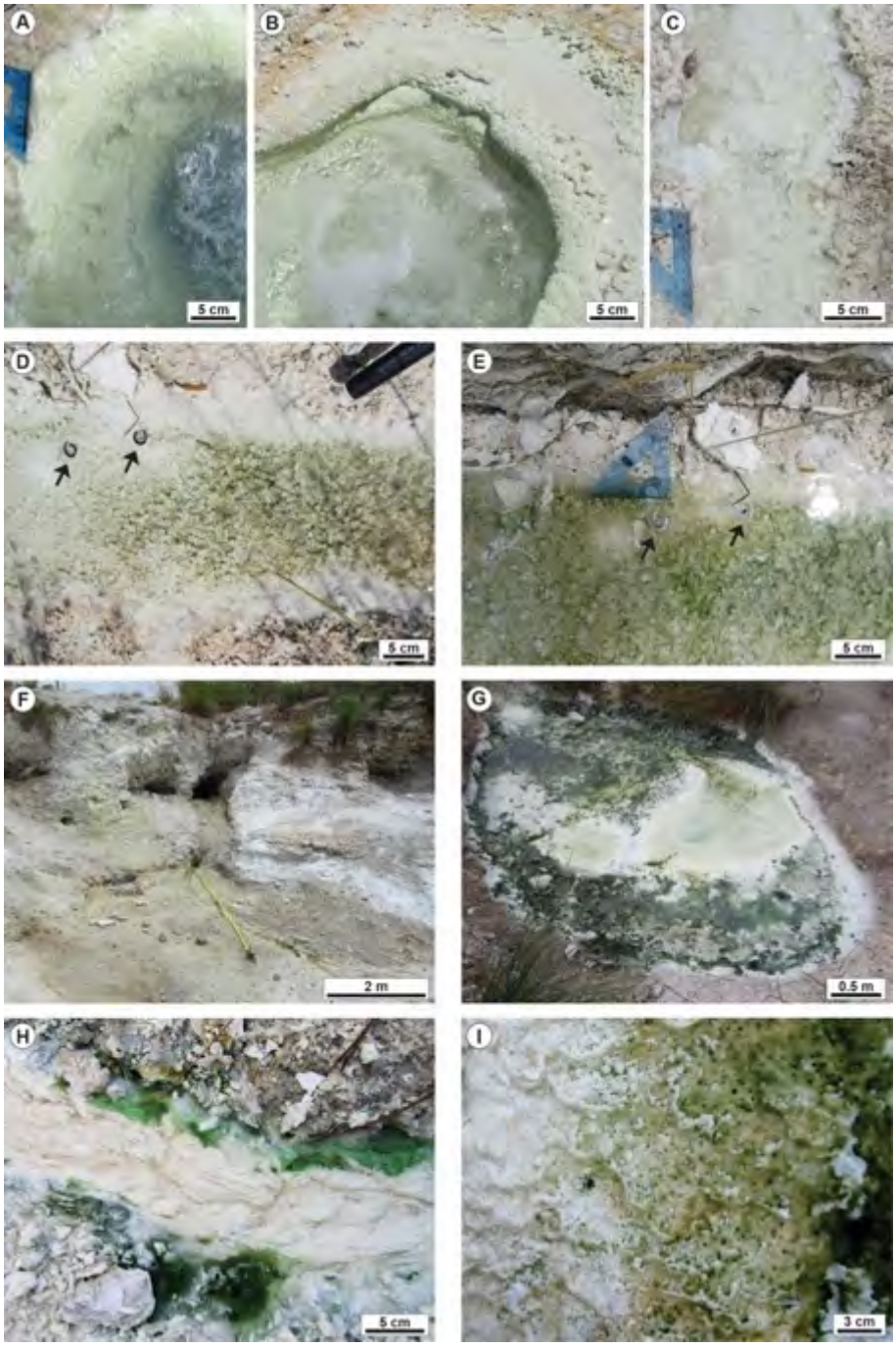

Figure S3. Bollore (Bagni San Filippo) active hydrothermal travertine system. (A, B) Close-up views of the vent orifices with the pool rims encrusted by carbonate as coated filaments and dendrites. (C) Proximal channel with white carbonate-encrusted bundles of filaments and paper thin rafts. (D, E) Distal channel 12 m from the vent with the channel floor draped by green microbial mat with abundant carbonate-coated gas bubbles. The two images were taken during two following days: to notice that the two dead worms (black arrows) are not coated by carbonate in Figure S3D whereas are carbonate-coated in the image in Figure S3E taken the following day. This confirms the fast rates of carbonate precipitation producing millimetres-thick carbonate coatings in 24 hours. (F) Second vent and channel in a lower topographic position. The yellow colour of the sediment is provided by abundant sulphur draping the precipitated travertines. (G, H, I) During the winter humid season (January), the main Bollore vent and channel thrive with dark green microbial mats, whereas during the summer sampling (July) the green microbial mat was absent and the channel floor colour was white to light pink.

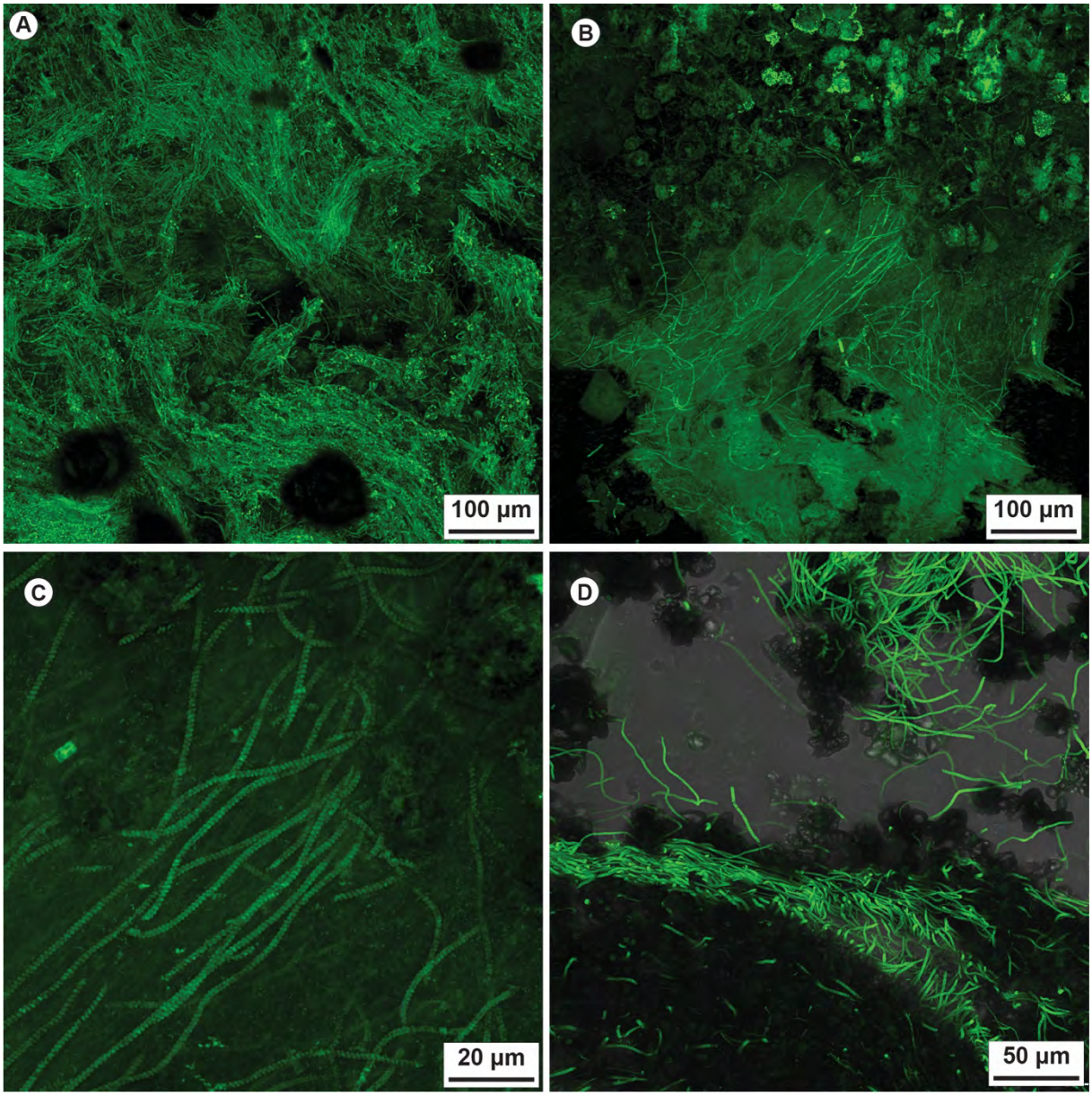

Figure S4. Confocal laser scanning microscope images of samples stained with calcein from Bollore proximal (A, 0.8 m from vent, sample BF 1.3; B-C, 2 m from second vent, sample BF2-2) and distal channel (D, 14 m from vent, sample BF 14). Calcein, which can be transported through the cell membrane into living cells, is able to chelate calcium within the cell, resulting in green fluorescence. (A) Filamentous microbes, likely Chloroflexi and sulphide-oxidizing bacteria, from the calcified streamers sampled in the proximal channel. (B, C) Bollore second vent channel with EPS embedding filamentous microbes and *Spirulina* cyanobacteria. (D) Distal channel with microbial mat dominated by *Spirulina* cyanobacteria.

1.3 Gorello Waterfall (Saturnia)

The Gorello Waterfall travertine deposits form a slope apron fed by a channel running for 1170 m from the thermal spa vent and discharging thermal water at a morphologic break in slope (Figure 12, S5). The travertine slope apron consists of a waterfall (5 m high) and a terraced slope system that distally merges into a river (Figure 12A-B).

Travertine deposits precipitate along the channel, at the waterfall and form the terraced slope (20 m long) with metre-scale sub-horizontal pools separated by rounded rims and sub-vertical walls 0.1-1.5 m high (Figure 12B). Water temperature is nearly 33-33.8°C in the pools; pH values are 7.8-7.9 and alkalinity 9 meq/l (Table 3). The channel levee and the pool rims are coated by olive green millimetre-thick microbial mat (Figure 12C). The pool walls are draped by white and dark to light green filamentous mat encrusted by carbonate (Figure 12D). Pool floors, rims and walls consist of several centimetres to decimetres thick laminated travertine boundstone. The pool floor includes terrigenous mud to sand-size detrital sediment, carbonate coated plant fragments and millimetre- to centimetre-size carbonate coated grains (oncoids; Figure 12E-F). The outer surface of these oncoids appears irregular and pitted by green microbial mat (Figure 12F). Areas of the terraced slope temporarily not flooded by thermal water are sites of vegetation growth, mostly reeds, which are encrusted by carbonate at renewed flows.

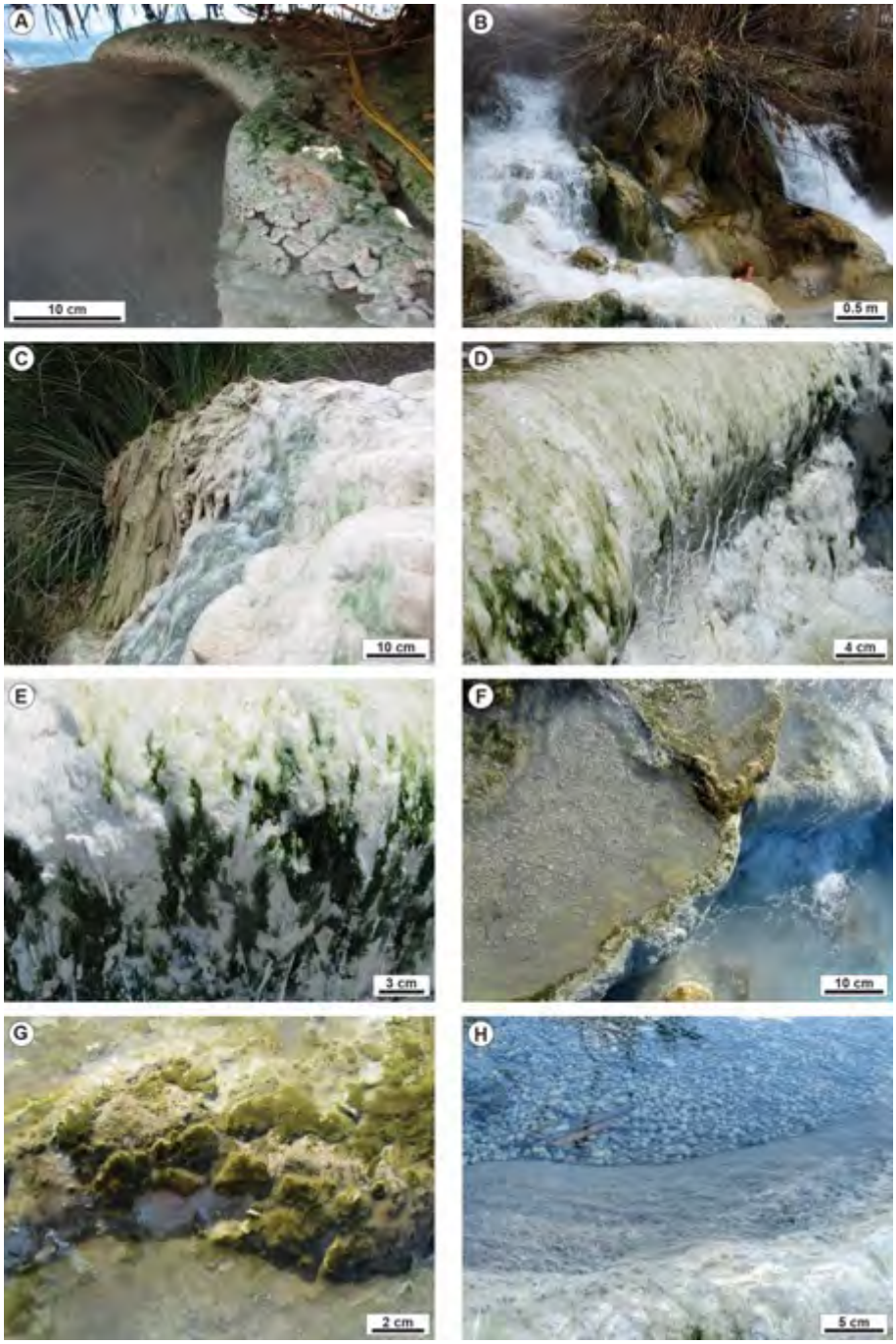

Figure S5. Gorello Waterfall (Saturnia) active hydrothermal travertine system. (A) Photograph showing the channel deriving from the thermal spa more than 1 km away before the break in slope that generates the waterfall. The channel levees are draped by green to pink microbial mats. (B) The nearly 5 m high waterfall developed at the channel topographic break in slope. (C) Areas of the pool rims and walls not flooded by thermal water are temporarily colonized by reed vegetation coated by carbonate precipitates when thermal water flow is resumed. (D, E) The vertical walls of the pools of the terraced slope are coated by white to dark green microbial mat. (F, G) The rims of the pools of the terraced slope are coated by olive green microbial mat. (H) Centimetre-size carbonate coated grains (oncoids) forming on the pool floor.

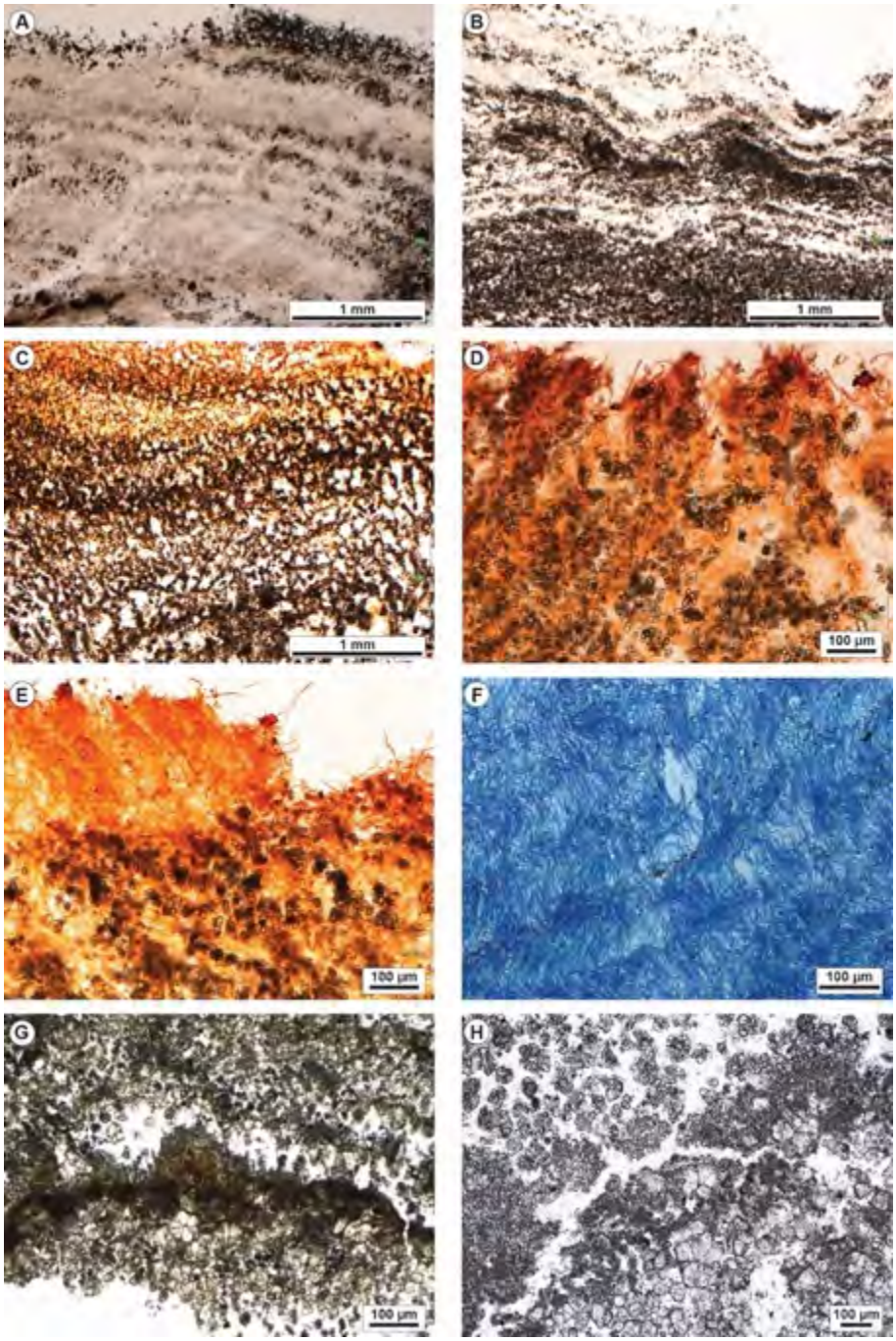

Figure S6. Gorello Waterfall (Saturnia) travertine precipitates from the rims and walls of the terraced slope system. (A) Photomicrograph showing the micritic laminated boundstone with alternation of carbonate precipitates and microbial mat that acted as organic matter substrate for carbonate precipitation. (B) Laminated boundstone showing the wavy lamination made of precipitated calcite crystals alternating with organic matter from the microbial mat. (C) Calcein-stained laminated boundstone showing that carbonate crystals precipitated following the alveolar fabric of the biofilm EPS. (D) Calcein-stained sample showing the microsparite crystals forming rosettes precipitating in between the erect filamentous microbes making the outer layer of the microbial mat. (E) Calcein-stained sample showing the erect filamentous microbes making the outer layer of the microbial mat with below micrite and microsparite precipitated following the spatial distribution of the filamentous microbes. (F) Paraffin sample stained with alcian blue showing the undulose pattern of filamentous microbes in the microbial mats mimicked by the laminated carbonate precipitates. (G) Laminated boundstone with microsparite/sparite rosettes and clotted peloidal micrite laminae. (H) Framework made of microsparite/sparite calcite crystal rosettes and clotted peloidal micrite.

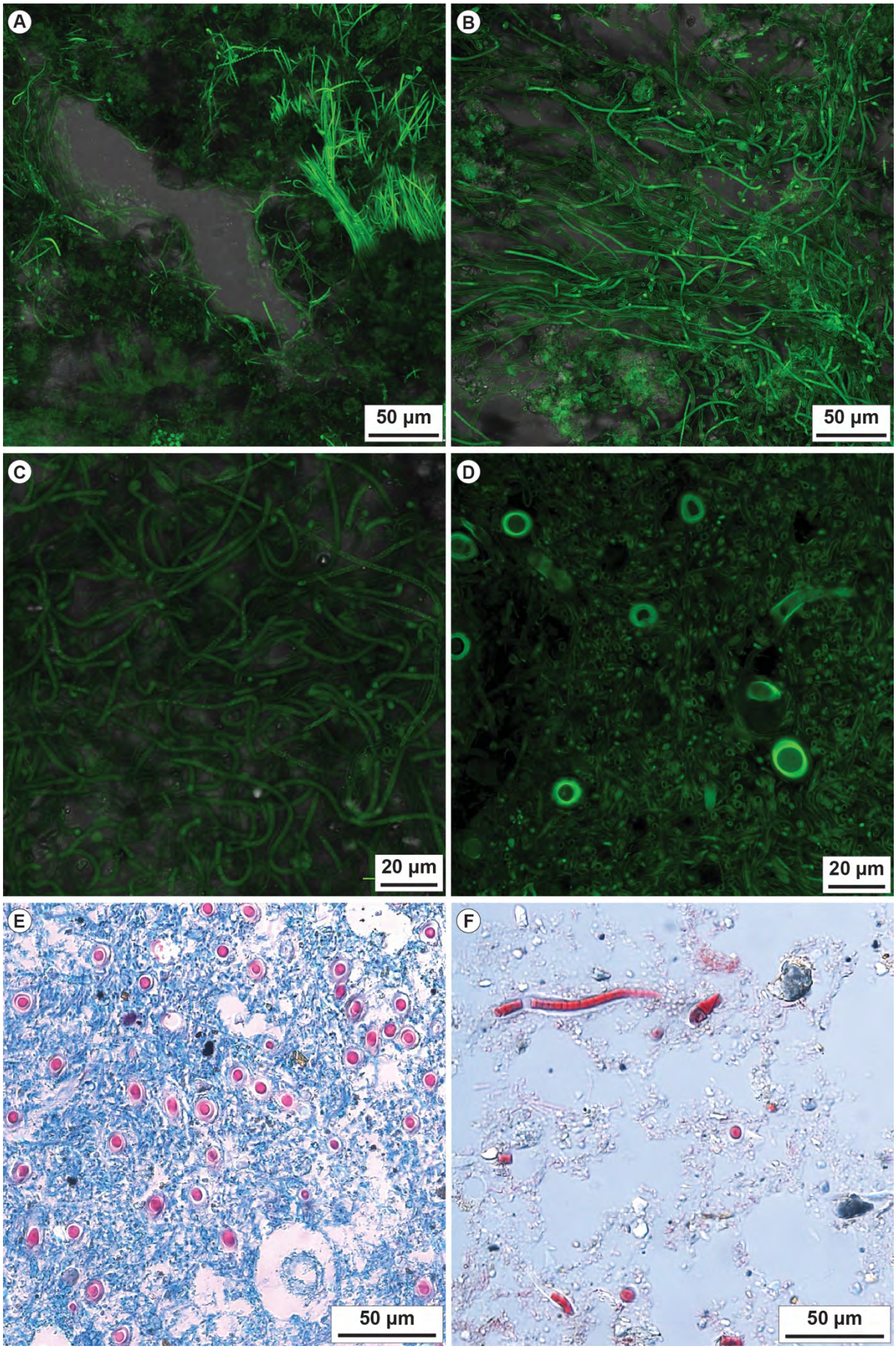
A
50 µm
B
50 µm
C
20 µm
D
20 µm
E
50 µm
F
50 µm

Figure S7 previous page. Confocal laser scanning microscope images of samples stained with calcein from and Gorello Waterfall (5-10 m from waterfall, samples GOR 5, 6, 8, 12). Calcein, which can be transported through the cell membrane into living cells, is able to chelate calcium within the cell, resulting in green fluorescence. (A) Laminated boundstone with carbonate precipitates embedded in EPS and filamentous cyanobacteria including *Spirulina* and segmented forms. The porosity within the microbial mat lacks carbonate precipitates. (B) Erect filamentous cyanobacteria alternating with prostrated filamentous microbes controlling the formation of lamination in the pool rim boundstone. (C) Entangled filamentous cyanobacteria of the Gorello Waterfall microbial mat including also segmented specimens. (D) Confocal laser scanning microscope image showing the cross-section of the thinner filamentous cyanobacteria and the sparse larger size putative *Calothrix* with thick sheath. (E) Paraffin prepared sample stained with alcian blue and cell centre red staining (Kernechtrot) showing the blue network of filamentous cyanobacteria associated with larger size cyanobacteria with a thick sheath, probably *Calothrix thermalis*. Alcian blue is a polysaccharide stain characterising EPS with abundant COO- groups. (F) Paraffin prepared sample stained with Masson-Goldener solution showing the longitudinal section and the segmented appearance of the larger size cyanobacteria inferred as *Calothrix*.

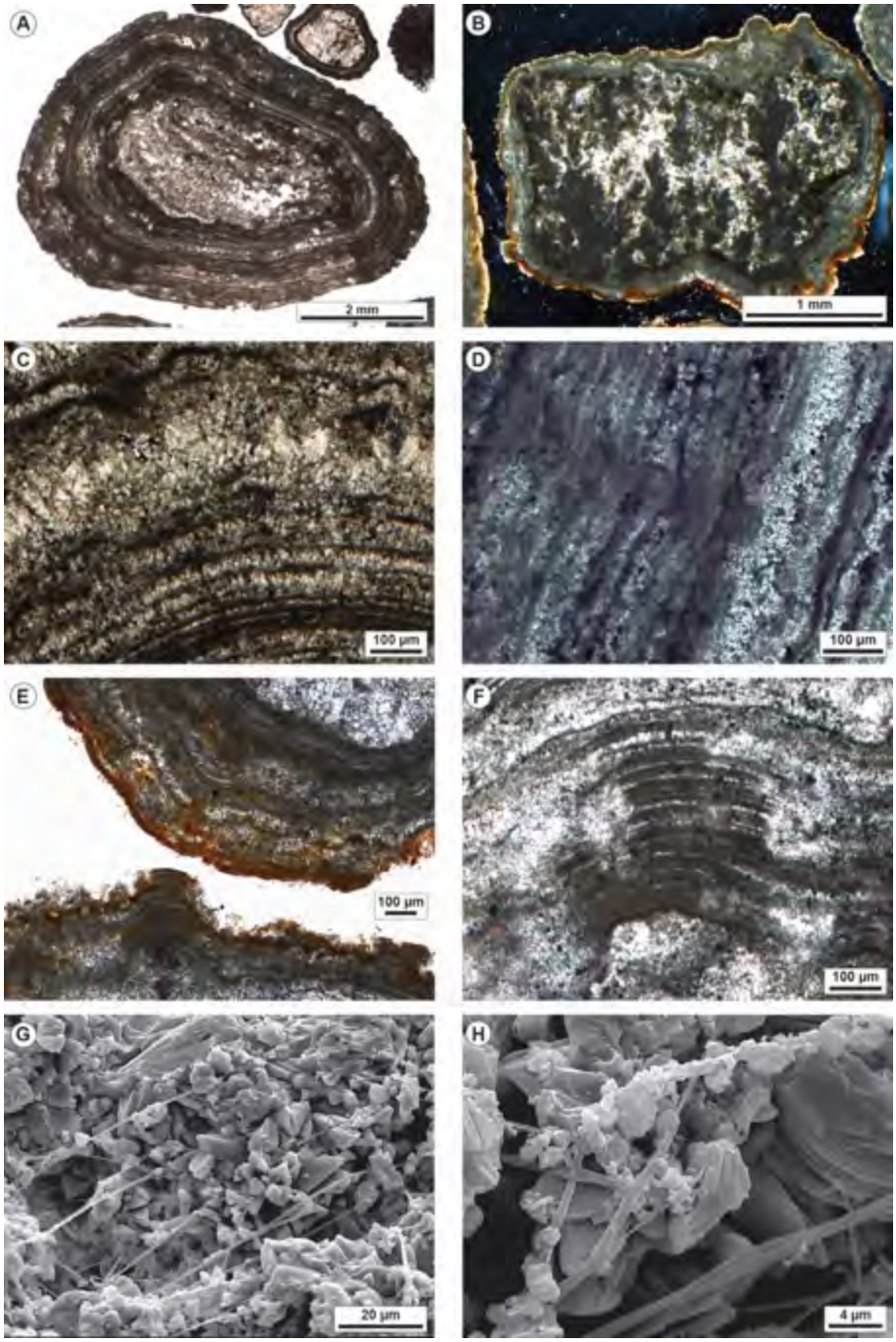

Figure S8. Petrographic and SEM images of the Gorello Waterfall (Saturnia) oncoids from the pools of the terraced slope system (sample Gor 7). (A) Photomicrograph of oncoids with regular parallel undulated laminae made of micrite and microsparite and nuclei made of travertine intraclasts. (B) Crossed polarizers image of an oncoid with the outer surface draped by microbial organic matter stained by tetracycline and nucleus made of travertine intraclast with clotted peloidal micrite dendrites surrounded by calcite spar. (C) Crossed-polarizers image of oncoid laminae made of micrite alternating with palisades of bladed calcite crystals. (D) Micritic and microsparitic laminae of oncoids containing organic matter as evidenced by toluidine staining. (E) Outer portion of the cortex of two oncoids showing the microbial mat draping the outer surface as evidenced by the staining with calcein. The micritic laminae are locally eroded and truncated with organic matter infilling the microborings. (F) Close-up view of truncated micritic laminae and microsparite replacing and filling the void left by removal of the micritic laminae. (G) SEM image of calcite crystals forming the oncoid laminae with filamentous microbes extending perpendicular to the laminae surface. (H) Filamentous microbes within the oncoid cortex encrusted by precipitated micrite.

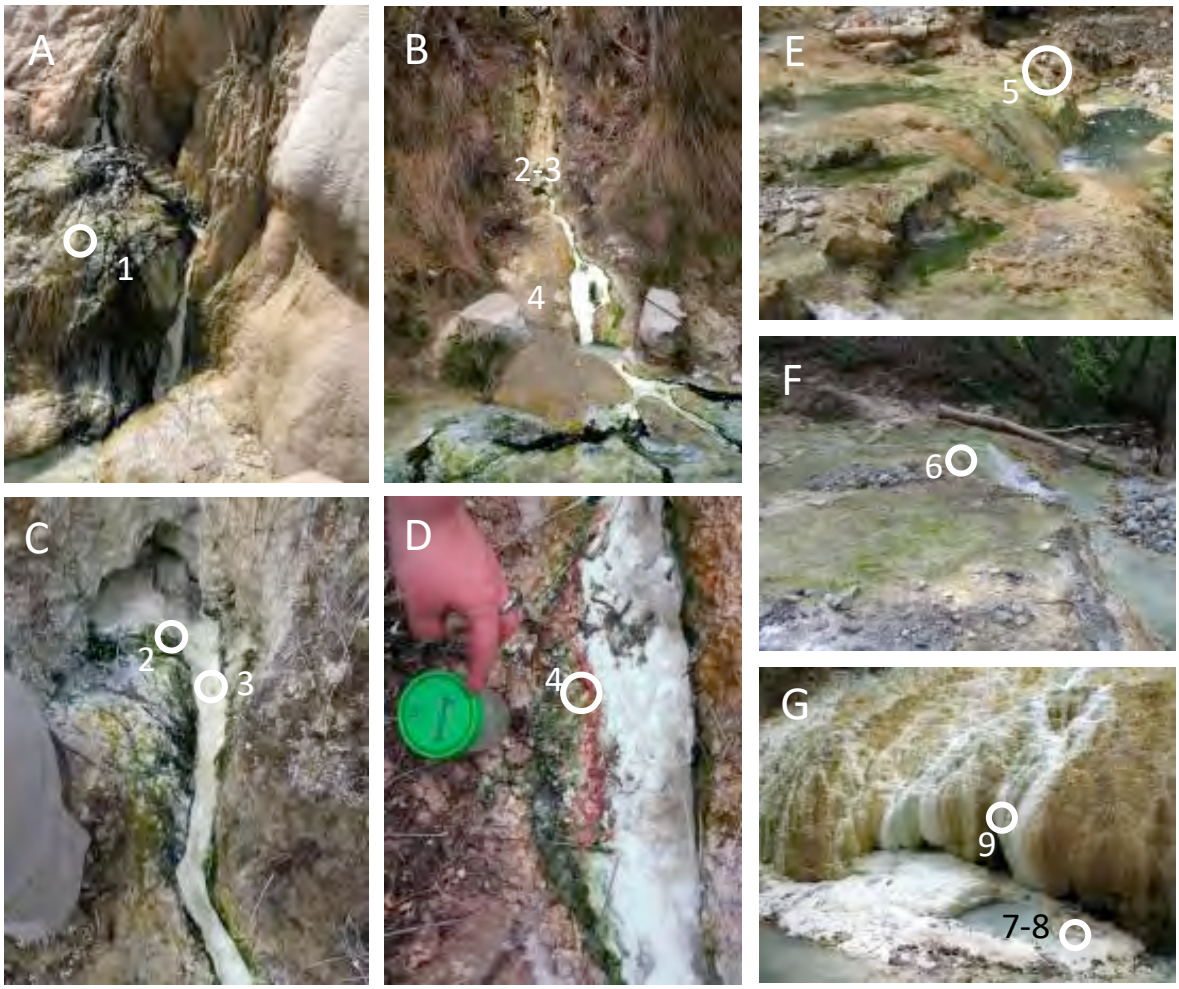

Figure S9. Bagni San Filippo (Fosso Bianco and Balena Bianca) sampling site for geomicrobiological analyses (samples from I4.1 to I4.9 in Table 4). Sampling spots are marked with a white circle and numbers from 1 to 9 indicative of the samples from I4.1 to I4.9 in Table 4. (A) Outflowing water percolating over a travertine cascade covered by a greenish/whitish microbial mat. (B, C, D) Outflow creek of thermal water showing a distinct zonation of differently coloured microbial mats. In (B) the overview of the sampling sites of the cascade with the flowing water creek. In (C) the spot of sample 2 (greenish mat) and 3 (whitish mat in the centre of the creek). In (D) sampling spot of sample 4 with reddish/purple and green microbial mats. (E) Sampling spot 5 in a terrace where the thermal water creek starts to mix with a freshwater stream showing signs of iron oxide/hydroxide precipitation. (F) Terrace wall and adjacent pool formed in the stream with mixed thermal and freshwater with greenish and brown microbial mats. (G) Balena Bianca sampling site with samples 7, 8 and 9 at the toe of the site travertine cascade sourced by the thermal spa. The micro-terraced surface of the travertine cascade is draped by white to pale green and yellow/brown microbial mats.

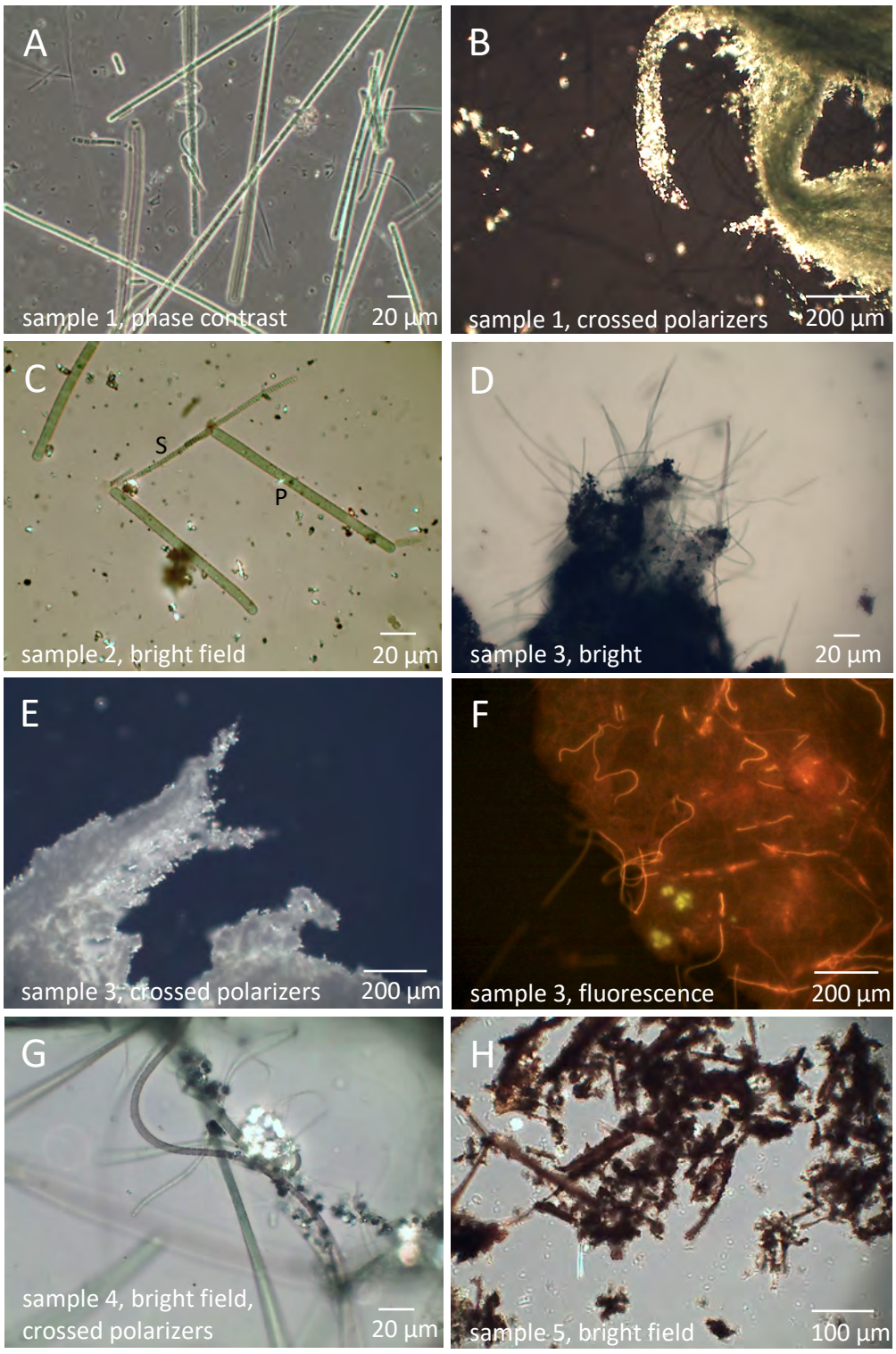

Figure S10. Representative light micrographs of samples from Bagni San Filippo (Fosso Bianco and Balena Bianca). Numbers from 1 to 5 are indicative of the samples from I4.1 to I4.5 in Table 4. (A) Filamentous cyanobacterial, *Phormidium*-like morphotype, which correlates with the dominance of a *Phormidium* ETS-05-related ACV. (B) Crossed polarizers reveal a tuft of light green cyanobacterial filaments with loosely attached, bright shining calcite crystals. (C) The abundant *Phormidium* (P) and *Spirulina* (S) morphotypes, as also confirmed by the most abundant cyanobacterial ACVs in this sample. (D) Thin filaments of putative Cyanobacteria and Chloroflexi morphotypes emerging from precipitates. (E) Calcite precipitate as depicted in D at low magnification. (F) Cyanobacterial filaments attached to a calcite crystal and also encased by calcite showing strong red chlorophyll autofluorescence. The mineral shows a red background fluorescence. (G) Calcite crystals (bright particles in the centre of the image) attached to various cyanobacterial filaments. (H) Filamentous and tubular shapes encrusted by brownish iron oxide/hydroxide are indicative for the presence of iron-oxidizing bacteria (Gallionellaceae-related ASVs).

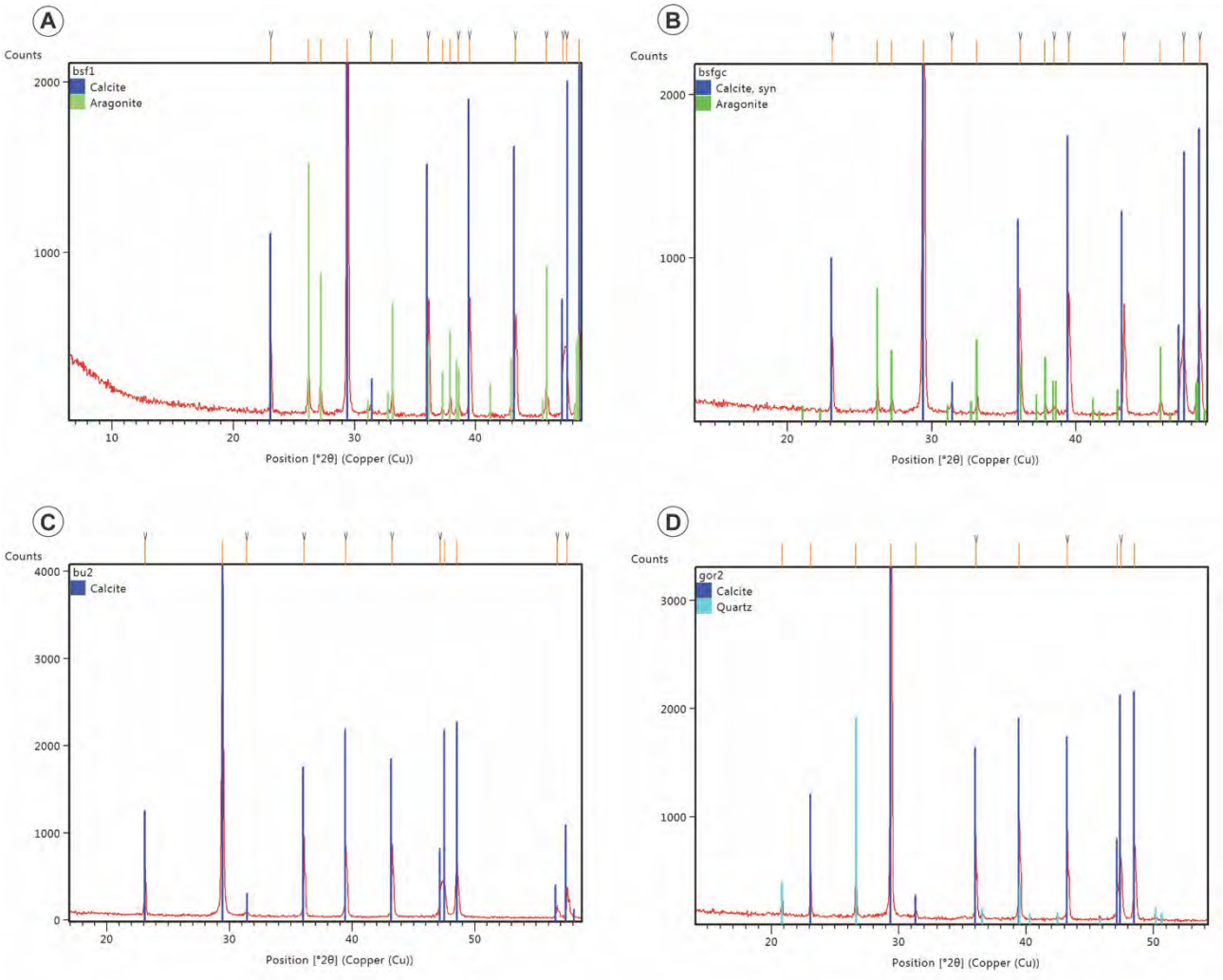

Figure S11. Results of XRD analyses. (A, B) Bollore (Bagni San Filippo) travertine from proximal channel showing the presence of calcite and aragonite. (C) Bullicame travertine from distal channel showing only calcite. (D) Gorello Waterfall sample from terraced slope consisting of calcite associated with detrital quartz.

Figures from S12 to S18 show some of the results of SEM-EDX analyses.

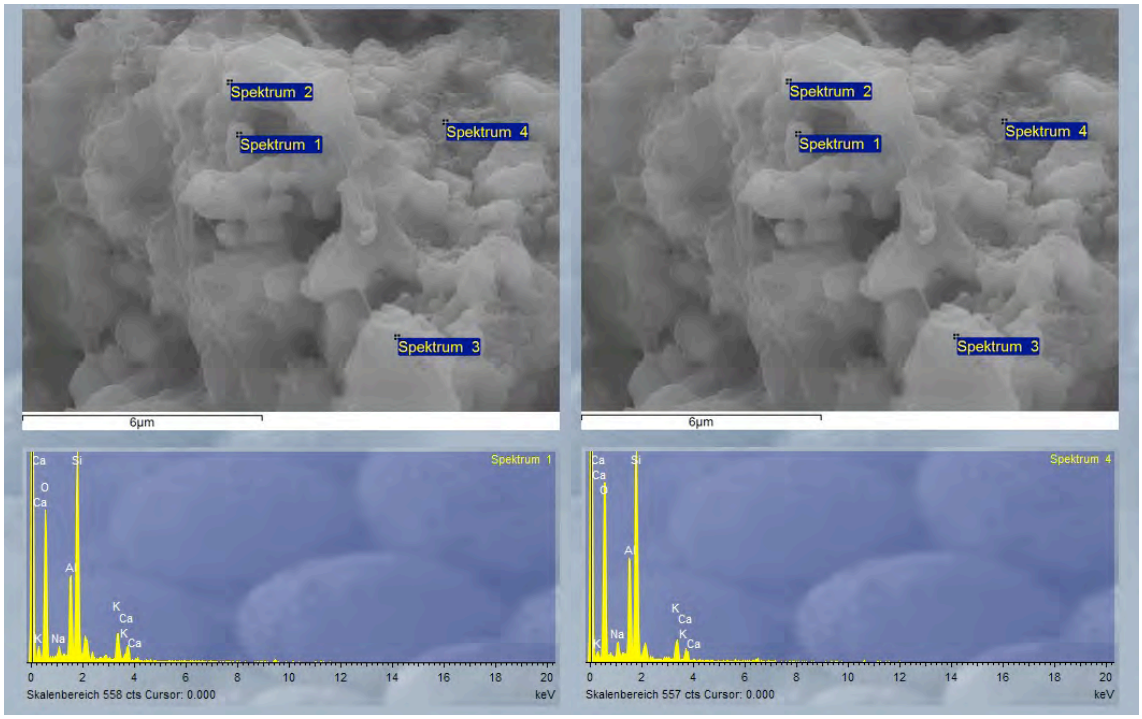

Figure S12. SEM-EDX analysis of Bullicame sample Bul-A-9 from proximal channel 21.5 m from vent. Both analyses on organic matter coating calcite crystals show enrichment in Si, Al, K and Na in addition to Ca.

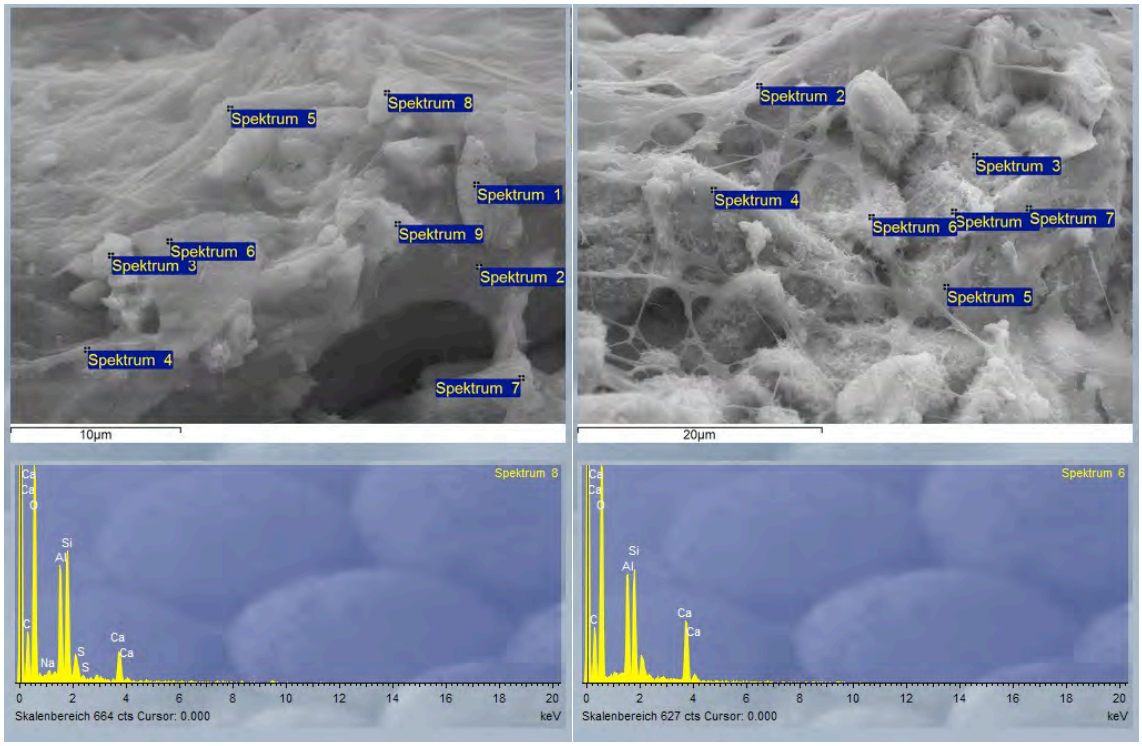

Figure S13. SEM-EDX analysis of Bullicame sample Bul-A-9 from proximal channel 21.5 m from vent. Both analyses on organic matter coating calcite crystals show enrichment in Si, Al, S and Na in addition to Ca.

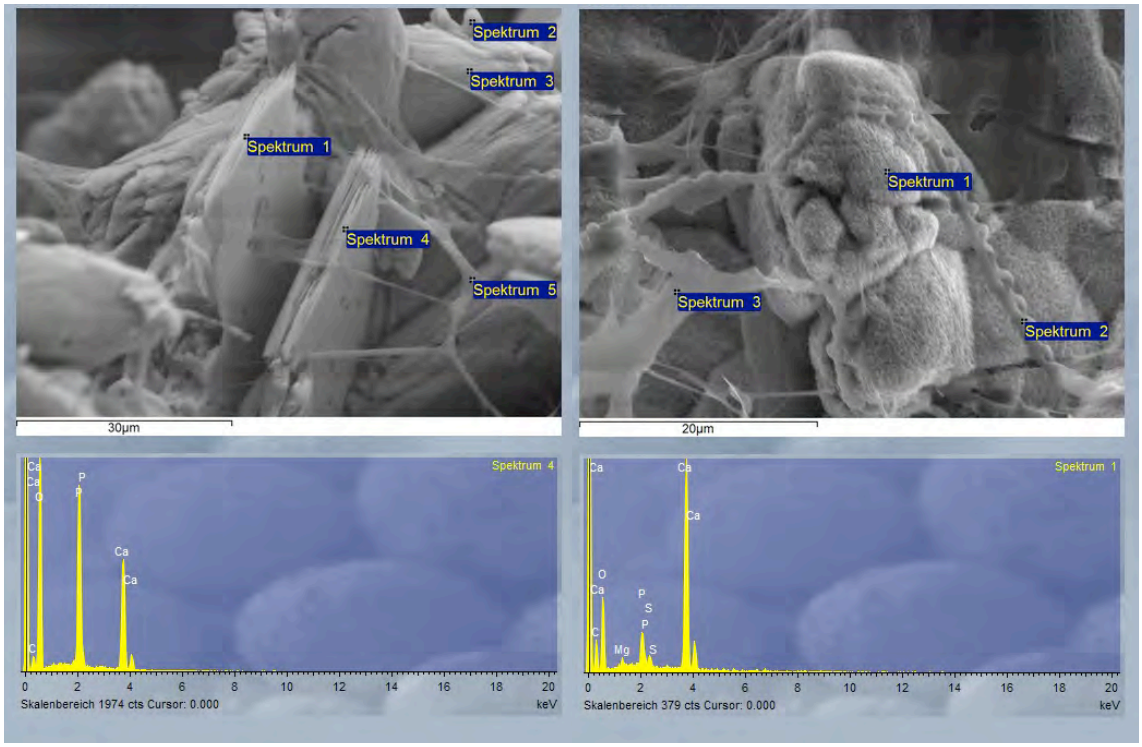

Figure S14. SEM-EDX analysis of Bullicame sample Bul-B-12 from distal channel 61.5 m from vent.
Both analyses show the presence of calcium phosphate as crystals and as coating crystals.
This phosphate might be an artifact related to the use of PBS solution for the glutaraldehyde fixative.
However, EPS and microbes cover the phosphate crystals and coatings on calcite.

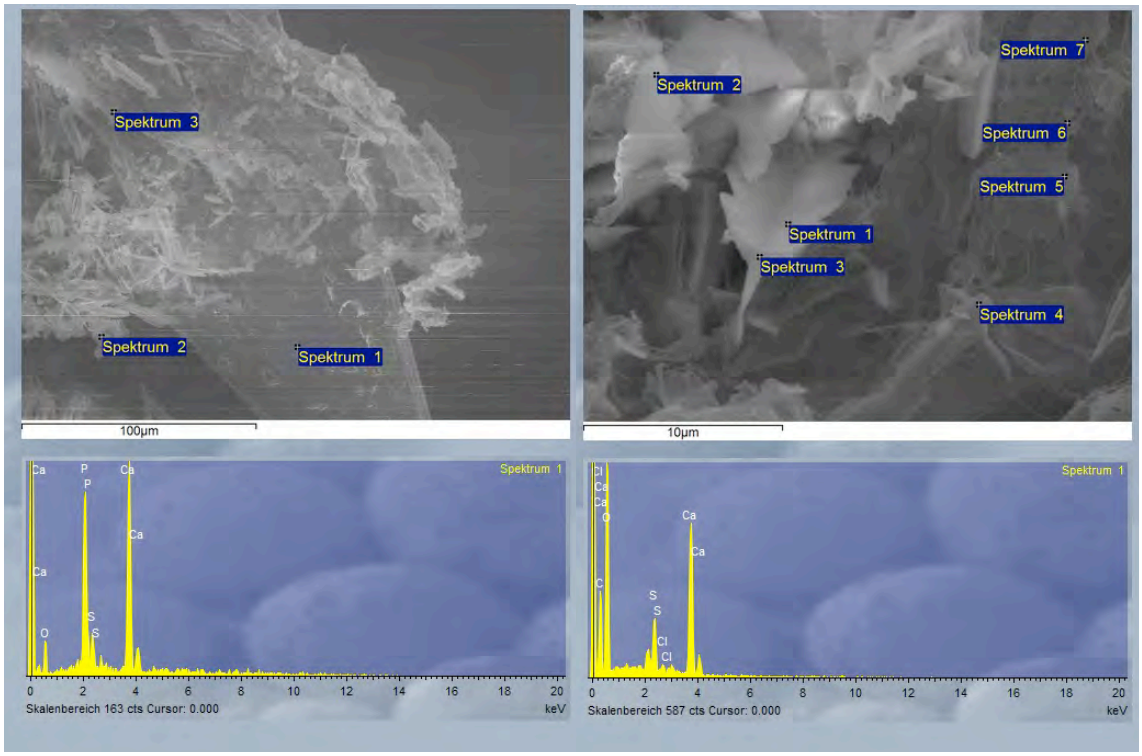

Figure S15. SEM-EDX analysis of Bollore sample BF 1.3 close to the vent (0.8 m).
The analysis on the left shows a calcium phosphate crystal; on the right a gypsum crystal is identified.

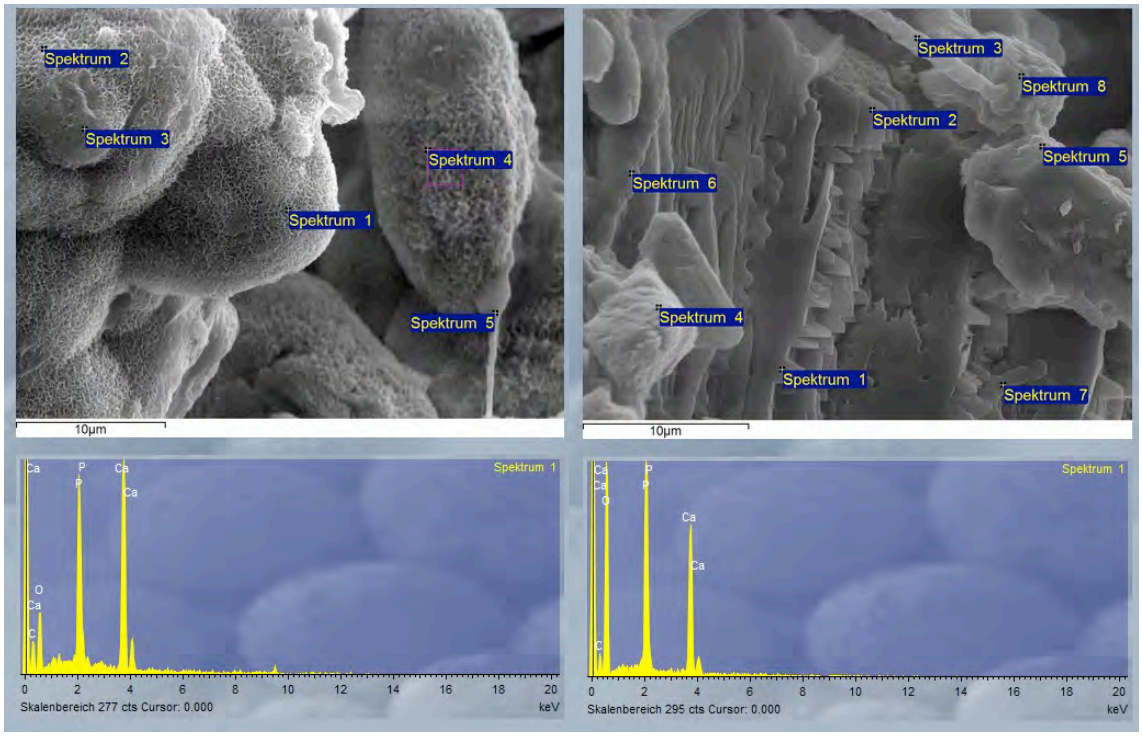

Figure S16. SEM-EDX analysis of Gorello Waterfall sample Gor 8, 5 m from waterfall. Both analyses show enrichment in calcium phosphate both draping calcite crystals on the left and forming calcium phosphate crystals. This phosphate might be an artifact related to the use of PBS solution for the glutaraldehyde fixative.

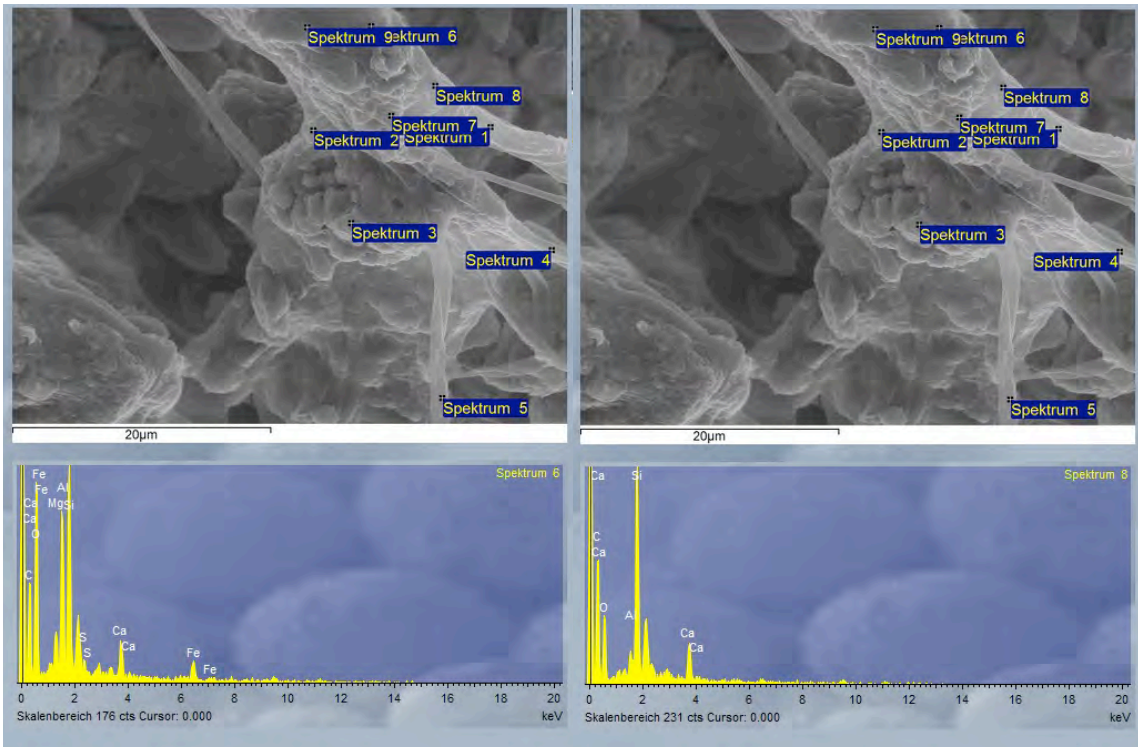

Figure S17. SEM-EDX analysis of Gorello Waterfall sample Gor 8, 5 m from waterfall.
Both analyses on organic matter coating calcite crystals show enrichment in Si, Al, Mg and Fe in addition to Ca.

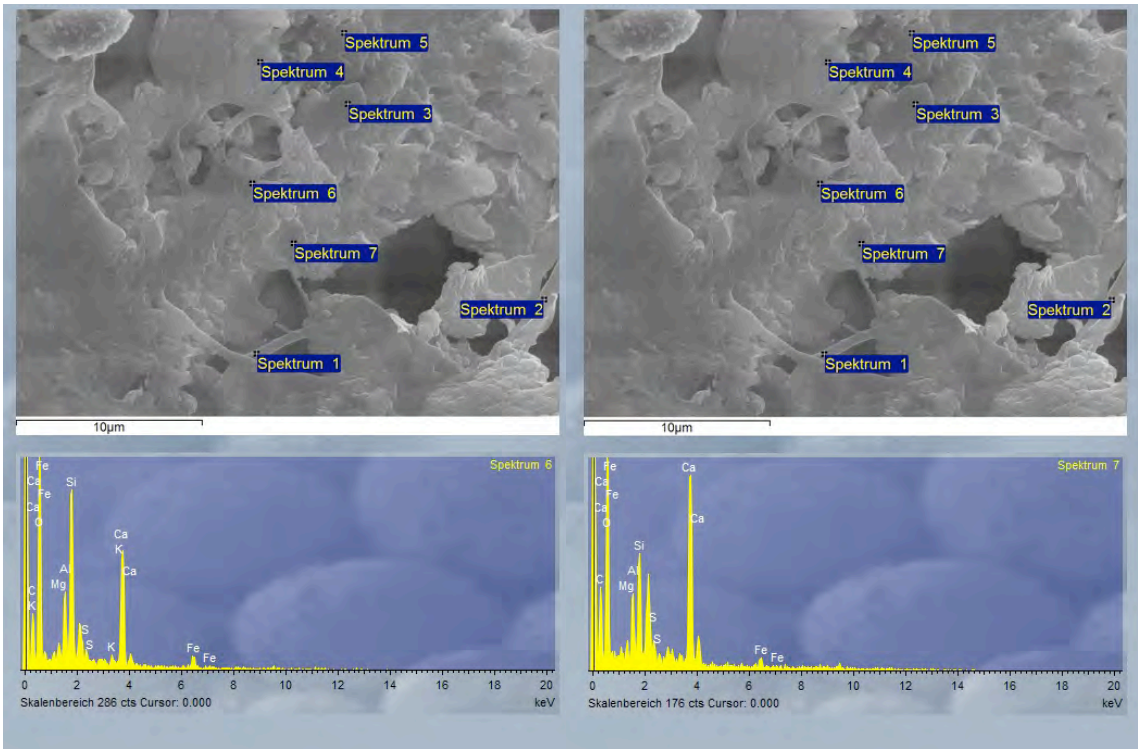

Figure S18. SEM-EDX analysis of Gorello Waterfall sample Gor 8, 5 m from waterfall.
Both analyses on organic matter coating calcite crystals show enrichment in Si, Al, Mg, Fe and K in addition to Ca.

Table S1. Results of stable carbon and oxygen isotope analyses from the travertine study sites. Samples reported as "fossil" were collected in inactive portions of the system and they had been deposited in previous seasons or years.

Samples Bullicame (Viterbo)	Distance from vent	Mineralogy	$\delta^{13}C$ (‰ V-PDB)	$\delta^{18}O$ (‰ V-PDB)
Streamers				
BUL-A-18	30.5 m	calcite; aragonite	5.4	-12.1
BUL-1	35 m	calcite; aragonite	5.5	-11.6
BUL-1b	35 m	calcite; aragonite	5.4	-11.6
Average streamers (n = 3)			5.4	-11.8
Standard Deviation			0.1	0.3
Rafts and coated bubbles				
BUL-A-9R rim at proximal channel margin	21.5 m	calcite; aragonite	7.2	-11.0
BUL-3A	60.5 m	calcite	7.3	-9.2
BUL-3B	70 m	calcite	7.5	-8.7
BUL-3C	70 m	calcite	7.4	-8.9
Average rafts and coated bubbles (n = 4)			7.3	-9.4
Standard Deviation			0.2	1.0
Coated reeds				
BUL-2B	fossil	calcite	6.8	-9.0
BUL-2A	fossil	calcite	6.7	-10.0
Average reeds (n = 2)			6.7	-9.4
Standard Deviation			0.0	0.6
Bullicame all analyses regression line	y=0.5635x+12.328			
R^2	0.8			
Pearson correlation coefficient	0.9			

Bollore (Bagni San Filippo)	Distance from vent	Mineralogy	$\delta^{13}C$ (‰ V-PDB)	$\delta^{18}O$ (‰ V-PDB)
Streamers				
BF-1.3d	0.8 m	calcite; aragonite	4.2	-12.9
BF 1.3b	0.8 m	calcite; aragonite	4.1	-12.8
BSF-GA1	2 m	calcite	4.4	-12.4
BSF-GA2	3 m	calcite	4.9	-12.4
BSF-GA3	3 m	calcite	4.8	-12.5
Average streamers (n = 5)			4.5	-12.6
Standard Deviation			0.3	0.2
Rafts and coated bubbles				
BSF-GC	2 m	calcite; aragonite	4.9	-12.5
BSF-GC-1	2 m	calcite; aragonite	5.2	-12.5
BSF-GC-2	2 m	calcite; aragonite	5.0	-12.6

BSF 1a	4 m	calcite; aragonite	5.8	-11.4
BSF 1b	4 m	calcite; aragonite	5.7	-11.4
BSF 14G	14 m	calcite	5.6	-11.6
BSF-R	fossil	calcite	5.1	-12.0
BSF-Rb	fossil	calcite	5.1	-12.2
Average rafts and coated bubbles (n = 8)			5.3	-12.0
Standard Deviation			0.3	0.5
Dendrites				
BSF GBa	16 m	calcite	4.8	-12.6
BSF-GBb	16 m	calcite	5.9	-12.1
Average dendrites (n = 2)			5.4	-12.4
Standard Deviation			0.8	0.4
Bollore all analyses regression line	y=0.954x+16.737			
R^2	0.7			
Pearson correlation coefficient	0.8			

Gorello Waterfalls (Saturnia)	**Distance from vent All samples 5-10 m from waterfall located ca. 1170 m far from vent**	**Mineralogy**	**$\delta^{13}C$ (‰ V-PDB)**	**$\delta^{18}O$ (‰ V-PDB)**
Laminated boundstone rims and walls				
GOR-13		calcite	3.3	-8.3
GOR-14		calcite	3.1	-8.3
GOR-15		calcite	3.5	-8.2
GOR-16		calcite	2.7	-8.8
GOR-17		calcite	3.5	-8.3
GOR-18		calcite	2.9	-8.8
GOR-19		calcite	2.2	-8.9
SAT-3ox		calcite	2.6	-8.6
SAT-ox		calcite	2.9	-8.5
SAT-1ox		calcite	2.5	-8.6
SAT-3		calcite	2.6	-8.5
SAT-F1		calcite	3.0	-8.6
SAT-F2		calcite	3.0	-8.5
SAT-F3		calcite	3.0	-8.6
SAT-2b		calcite	2.5	-8.6
SAT-2ox		calcite	3.1	-8.5
SAT-1ox		calcite	3.0	-8.6
Average laminated boundstone rims and walls (n = 17)			2.9	-8.5
Standard Deviation			0.4	0.2
Coated grains (oncoids) in pools				
GOR-3		calcite	2.6	-8.5
GOR-4		calcite	2.8	-8.2
SAT-S2		calcite	2.6	-8.6
SAT-S1ox		calcite	2.7	-8.5
SAT-S2ox		calcite	2.7	-8.6

Average coated grains (oncoids) in pools (n = 5)			2.7	-8.5
Standard Deviation			0.1	0.2
Rafts and coated bubbles				
GOR-2		calcite	2.2	-8.4
Coated reeds		calcite		
GOR-1		calcite	3.1	-8.2
Gorello Waterfall all analyses regression line	y=1.2008x+13.063			
R^2	0.4			
Pearson correlation coefficient	0.6			